Directional Tensor Product Complex Tight Framelets

by

Zhenpeng Zhao

A thesis submitted in partial fulfillment of the requirements for the degree of

Doctor of Philosophy

in

Applied Mathematics

Department of Mathematical and Statistical Sciences

University of Alberta

Abstract

This thesis concentrates on the construction of directional tensor product complex tight framelets (TP-$\mathbb{C}\mathrm{TF}_m$). It uses a complex tight framelet filter bank ($\mathbb{C}\mathrm{TF}_m$) in one dimension and the tensor product of the one-dimensional filter bank to obtain high-dimensional filter banks. It has a number of advantages over the traditional tensor product real wavelet transform.

Motivated by two-dimensional dual tree complex wavelet transform, the complex tight framelet filter banks with frequency separation are constructed in the frequency domain. Then the high-dimensional framelet filter banks via tensor product and corresponding frames will have directional selectivity.

The computational cost increases exponentially as dimension and redundancy rate grow, which restricts the application of framelet filter banks in high-dimensional data processing. In the frequency domain, we propose complex tight framelet filter banks with mixed sampling factor to reduce the redundancy rate.

The tensor product complex tight framelet filter banks constructed in the frequency domain are bandlimited. They are not finitely supported in the time domain. Compactly supported wavelets or framelets are essential to many applications due to their good space-frequency localization and fast computational algorithm. We have proved a theoretical result on directional selectivity and provided step-by-step algorithms to construct compactly supported complex tight framelet filter banks $\mathbb{C}\mathrm{TF}_3$, $\mathbb{C}\mathrm{TF}_4$, and $\mathbb{C}\mathrm{TF}_6$. Then the directional compactly supported tensor product complex tight framelet filter banks TP-$\mathbb{C}\mathrm{TF}_3$, TP-$\mathbb{C}\mathrm{TF}_4$, and TP-$\mathbb{C}\mathrm{TF}_6$ in high dimensions can be obtained via tensor product.

The directional tensor product complex tight framelet is used to the application of image denoising and video denoising. Experimental results show that our constructed TP-$\mathbb{C}\mathrm{TF}_m$ succeeds in providing improved image denoising results combined with advanced statistical models comparing with many other state-of-the-art transform based image denoising methods.

To my wife Fei Wang and my parents

Acknowledgement

I would like to express my sincere gratitude to my supervisor Dr. Bin Han and vice supervisor Dr. Yau Shu Wong for their patience, knowledge, inspirations, guidances, and supportive attitudes throughout my studies. Dr. Han first introduced me to the topic of constructing directional tensor product complex tight framelets. Dr. Wong helped me to establish the connection between my research project to real industry applications. I sincerely appreciate their time for writing reference letter for me and giving suggestions on my career. Without their efforts, this thesis would not have been possible.

I am deeply indebted to Dr. Rong-Qing Jia, Dr. Michael Y. Li, Dr. Vicky Zhao, and Dr. Ivan Selesnick for serving in my supervisory committee or final examine committee and reading my thesis carefully. My heartfelt appreciation also goes to Dr. Qun Mo, Dr. Xiaosheng Zhuang, and Dr. Yi Shen for their helpful discussions. I have learned a lot from them. I would like to thank Dr. Wei Song from Harbin Institute of Technology for the last-minute proofreading.

Many thanks to Department of Mathematical and Statistical Sciences at University of Alberta for the financial support and the excellent service provided for the last five years. I am also grateful to Dr. Dang Dinh Hai, Dr. Chuanxi Qian, Dr. Seongjai Kim, and Dr. Xingzhou Yang at Department of Mathematics and Statistics, Mississippi State University. Special thanks go to all my friends in Edmonton.

Last but not least, I would like to thank my wife and my parents for their love, tolerance, and support throughout my life. To them, all this has been done.

List of Figures

List of Tables

Table of Contents

Chapter 1

Introduction

1.1 Definitions, background, and motivations

In order to introduce the background and motivations, we first need some definitions and notion. By $l_2(\mathbb{Z})$ we denote the linear space of all complex-valued sequences $u = \{u(k)\}_{k\in\mathbb{Z}} : \mathbb{Z} \to \mathbb{C}$ such that $\|u\|_{l_2(\mathbb{Z})} := \left(\sum_{k\in\mathbb{Z}} |u(k)|^2\right)^{\frac{1}{2}} < \infty$. The Fourier series (or symbol) of a sequence $u \in l_2(\mathbb{Z})$ is defined to be

$$\widehat{u}(\xi) := \sum_{k\in\mathbb{Z}} u(k)e^{-ik\xi}, \quad \xi \in \mathbb{R},$$

which is a 2π-periodic measurable function in $L_2(\mathbb{T})$ since

$$\|\widehat{u}\|^2_{L_2(\mathbb{T})} := \frac{1}{2\pi}\int_{[-\pi,\pi)} |\widehat{u}(\xi)|^2 d\xi = \sum_{k\in\mathbb{Z}} |u(k)|^2 = \|u\|^2_{l_2(\mathbb{Z})} < \infty,$$

where $\mathbb{T}$ is defined as the quotient $\mathbb{R}/2\pi\mathbb{Z}$. If $u \in l_1(\mathbb{Z})$, that is, $\|u\|_{l_1(\mathbb{Z})} := \sum_{k\in\mathbb{Z}} |u(k)| < \infty$, then $u \in l_2(\mathbb{Z})$ and $\widehat{u} \in C(\mathbb{T})$ is a continuous function.

For $a, b_1, \dots, b_s \in l_1(\mathbb{Z})$, $\{a; b_1, \dots, b_s\}$ is called a (dyadic) tight framelet filter bank if

$$\begin{aligned} &|\widehat{a}(\xi)|^2 + \sum_{\ell=1}^{s} |\widehat{b_\ell}(\xi)|^2 = 1, \\ &\widehat{a}(\xi)\overline{\widehat{a}(\xi+\pi)} + \sum_{\ell=1}^{s} \widehat{b_\ell}(\xi)\overline{\widehat{b_\ell}(\xi+\pi)} = 0, \end{aligned} \tag{1.1.1}$$

for $\xi \in \mathbb{R}$. (1.1.1) is also called the property of perfect reconstruction and it is one of the fundamental properties for filter banks. The filter a is called a low-pass filter since it is often required that $\widehat{a}(0) = 1$, and all the filters $b_1, \ldots, b_s$ are called high-pass filters since they often have $\widehat{b_1}(0) = \ldots = \widehat{b_s}(0) = 0$. Note that if $\widehat{a}(0) = 1$, it follows from (1.1.1) that $\widehat{b_1}(0) = \ldots = \widehat{b_s}(0) = 0$. When $s = 1$, the (dyadic) tight framelet filter bank $\{a; b_1\}$ is called a (dyadic) wavelet filter bank.

A (dyadic) wavelet system comprises a set of functions $\{\psi_{j,k}\}_{j,k\in\mathbb{Z}}$, which is generated from one single function or more functions by dilations and shifts. It forms an orthogonal basis for the function space $L_2(\mathbb{R})$. Each member in this set is defined as

$$\psi_{j,k} = 2^{j/2}\psi(2^j \cdot -k), \quad j,\ k \in \mathbb{Z},$$

where ψ is called the mother wavelet, which plays an important role in wavelet analysis.

Mallat [37] and Meyer introduced multiresolution analysis (MRA) to generate mother wavelet ψ. Let V_0 be a subspace of $L_2(\mathbb{R})$ and $V_j := \{f(2^j\cdot) \ : \ f \in V_0\}$. As outlined in Chapter 5 by Daubechies [4], MRA is a decomposition of $L_2(\mathbb{R})$ into a nested chain of closed subspaces such that

(1) $\cdots \subset V_{-k} \subset \cdots \subset V_{-1} \subset V_0 \subset V_1 \subset \cdots \subset V_k \subset \cdots$;

(2) $\bigcap_{j\in\mathbb{Z}} V_j = \{0\}$;

(3) $\bigcup_{j\in\mathbb{Z}} V_j$ is dense in $L_2(\mathbb{R})$;

(4) there exists a function $\phi \in L_2(\mathbb{R})$ such that $V_0 = \overline{\text{span}\{\phi(\cdot - k)\}_{k\in\mathbb{Z}}}$;

(5) the mother wavelet function $\psi \in L_2(\mathbb{R})$ can be constructed such that $V_1 = V_0 \oplus W$ where $W = \overline{\text{span}\{\psi(\cdot - k)\}_{k\in\mathbb{Z}}}$.

The MRA is completely determined by the function ϕ in item (4). Thus we have to construct such a function ϕ first. Since by item (4) $V_0 = \overline{\text{span}\{\phi(\cdot - k)\}_{k\in\mathbb{Z}}}$,

$\phi \in V_0$. Also by the definition of V_1, we have $V_1 = \overline{\text{span}\{\phi(2\cdot - k)\}_{k\in\mathbb{Z}}}$. Since $\phi \in V_0 \subset V_1$, the following refinement equation holds:

$$\phi = 2\sum_{k\in\mathbb{Z}} a(k)\phi(2\cdot - k),$$

where $a = \{a(k)\}_{k\in\mathbb{Z}}$ is a sequence on $\mathbb{Z}$. ϕ is called refinable function if $\phi \in L_2(\mathbb{R})$ and satisfies the refinement equation. The MRA can be constructed from a refinable function ϕ under mild conditions on the sequence a. From an MRA, a wavelet system can be constructed.

A wavelet system has many advantages. First, it is a time and frequency representation [1] comparing with Fourier transform. The Fourier transform of $f \in L_1(\mathbb{R})$ is defined to be $\widehat{f}(\xi) = \int_{\mathbb{R}} f(x)e^{-ix\xi}d\xi$, for $\xi \in \mathbb{R}$. Since all the information in the time domain is involved in the Fourier transform, the time and frequency information cannot be seen simultaneously. The wavelet system enjoys a multiscale structure: for $j \in \mathbb{Z}$, $\psi_{j,k}$ corresponds to a frequency scale. The frequency information can be reflected by the wavelet function $\psi_{j,k}$ with different j. Therefore, the wavelet system can describe the time-frequency localization very well. Second, a wavelet system offers a sparse representation for smooth or piecewise smooth signals [38]. A wavelet function ψ is called to have vanishing moments of order m if

$$\int_{\mathbb{R}} x^k\psi(x)dx = 0, \qquad k = 0, 1, \ldots, m-1.$$

The wavelet function with high order vanishing moments makes only a few wavelet coefficients large while the other coefficients very small.

For practical applications, The decimated dyadic filter bank tree proposed by Mallat [37] is the most acknowledged form in application. The most popular set of wavelet filter banks was proposed by Ingrid Daubechies [4].

Although wavelets have many applications in compression and signal processing, the requirements on wavelets to be orthonormal or biorthogonal are too restrictive to construct bases with extra conditions. For example, it is well known that the dyadic real-valued orthogonal compactly supported wavelets cannot have symmetry except Haar wavelet. As a generalization of wavelet representation, frames are over-complete systems that allow us to have more flexibility. Frames of a vector space were introduced by Duffin and Schaeffer in [6].

A sequence $\{f_n\}_{n\in\Gamma}$ is a frame for $L_2(\mathbb{R})$ if there exist two constants $B \geqslant A > 0$ such that

$$A\|f\|^2_{L_2(\mathbb{R})} \leqslant \sum_{n\in\Gamma} |\langle f, f_n\rangle|^2 \leqslant B\|f\|^2_{L_2(\mathbb{R})}, \quad f \in L_2(\mathbb{R}).$$

A frame $\{f_n\}_{n\in\Gamma}$ is tight if $A = B$. For a tight frame, A and B can be normalized to one such that the Parseval identity holds:

$$\|f\|^2_{L_2(\mathbb{R})} = \sum_{n\in\Gamma} |\langle f, f_n\rangle|^2, \quad f \in L_2(\mathbb{R}).$$

Throughout this thesis, the word framelets is a synonym for wavelet frames.

One problem with the real wavelets and framelets is a lack of directional selectivity in high dimensions. Multidirectional representation systems can represent curve or edge singularities effectively and offer a sparse expression for the hight-dimensional data which simplifies the processing and modeling of geometric features of the data in high dimensions.

To better understand directionality, consider the Haar orthogonal wavelet filter bank in two dimensions. The one-dimensional Haar orthogonal wavelet filter bank is $\{a; b\}$ with $a = \{\frac{1}{2}, \frac{1}{2}\}_{[0,1]}$ and $b = \{\frac{1}{2}, -\frac{1}{2}\}_{[0,1]}$ on discrete support $[0, 1]$. The two-dimensional Haar orthogonal wavelet filter bank is obtained by the tensor product $\{a\otimes a; a\otimes b, b\otimes a, b\otimes b\}$. More specifically, they are

$$a\otimes a=\begin{bmatrix}\frac{1}{4} & \frac{1}{4}\\ \frac{1}{4} & \frac{1}{4}\end{bmatrix},\ a\otimes b=\begin{bmatrix}-\frac{1}{4} & -\frac{1}{4}\\ \frac{1}{4} & \frac{1}{4}\end{bmatrix},\ b\otimes a=\begin{bmatrix}\frac{1}{4} & -\frac{1}{4}\\ \frac{1}{4} & -\frac{1}{4}\end{bmatrix},\ b\otimes b=\begin{bmatrix}-\frac{1}{4} & \frac{1}{4}\\ \frac{1}{4} & -\frac{1}{4}\end{bmatrix},$$

on discrete support $[0,1]^2$. The two-dimensional transform can be implemented separately because of the tensor product filter: each row of the two-dimensional input data is convolved with the one-dimensional filter in the first dimension of the tensor product filter, then each column of the resulting two-dimensional data is convolved with the one-dimensional filter in the second dimension. Worthy of note is both $a\otimes b$ and $b\otimes a$ are able to select horizontal and vertical edges, respectively. But $b\otimes b$ is oriented along two diagonal orientations simultaneously and produces a checkerboard pattern. See Figure 1.1 for the demonstration.

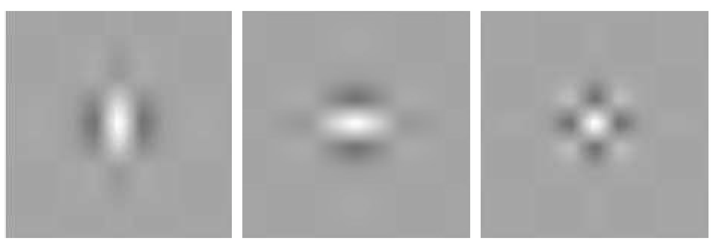

Figure 1.1: Two-dimensional tensor product real-valued wavelets in the time domain. The third graph demonstrates the checkerboard artifact of $b\otimes b$. Figure adapted from [44].

This is because u is real (that is, $u:\mathbb{Z}\to\mathbb{R}$) if and only if $\overline{\widehat{u}(\xi)}=\widehat{u}(-\xi)$. Thus, we always have $|\widehat{u}(-\xi)|=|\widehat{u}(\xi)|$ for a real filter u, and the magnitude of its frequency spectrum is symmetric about the origin. If both u and v are one-dimensional real high-pass filters, then the frequency spectrum of the tensor product filter $u\otimes v$ concentrates equally in all four quadrants (more precisely, the four corners) of the basic frequency square $[-\pi,\pi]^2$. Consequently, the filter $u\otimes v$ behaves like a saddle point and lacks directional selectivity.

The same argument applies to the tensor product of real-valued functions. This lack of directional selectivity complicates the image modeling and processing of ridges or edges singularities. Since the edges and textures are ubiquitous in images, directional representations have to be devised to handle the geometric features by offering effective and sparse expansions.

In order to remedy this drawback, it is natural to design the spectra of high-dimensional filters in separate quadrants of the frequency plane. Several approaches have been proposed in the literature: for example, the curvelet transform [2] and the shearlet transform [21, 29, 30, 34] in two dimensions on $\mathbb{R}^2$, contourlets [5] in the discrete domain $\mathbb{Z}^2$, symmetric complex orthogonal wavelet filter banks [13, 15, 35], and the dual tree complex wavelet transform (DT-$\mathbb{C}$WT) in [27, 28, 43, 44], and etc.

Curvelets are one type of tight frames proposed by E. Candès and D. Donoho [2, 3]. In the frequency domain, curvelet transforms apply angle-trapezoid filters to achieve directional selectivity. However, it is a challenge for curvelets to develop an efficient algorithm for practical applications in discrete setting. Based on unequall-spaced fast Fourier transform, discrete curvelet transform was proposed in [2]. The construction requires a rotation and partition of the two-dimensional frequency plane in polar coordinate perspective. Even so, it still suffers high redundancy rate.

Shearlets were introduced for the approximation of functions $f \in L_2(\mathbb{R}^2)$ in 2006 [10]. Shearlets constitute an affine system from one single shearlet function by scaling, shearing, and translation operations. The scaling operation can elongate the elements in the affine system. The shearing operation captures the directionality of the curve singularities. The translation operation offers the spatial localizations. In order to have discrete transform, one has to calculate the coefficients in the continuum setting and pseudopolar Fourier transform is applied. However, to achieve nearly perfect reconstruction of the obtained discrete shearlet transform, the oversampling rate used in pseudopolar Fourier transform is often very large, and this results in high redundancy rate.

Contourlets, proposed by Do and Vetterli [5], are one of the multidirectional representation systems. Contourlets can handle piecewise smooth images with steady contours effectively. The construction of contourlets is directly from the discrete domain. The contourlet transform can be treated as a discrete version of certain curvelet transforms. One drawback of the contourlets lies in its shift-sensitivity.

The $\mathrm{DT}\text{-}\mathbb{C}\mathrm{WT}$ is probably the most popular and successful among all these approaches mentioned above. The success of the $\mathrm{DT}\text{-}\mathbb{C}\mathrm{WT}$ depends on three major advantages [44]:

- the two-dimensional $\mathrm{DT}\text{-}\mathbb{C}\mathrm{WT}$ offers six directions (roughly along $\pm 15°$, $\pm 45°$, $\pm 75°$), comparing with only two (horizontal and vertical) directions of classical tensor product real wavelets;

- the $\mathrm{DT}\text{-}\mathbb{C}\mathrm{WT}$ is nearly shift-invariant without high redundancy, comparing with the shift-invariant undecimated wavelet transform, see Figure 1.2 for the wavelets of the two-dimensional $\mathrm{DT}\text{-}\mathbb{C}\mathrm{WT}$;

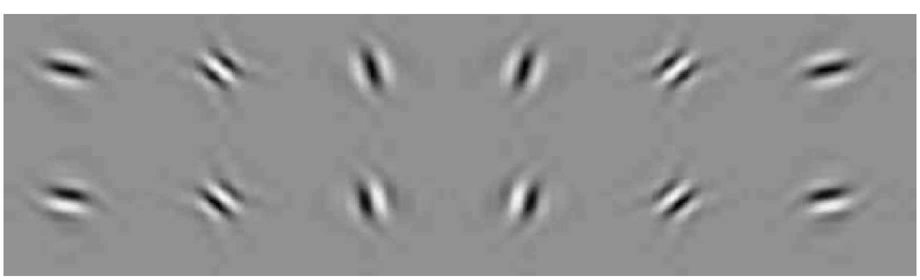

Figure 1.2: Typical wavelets associated with the $\mathrm{DT}\text{-}\mathbb{C}\mathrm{WT}$ in two dimensions. The first row illustrates the real part of each complex wavelet; the second row illustrates the imaginary part. Figure adapted from [44].

- the d-dimensional $\mathrm{DT}\text{-}\mathbb{C}\mathrm{WT}$ can be implemented by applying 2^d tensor product discrete orthogonal wavelet transforms in parallel.

The one-dimensional $\mathrm{DT}\text{-}\mathbb{C}\mathrm{WT}$ employs two trees of finitely supported orthogonal real wavelet filter banks with three sets: $\{a^0; b^0\}$, $\{a^1; b^1\}$, and $\{a^2; b^2\}$ such that $|\widehat{a^\ell}(\xi)|^2 + |\widehat{a^\ell}(\xi+\pi)|^2 = 1$ and $\widehat{b^\ell} = e^{-i\xi}\overline{\widehat{a^\ell}(\xi+\pi)}$ for $\ell = 0, 1, 2$. The filter banks $\{a^0; b^0\}$ and $\{a^0(\cdot - 1); b^0(\cdot - 1)\}$ used for the first level of the two trees can be any finitely supported orthogonal real wavelet filter bank, where $a^0(\cdot - 1)$ and $b^0(\cdot - 1)$ are the shifted versions of sequences a^0 and b^0, respectively. The correlated pair of finitely supported orthogonal real wavelet filter banks $\{a^1; b^1\}$ and $\{a^2; b^2\}$ used for all other levels of the two trees are linked to each other through the half-shift condition [42, 43, 44]:

$$\widehat{a^2}(\xi) \approx e^{-i\xi/2}\widehat{a^1}(\xi), \quad \xi \in [-\pi, \pi).$$

Then complex wavelet coefficients are generated by taking the wavelet coefficients from two trees as the real part and imaginary part, respectively. Equivalently, complex wavelet coefficients in the $\mathrm{DT}\text{-}\mathbb{C}\mathrm{WT}$ are obtained by employing the complex high-pass filters $b^1 + ib^2$ and $b^1 - ib^2$. Due to the half-shift condition, the two high-pass filters b^1 and b^2 satisfy

$$\widehat{b^2}(\xi) \approx -i\,\mathrm{sgn}(\xi)e^{i\xi/2}\widehat{b^1}(\xi), \quad \xi \in [-\pi, \pi),$$

where $\mathrm{sgn}(\xi) = 1$ for $\xi \geqslant 0$ and $\mathrm{sgn}(\xi) = -1$ for $\xi < 0$. Consequently, the underlying complex high-pass filters $b^1 + ib^2$ and $b^1 - ib^2$ enjoy the following frequency separation:

$$\widehat{b^1}(\xi) + i\widehat{b^2}(\xi) \approx 0, \quad \xi \in [-\pi, 0] \quad \text{and} \quad \widehat{b^1}(\xi) - i\widehat{b^2}(\xi) \approx 0, \quad \xi \in [0, \pi].$$

The frequency separation plays a critical role to produce the desired directional selectivity of DT-$\mathbb{C}$WT in high dimensions.

The half-shift condition for a^1 and a^2 in the DT-$\mathbb{C}$WT is not trivial in discrete setting in the time domain. Instead of using pairs of correlated orthogonal real wavelet filter banks to achieve frequency separation, in this thesis, we propose complex tight framelet filter banks with frequency separation so that the high-pass filters in high dimensions via tensor product achieve directional selectivity.

1.2 Discrete framelet transform

Let us introduce the discrete framelet transform using the one-dimensional tight framelet filter bank $\{u_0; u_1, \ldots, u_s\}$. The discrete framelet transform can be described by two linear operators – the subdivision operator and the transition operator [19]. For a filter $u \in l_0(\mathbb{Z})$, the subdivision operator $\mathcal{S}_u : l(\mathbb{Z}) \to l(\mathbb{Z})$ is defined to be

$$[\mathcal{S}_u v](n) = 2\sum_{k\in\mathbb{Z}} v(k)u(n-2k), \qquad n \in \mathbb{Z},$$

and the transition operator $\mathcal{T}_a : l(\mathbb{Z}) \to l(\mathbb{Z})$ is defined to be

$$[\mathcal{T}_u v](n) = 2\sum_{k\in\mathbb{Z}} v(k)\overline{u(k-2n)}, \qquad n \in \mathbb{Z}.$$

The transition operation often averages data to lower frequency resolution levels; while the subdivision operator refines data to higher resolution levels.

The subdivision and transition operators can be implemented through convolution, upsampling, and downsampling operators. For $u \in l_0(\mathbb{Z})$ and $v \in l(\mathbb{Z})$, the convolution $u * v$ is defined to be

$$[u * v](n) := \sum_{k\in\mathbb{Z}} u(k)v(n-k), \quad n \in \mathbb{Z}.$$

The upsampling operator $\uparrow \mathsf{d} : l(\mathbb{Z}) \to l(\mathbb{Z})$ and downsampling operator $\downarrow \mathsf{d} : l(\mathbb{Z}) \to l(\mathbb{Z})$ with the sampling factor d are defined to be

$$[v\uparrow\mathsf{d}](n) := \begin{cases} v\,(n/\mathsf{d}) & \text{if } \frac{n}{\mathsf{d}} \text{ is an integer,} \\ 0 & \text{otherwise,} \end{cases} \quad \text{and} \quad [v\downarrow\mathsf{d}](n) := v(\mathsf{d}n),\ n \in \mathbb{Z}.$$

Using convolution, upsampling, and downsampling, we have

$$\mathcal{T}_u v = 2(v * u^\star)\downarrow 2 \quad \text{and} \quad \mathcal{S}_u v = 2(v\uparrow 2) * u,$$

where the adjoint filter $u^\star$ is defined by $u^\star(n) := \overline{u(-n)}, \quad n \in \mathbb{Z}$.

In terms of Fourier series, we have $\widehat{u * v}(\xi) = \widehat{u}(\xi)\widehat{v}(\xi),\ \widehat{v^\star}(\xi) = \overline{\widehat{v}(\xi)}$, and

$$\widehat{v\uparrow 2}(\xi) = \widehat{v}(2\xi), \quad \widehat{v\downarrow 2}(\xi) = 2^{-1}[\widehat{v}(\xi/2) + \widehat{v}(\xi/2+\pi)].$$

Then, the subdivision and transition operators can be expressed as

$$\begin{aligned} &\widehat{\mathcal{S}_u v}(\xi) = 2\widehat{v}(2\xi)\widehat{u}(\xi), \\ &\widehat{\mathcal{T}_u v}(\xi) = \widehat{v}(\xi/2)\overline{\widehat{u}(\xi/2)} + \widehat{v}(\xi/2+\pi)\overline{\widehat{u}(\xi/2+\pi)}, \quad \xi \in \mathbb{R}. \end{aligned}$$

The one-level discrete framelet transform consists of two parts: decomposition and reconstruction. Let $\{u_0; u_1, \ldots, u_s\}$ be a tight framelet filter bank. For given data $v \in l(\mathbb{Z})$, the one-level framelet decomposition is

$$w_\ell := \frac{\sqrt{2}}{2}\mathcal{T}_{u_\ell} v, \quad \ell = 0, \ldots, s,$$

where w_ℓ's are called sequences of framelet coefficients of the input signal v. We can group all coefficient sequences together to define the framelet decomposition operator $\mathcal{W}$:

$$\mathcal{W}v := \frac{\sqrt{2}}{2}\left(\mathcal{T}_{u_0} v, \ldots, \mathcal{T}_{u_s} v\right), \quad v \in l(\mathbb{Z}).$$

The one-level framelet reconstruction employing the filter bank $\{u_0; u_1, \ldots, u_s\}$

can be described by a framelet reconstruction operator $\mathcal{V}$ which is defined to be

$$\mathcal{V}(w_0, \ldots, w_s) := \frac{\sqrt{2}}{2} \sum_{\ell=0}^{s} \mathcal{S}_{u_\ell} w_\ell, \quad w_0, \ldots, w_s \in l(\mathbb{Z}).$$

The factor $\frac{\sqrt{2}}{2}$ is applied to balance the energy between the input data and its framelet coefficients.

The simplest way to obtain tight framelet filter banks in high dimensions is by the tensor product of one-dimensional tight framelet filter banks. The main advantage of tensor product wavelets and framelets lies in their easy construction and fast computational algorithms.

For one-dimensional filters $u, v \in l_1(\mathbb{Z})$, the tensor product filter $u \otimes v$ in two dimensions is defined to be

$$[u \otimes v](j, k) = u(j)v(k), \quad j, k \in \mathbb{Z}.$$

Let $\{a; b_1, \ldots, b_s\}$ be a one-dimensional tight framelet filter bank. The tensor product d-dimensional tight framelet filter bank is defined by $\otimes^d \{a; b_1, \ldots, b_s\}$, with $\otimes^d a$ being the low-pass filter and all other filters being the high-pass filters.

For d-dimensional filters $a, b_1, \ldots, b_s \in l_1(\mathbb{Z}^d)$, following (1.1.1), $\{a; b_1, \ldots, b_s\}$ is called a (d-dimensional dyadic) tight framelet filter bank if

$$|\widehat{a}(\xi)|^2 + \sum_{\ell=1}^{s} |\widehat{b_\ell}(\xi)|^2 = 1, \tag{1.2.1}$$

$$\widehat{a}(\xi)\overline{\widehat{a}(\xi + \pi\omega)} + \sum_{\ell=1}^{s} \widehat{b_\ell}(\xi)\overline{\widehat{b_\ell}(\xi + \pi\omega)} = 0, \tag{1.2.2}$$

for all $\xi \in \mathbb{R}^d$ and all $\omega \in \Omega \backslash \{0\}$, where $\Omega := [0, 1]^d \cap \mathbb{Z}^d$. The filter a is called the low-pass filter since we often have $\widehat{a}(0) = 1$, and all the filters $b_1, \ldots, b_s$ are called high-pass filters since it is often required that $\widehat{b_1}(0) = \cdots = \widehat{b_s}(0) = 0$. Note that if $\widehat{a}(0) = 1$ in a tight framelet filter bank $\{a; b_1, \ldots, b_s\}$, then it follows directly from (1.2.1) that $\widehat{b_1}(0) = \cdots = \widehat{b_s}(0) = 0$. When $s = 2^d - 1$, the (d-dimensional dyadic) tight framelet filter bank $\{a; b_1, \dots, b_{2^d-1}\}$ is called the (d-dimensional dyadic) orthogonal wavelet filter bank. Let $\{a; b_1, \dots, b_s\}$ be a d-dimensional tight framelet filter bank. Under the mild condition $|1 - \widehat{a}(\xi)| \leqslant C|\xi|^\tau, \xi \in [-\pi, \pi]^d$ for some positive numbers C and τ (all the tight framelet filter banks constructed in Chapter 2 satisfy this condition with $\tau = 1$), the function $\widehat{\phi}(\xi) := \prod_{j=1}^{\infty} \widehat{a}(2^{-j}\xi)$ is a well-defined function in $L_2(\mathbb{R}^d)$ and $\{\phi; \psi^1, \dots, \psi^s\}$ is a tight frame for $L_2(\mathbb{R}^d)$, where the functions $\psi^1, \dots, \psi^s$ are defined by $\widehat{\psi^\ell}(\xi) := \widehat{b_\ell}(\xi/2)\widehat{\phi}(\xi/2),\ \ell = 1, \dots, s$. That means the system

$$\left\{\phi(\cdot - k) \ : \ k \in \mathbb{Z}^d\right\} \bigcup \left\{2^{dj/2}\psi^\ell(2^j \cdot -k) \ : \ k \in \mathbb{Z}^d, j \in \mathbb{N} \cup \{0\}, \ell = 1, \dots, s\right\} \tag{1.2.3}$$

is a (normalized) tight frame for $L_2(\mathbb{R}^d)$ satisfying

$$\|f\|^2_{L_2(\mathbb{R}^d)} = \sum_{k \in \mathbb{Z}^d} |\langle f, \phi(\cdot - k)\rangle|^2 + \sum_{j=0}^{\infty} \sum_{\ell=1}^{s} \sum_{k \in \mathbb{Z}^d} |\langle f, 2^{dj/2}\psi^\ell(2^j \cdot - k)\rangle|^2, \quad f \in L_2(\mathbb{R}^d).$$

Due to this connection between a tight framelet filter bank and a tight frame for the function space $L_2(\mathbb{R}^d)$, we concentrate on tight framelet filter banks instead of tight frames for $L_2(\mathbb{R}^d)$ in the whole thesis. In fact, it is more natural to study its underlying discrete affine systems instead of the functional systems (1.2.3) in $L_2(\mathbb{R}^d)$.

1.3 Overview

Chapter 2 and Chapter 3 comprise the construction of directional tensor product complex tight framelet filter banks in the frequency domain. Chapter 2 begins with the definition of discrete affine systems, explains the connection between the tight framelet filter banks and the tight frames for the function space $L_2(\mathbb{R})$, and finally discusses the construction of tight complex framelet filter banks with frequency separation in one dimension. Though a tight frame with higher redundancy often leads to superior performance, the computational cost magnifies exponentially as the dimension increases. This restricts the usage of frame with immense over-complete rate. Chapter 3 introduces a complex tight framelet filter bank with mixed sampling factors to reduce the computational cost in high-dimensional applications.

The complex tight framelet filter banks constructed in Chapter 2 and 3 are bandlimited in the frequency domain. They do not have compact support in the time domain. Compactly supported wavelets and framelets are of importance due to their good space-frequency localization and computational efficiency in applications. It is still an unsolved problem whether there exist compactly supported tensor product complex tight framelets with directionality. Chapter 4 covers the answer to this question by proving theoretical results and providing step-by-step algorithms to construct compactly supported complex tight framelet filter bank $\{a; b^p, b^n\}$. Built on Chapter 4, Chapter 5 continues to work on compactly supported tight framelet filter banks so that their tensor product filters in hight dimensions have more directions.

Finally, the directional tensor product complex tight framelets are tested in the applications of image and video denoising. Experimental results demonstrate that our proposed system shows superior performance comparing with the DT-$\mathbb{C}$WT and many other transform-based methods.

Chapter 2

Directional Tensor Product Complex Tight Framelets

This chapter develops the idea of the frequency separation. The directional tensor product complex tight framelets are systematically constructed and studied. The notion of discrete affine systems associated with a multilevel discrete framelet transform is introduced in [19]. It allows us to analyze the frequency separation of high-pass filters in the multilevel tight framelet filter bank. Following this, one-dimensional complex tight framelet filter banks with good frequency separation are constructed. Finally, we explain how and why one-dimensional complex wavelets and framelets with frequency separation lead to directional selectivity in high dimensions via tensor product. Several examples are provided to illustrate our construction. The results in this chapter have been published in *SIAM Journal on Imaging Sciences* [24].

2.1 Discrete affine systems

The advantage of discrete framelet transform lies in the ability to extract the multiscale information from the input signals. Hence a multilevel discrete framelet transform is applied. The multilevel discrete framelet transform applies the filter bank recursively in both decomposition and reconstruction procedures.

Let $\{a; b_1, \dots, b_s\}$ be the tight framelet filter bank used in the discrete framelet transform. For a positive integer J, the J-level discrete framelet decomposition is given by the following recursive formulas:

$$v_j := 2^{-d/2}\mathcal{T}_a v_{j-1}, \quad w_{\ell,j} := 2^{-d/2}\mathcal{T}_{b_\ell} v_{j-1}, \quad \ell = 1, \dots, s, \ j = 1, \dots, J,$$

where $v_0 = v \in l_2(\mathbb{Z}^d)$ is the input signal. The original input data v is decomposed into one low-pass subband and sJ high-pass subbands after the J-level discrete framelet decomposition.

Now the J-level discrete framelet reconstruction is used to rebuild the original signal recursively as follows:

$$\mathring{v}_{j-1} := 2^{-d/2}\mathcal{S}_a \mathring{v}_j + 2^{-d/2}\sum_{\ell=1}^{s} \mathcal{S}_{b_\ell} \mathring{w}_{\ell,j}, \qquad j = J, \dots, 1.$$

It is convenient for us to define the associated discrete affine systems to analyze multilevel discrete framelet transforms.

Following [19], the multilevel filters a_j and $b_{\ell,j}$ with $j \in \mathbb{N}$ and $\ell = 1, \dots, s$ are defined by

$$\widehat{a_j}(\xi) := 2^{dj/2}\widehat{a}(\xi)\widehat{a}(2\xi)\cdots\widehat{a}(2^{j-2}\xi)\widehat{a}(2^{j-1}\xi),$$
$$\widehat{b_{\ell,j}}(\xi) := 2^{dj/2}\widehat{a}(\xi)\widehat{a}(2\xi)\cdots\widehat{a}(2^{j-2}\xi)\widehat{b_\ell}(2^{j-1}\xi),$$

with $a_1 = 2^{d/2}a$ and $b_{\ell,1} = 2^{d/2}b_\ell$. Now their shifts in the time domain are defined by

$$a_{j;k} := a_j(\cdot - 2^j k) \quad \text{and} \quad b_{\ell,j;k} := b_{\ell,j}(\cdot - 2^j k), \quad k \in \mathbb{Z}^d, \ j \in \mathbb{N}, \ \ell = 1, \dots, s. \tag{2.1.1}$$

Since $l_2(\mathbb{Z}^d)$ is a Hilbert space with the inner product $\langle v, w\rangle = \sum_{k\in\mathbb{Z}^d} v(k)\overline{w(k)}$, as shown in [19], we have

$$v_j(k) = \langle v, a_{j;k} \rangle \quad \text{and} \quad w_{\ell,j}(k) = \langle v, b_{\ell,j;k} \rangle, \; k \in \mathbb{Z}^d, \; j \in \mathbb{N}, \; \ell = 1, \ldots, s,$$

Consequently, a J-level discrete framelet transform is to compute the following representation:

$$v = \sum_{k \in \mathbb{Z}^d} \langle v, a_{J;k} \rangle a_{J;k} + \sum_{j=1}^{J} \sum_{\ell=1}^{s} \sum_{k \in \mathbb{Z}^d} \langle v, b_{\ell,j;k} \rangle b_{\ell,j;k}, \qquad v \in l_2(\mathbb{Z}^d) \tag{2.1.2}$$

with the series converging unconditionally in $l_2(\mathbb{Z}^d)$. Moreover, we have the following cascade structure:

$$\sum_{k \in \mathbb{Z}^d} \langle v, a_{j-1;k} \rangle a_{j-1;k} = \sum_{k \in \mathbb{Z}^d} \langle v, a_{j;k} \rangle a_{j;k} + \sum_{\ell=1}^{s} \sum_{k \in \mathbb{Z}^d} \langle v, b_{\ell,j;k} \rangle b_{\ell,j;k}, \quad j \in \mathbb{N}, \; v \in l_2(\mathbb{Z}^d).$$

The fast discrete framelet transform algorithm is built on this cascade structure.

The J-level discrete affine system associated with the filter bank $\{a; b_1, \ldots, b_s\}$ is defined to be

$$\mathsf{DAS}_J(\{a; b_1, \ldots, b_s\}) := \{a_{J;k} \; : \; k \in \mathbb{Z}^d\} \bigcup \bigcup_{j=1}^{J} \{b_{\ell,j;k} \; : \; k \in \mathbb{Z}^d, \; \ell = 1, \ldots, s\}. \tag{2.1.3}$$

Following the general theory in [19], we have the following result for discrete affine systems.

Theorem 1. *Let* $a, b_1, \ldots, b_s \in l_1(\mathbb{Z}^d)$*. For* $J \in \mathbb{N}$*, define* $\mathrm{DAS}_J(\{a; b_1, \ldots, b_s\})$ *as in (2.1.3) with* $a_{J;k}$ *and* $b_{\ell,j;k}$ *being given in (2.1.1), respectively. Then the following statements are equivalent:*

(1) $\{a; b_1, \ldots, b_s\}$ *is a tight framelet filter bank.*

(2) The following identity holds:

$$v = \sum_{k\in\mathbb{Z}^d} \langle v, a_{1;k}\rangle a_{1;k} + \sum_{\ell=1}^{s}\sum_{k\in\mathbb{Z}^d} \langle v, b_{\ell,1;k}\rangle b_{\ell,1;k}, \quad v \in l_2(\mathbb{Z}^d). \tag{2.1.4}$$

(3) $\mathrm{DAS}_1(\{a; b_1, \dots, b_s\})$ is a (normalized) tight frame for $l_2(\mathbb{Z}^d)$, that is,

$$\|v\|^2_{l_2(\mathbb{Z}^d)} = \sum_{k\in\mathbb{Z}^d} |\langle v, a_{1;k}\rangle|^2 + \sum_{\ell=1}^{s}\sum_{k\in\mathbb{Z}^d} |\langle v, b_{\ell,1;k}\rangle|^2, \quad v \in l_2(\mathbb{Z}^d). \tag{2.1.5}$$

(4) For every $j \in \mathbb{N}$, the following identity holds:

$$\sum_{k\in\mathbb{Z}^d} \langle v, a_{j-1;k}\rangle a_{j-1;k} = \sum_{k\in\mathbb{Z}^d} \langle v, a_{j;k}\rangle a_{j;k} + \sum_{\ell=1}^{s}\sum_{k\in\mathbb{Z}^d} \langle v, b_{\ell,j;k}\rangle b_{\ell,j;k}, \quad v \in l_2(\mathbb{Z}^d),$$

with convention $a_0 := \boldsymbol{\delta}$ and $a_{0;k} := \boldsymbol{\delta}(\cdot - k)$ for $k \in \mathbb{Z}^d$, where $\boldsymbol{\delta}$ is the Dirac/Kronecker sequence on $\mathbb{Z}^d$:

$$\boldsymbol{\delta}(n) = \begin{cases} 1, & \text{if } n = 0, \\ 0, & \text{if } n \neq 0. \end{cases}$$

(5) For every $J \in \mathbb{N}$, the identity in (2.1.2) holds.

(6) For every $J \in \mathbb{N}$, $\mathrm{DAS}_J(\{a; b_1, \dots, b_s\})$ is a (normalized) tight frame for $l_2(\mathbb{Z}^d)$, that is,

$$\|v\|^2_{l_2(\mathbb{Z}^d)} = \sum_{k\in\mathbb{Z}^d} |\langle v, a_{J;k}\rangle|^2 + \sum_{j=1}^{J}\sum_{\ell=1}^{s}\sum_{k\in\mathbb{Z}^d} |\langle v, b_{\ell,j;k}\rangle|^2, \quad v \in l_2(\mathbb{Z}^d).$$

Proof. These claims have been proved in [19] for the general downsampling matrix M. This theorem is a special case with downsampling matrix $\mathsf{M} = 2\mathsf{I}_d$. For the completeness, we only present a sketch of the proof here.

Plugging $v = \boldsymbol{\delta}(\cdot - n)$ with all $n \in \mathbb{Z}^d$ into (2.1.4), we deduce that the resulting equations in (2.1.4) with $v = \boldsymbol{\delta}(\cdot - n)$ are exactly the time domain version of the conditions in (1.2.1) and (1.2.2) in the frequency domain. Hence, (1) $\iff$ (2).

(2)$\Longrightarrow$(3) is by direct calculation. (3)$\Longrightarrow$(2) is an application of the polarization identity to (2.1.5). Hence, (2) $\iff$ (3).

It follows from the convention $a_0 = \boldsymbol{\delta}$ that

$$\sum_{k\in\mathbb{Z}^d} \langle v, a_{0;k}\rangle a_{0;k} = \sum_{k\in\mathbb{Z}^d} v(k)\boldsymbol{\delta}(\cdot - k) = v.$$

Thus, (4)$\Longrightarrow$(2).

We now prove (2)$\Longrightarrow$(4). By the definition of $b_{\ell,j}$ in (2.1.1) and $b_{\ell,1} = b_\ell$,

$$\begin{aligned} b_{\ell,j} &= a_{j-1} * (b_\ell \uparrow 2^{j-1}\mathsf{I}_d) = a_{j-1} * (b_{\ell,1}\uparrow 2^{j-1}\mathsf{I}_d) \\ &= \sum_{n\in\mathbb{Z}^d} a_{j-1}(\cdot - n)(b_{\ell,1}\uparrow 2^{j-1}\mathsf{I}_d)(n) = \sum_{m\in\mathbb{Z}^d} a_{j-1}(\cdot - 2^{j-1}\mathsf{I}_d m) b_{\ell,1}(m), \end{aligned}$$

where I_d is $d\times d$ identity matrix. Therefore, by the definition of $b_{\ell,j;k}$ in (2.1.1),

$$\begin{aligned} b_{\ell,j;k} &= 2^{dj} b_{\ell,j}(\cdot - 2^j\mathsf{I}_d k) = 2^{dj}\sum_{m\in\mathbb{Z}^d} a_{j-1}(\cdot - 2^j\mathsf{I}_d k - 2^{j-1}\mathsf{I}_d m) b_{\ell,1}(m) \\ &= 2^{dj}\sum_{m\in\mathbb{Z}^d} a_{j-1}(\cdot - 2^{j-1}\mathsf{I}_d m) b_{\ell,1}(m - 2\mathsf{I}_d k) = \sum_{m\in\mathbb{Z}^d} a_{j-1;m} b_{\ell,1;k}(m). \end{aligned}$$

Consequently,

$$\langle v, b_{\ell,j;k}\rangle = \sum_{m\in\mathbb{Z}^d} \langle v, a_{j-1;m}\rangle \overline{b_{\ell,1;k}(m)} = \langle\langle v, a_{j-1;\cdot}\rangle, b_{\ell,1;k}(\cdot)\rangle.$$

From the above two identities, we deduce that

$$\sum_{k\in\mathbb{Z}^d} \langle v, b_{\ell,j;k}\rangle b_{\ell,j;k} = \sum_{m\in\mathbb{Z}^d} a_{j-1;m}\left(\sum_{k\in\mathbb{Z}^d} \langle\langle v, a_{j-1;\cdot}\rangle, b_{\ell,1;k}\rangle b_{\ell,1;k}(m)\right).$$

The same argument can be applied to $a_{j;k}$ similarly by replacing $b_{\ell,j;k}$ and $b_{\ell,1;k}$ with $a_{j;k}$ and $a_{1;k}$, respectively. Therefore,

$$\sum_{k\in\mathbb{Z}^d} \langle v, a_{j;k}\rangle a_{j;k} + \sum_{\ell=1}^{s}\sum_{k\in\mathbb{Z}^d} \langle v, b_{\ell,j;k}\rangle b_{\ell,j;k}$$

$$
= \sum_{m\in\mathbb{Z}^d} a_{j-1;m} \left(\sum_{k\in\mathbb{Z}^d} \langle\langle v, a_{j-1;\cdot}\rangle, a_{1;k}\rangle a_{1;k}(m) + \sum_{\ell=1}^{s}\sum_{k\in\mathbb{Z}^d} \langle\langle v, a_{j-1;\cdot}\rangle, b_{\ell,1;k}\rangle b_{\ell,1;k}(m) \right)
$$

$$
= \sum_{m\in\mathbb{Z}^d} \langle v, a_{j-1;m}\rangle a_{j-1;m},
$$

where (2.1.4), i.e., item (2), is applied in the last identity. This proves (2)$\Longrightarrow$(4).

(4)$\Longrightarrow$(5) is from the summation of equation in item (4) with $j = 1, \dots, J$. Conversely, considering the differences between $J = j$ and $J = j - 1$ in (2.1.2), we see that (5)$\Longrightarrow$(4).

The equivalence between item (5) and item (6) is similar to the equivalence between item (2) and item (3). □

Therefore, the performance of a multilevel discrete framelet transform is completely determined by its underlying discrete affine systems. Similarly, $\{a; b_1, \dots, b_{2^d-1}\}$ is an orthogonal wavelet filter bank if and only if $\mathsf{DAS}_J(\{a; b_1, \dots, b_{2^d-1}\})$ is an orthonormal basis for $l_2(\mathbb{Z}^d)$ for every $J \in \mathbb{N}$.

2.2 Tensor product complex tight framelets $\mathrm{TP}\text{-}\mathbb{C}\mathrm{TF}_{2s+1}$ with $s \in \mathbb{N}$

We first provide a road map and some explanations. The one-dimensional complex tight framelet filter bank $\{a; b^{1,p}, \dots, b^{s,p}, b^{1,n}, \dots, b^{s,n}\}$ is constructed such that

(1) $\{a; b^{1,p}, \dots, b^{s,p}, b^{1,n}, \dots, b^{s,n}\}$ is a tight framelet filter bank. By definition, the following conditions are satisfied:

$$
|\widehat{a}(\xi)|^2 + \sum_{\ell=1}^{s} |\widehat{b^{\ell,p}}(\xi)|^2 + \sum_{m=1}^{s} |\widehat{b^{m,n}}(\xi)|^2 = 1,
$$

$$
\widehat{a}(\xi)\overline{\widehat{a}(\xi+\pi)} + \sum_{\ell=1}^{s} \widehat{b^{\ell,p}}(\xi)\overline{\widehat{b^{\ell,p}}(\xi+\pi)} + \sum_{m=1}^{s} \widehat{b^{m,n}}(\xi)\overline{\widehat{b^{m,n}}(\xi+\pi)} = 0,
$$

$$a.e. \xi \in [-\pi, \pi];$$

(2) the low-pass filter a is real and symmetric about the origin, and has $2m$ order linear-phase moments with zero phase: $\widehat{a}(\xi) = 1 + \mathcal{O}(|\xi|^{2m})$ as $\xi \to 0$ for some $m \in \mathbb{N}$;

(3) all $\widehat{b^{1,p}}, \dots, \widehat{b^{s,p}}$ concentrate in $[0, \pi]$ and almost vanish in $[-\pi, 0]$, while all $\widehat{b^{1,n}}, \dots, \widehat{b^{s,n}}$ concentrate in $[-\pi, 0]$ and almost vanish in $[0, \pi]$;

(4) $b^{\ell,n} = \overline{b^{\ell,p}}$, which is equivalent to $\widehat{b^{\ell,n}}(\xi) = \overline{\widehat{b^{\ell,p}}(-\xi)}$ for all $\ell = 1, \dots, s$.

The requirements in item (2) are not necessary for directionality except the condition $\widehat{a}(0) = 1$. However, the linear phase property (i.e., symmetry) and linear-phase moments of the low-pass filter are desired in numerical algorithms and applications. The linear-phase moments in item (2) imply that $\widehat{a}(0) = 1$ and all the high-pass filters $b^{\ell,p}$ and $b^{\ell,n}$ have at least m order vanishing moments (see [16]). The condition $\widehat{a}(0) = 1$ is indispensable for the existence of the refinable function $\widehat{\phi}(\xi) = \prod_{j=1}^{\infty} \widehat{a}(2^{-j}\xi)$. Item (3) is simply the frequency separation. Item (4) allows us to simplify the associated underlying high-dimensional real tight framelets which are obtained by separating the real and imaginary parts of the complex tight framelets. For simplicity, the following additional condition is imposed such that (1.2.2) holds automatically:

(5) $\widehat{a}(\xi)\widehat{a}(\xi + \pi) = 0$ and $\widehat{b^{\ell,p}}(\xi)\widehat{b^{\ell,p}}(\xi + \pi) = 0$ for $\xi \in \mathbb{R},\ \ell = 1, \dots, s$.

We now construct the one-dimensional directional complex tight framelet filter banks. Let $\mathsf{P}_m(x) := (1 - x)^m \sum_{j=0}^{m-1} \binom{m+j-1}{j} x^j$. Then P_m satisfies the identity $\mathsf{P}_m(x) + \mathsf{P}_m(1 - x) = 1$ (see [4]).

For $c_L < c_R$ and two positive numbers $\varepsilon_L, \varepsilon_R$ satisfying $\varepsilon_L + \varepsilon_R \leqslant c_R - c_L$, we define a bump function $\chi_{[c_L, c_R]; \varepsilon_L, \varepsilon_R}$ on $\mathbb{R}$ by

$$\chi_{[c_L,c_R];\varepsilon_L,\varepsilon_R}(\xi) := \begin{cases} 0, & \xi \leqslant c_L - \varepsilon_L \text{ or } \xi \geqslant c_R + \varepsilon_R, \\ \sin\left(\frac{\pi}{2}\mathsf{P}_m(\frac{c_L+\varepsilon_L-\xi}{2\varepsilon_L})\right), & c_L - \varepsilon_L < \xi < c_L + \varepsilon_L, \\ 1, & c_L + \varepsilon_L \leqslant \xi \leqslant c_R - \varepsilon_R, \\ \sin\left(\frac{\pi}{2}\mathsf{P}_m(\frac{\xi-c_R+\varepsilon_R}{2\varepsilon_R})\right), & c_R - \varepsilon_R < \xi < c_R + \varepsilon_R. \end{cases} \tag{2.2.1}$$

Note that $\chi_{[c_L,c_R];\varepsilon_L,\varepsilon_R}$ is a continuous function supported on $[c_L-\varepsilon_L, c_R+\varepsilon_R]$. This bump function (2.2.1) is actually a partition of unity and serves as our prototype for the one-dimensional complex tight framelet filters. Let $0 < c_1 < c_2 < \cdots < c_s < c_{s+1} := \pi$ and $\varepsilon_1, \dots, \varepsilon_s$ be positive numbers satisfying

$$0 < \varepsilon_1 \leqslant \min(c_1, \tfrac{\pi}{2} - c_1) \quad \text{and} \quad (c_{\ell+1} - c_\ell) + \varepsilon_{\ell+1} + \varepsilon_\ell \leqslant \pi, \quad \ell = 1, \dots, s. \tag{2.2.2}$$

Define the symmetric real low-pass filter a and $2s$ numbers of complex high-pass filters $b^{1,p}, \dots, b^{s,p}, b^{1,n}, \dots, b^{s,n}$ by

$$\widehat{a} := \chi_{[-c_1,c_1];\varepsilon_1,\varepsilon_1}, \quad \widehat{b^{\ell,p}} := \chi_{[c_\ell,c_{\ell+1}];\varepsilon_\ell,\varepsilon_{\ell+1}}, \quad \text{and} \quad \widehat{b^{\ell,n}} := \overline{\widehat{b^{\ell,p}}(-\cdot)}, \quad \ell = 1, \dots, s. \tag{2.2.3}$$

The conditions in (2.2.2) guarantee item (5): the short support length makes each term in item (5) zero. It is easy to check that all items (2) – (4) are fulfilled. In particular the low-pass filter a has infinite order linear-phase moments. Due to the bump function in (2.2.1), the condition in item (1) is satisfied. Therefore, $\mathbb{C}\mathrm{TF}_{2s+1} := \{a; b^{1,p}, \dots, b^{s,p}, b^{1,n}, \dots, b^{s,n}\}$ is a (one-dimensional dyadic) tight framelet filter bank satisfying all the requirements in items (1) – (5). For simplicity, c_1 and ε_1 are often set to be free parameters and

$$c_\ell := c_1 + \frac{\pi - c_1}{s}(\ell - 1), \quad \varepsilon_\ell = \varepsilon_1, \quad \ell = 1, \dots, s. \tag{2.2.4}$$

For this particular choice, due to the constraints in (2.2.2), the parameters c_1 and ε_1 must satisfy

$$0 < \varepsilon_1 \leqslant \min\left(c_1, \frac{\pi}{2} - c_1, \frac{c_1 + (s-1)\pi}{2s}\right). \tag{2.2.5}$$

Tensor product complex tight framelet filter bank $\text{TP-}\mathbb{C}\text{TF}_{2s+1}$ in d dimensions is defined to be

$$\text{TP-}\mathbb{C}\text{TF}_{2s+1} := \otimes^d\, \mathbb{C}\text{TF}_{2s+1} = \otimes^d \{a; b^{1,p}, \ldots, b^{s,p}, b^{1,n}, \ldots, b^{s,n}\},$$

where $\otimes^d$ means taking d times of tensor product and d is often omitted when $d = 2$. This tight framelet filter bank $\text{TP-}\mathbb{C}\text{TF}_{2s+1}$ has one real low-pass filter $a \otimes a$ and $(2s+1)^d - 1$ complex high-pass filters. And the associated J-level discrete affine system is given by

$$\mathsf{DAS}_J(\text{TP-}\mathbb{C}\text{TF}_{2s+1}) = \mathsf{DAS}_J(\otimes^d \{a; b^{1,p}, \ldots, b^{s,p}, b^{1,n}, \ldots, b^{s,n}\}).$$

It is important to understand how and why tensor product complex framelets $\text{TP-}\mathbb{C}\text{TF}_m$ and the DT-$\mathbb{C}$WT can achieve directionality in high dimensions. To do so, consider the complex-valued wavelet function $\psi : \mathbb{R}^2 \to \mathbb{C}$ in two dimensions. The same argument can be applied to the high-pass filter $u : \mathbb{Z}^2 \to \mathbb{C}$ similarly. Separating the real and imaginary parts, $\psi = \psi^{[r]} + i\psi^{[i]}$, where $\psi^{[r]}$ and $\psi^{[i]}$ are real-valued functions in two dimensions. For $\psi^{[r]}$ and $\psi^{[i]}$ to have directionality, $\widehat{\psi}$ often concentrates around a point $\zeta \in \mathbb{R}^2 \backslash \{0\}$ (i.e., a nonzero vector) in the frequency domain. More precisely, $\widehat{\psi}(\xi) = g(\xi - \zeta)$, where g is a function concentrating around the origin. Let f be the inverse Fourier transform of g, that is, $\widehat{f} = g$. For the $\text{TP-}\mathbb{C}\text{TF}_m$ and the DT-$\mathbb{C}$WT, f is often an isotropic real-valued function concentrating around the origin in the time domain. From the relation $\widehat{\psi}(\xi) =$

$g(\xi - \zeta) = \widehat{f}(\xi - \zeta)$, we deduce that

$$\psi(x) = f(x)e^{i\zeta\cdot x}, \quad \psi^{[r]}(x) = f(x)\cos(\zeta\cdot x), \quad \psi^{[i]}(x) = f(x)\sin(\zeta\cdot x), \quad x \in \mathbb{R}^2.$$

Even though the complex-valued function ψ does not exhibit any orientation with isotropic magnitude $|\psi(x)| = |f(x)|$, its real part $\psi^{[r]}$ and imaginary part $\psi^{[i]}$ indeed have directionality. The function f provides good spatial localizations as well as the magnitudes for $\psi^{[r]}$ and $\psi^{[i]}$. The factors $\cos(\zeta \cdot x)$ and $\sin(\zeta \cdot x)$ grant the directional selectivity to $\psi^{[r]}$ and $\psi^{[i]}$ according to ζ. Note that $\psi^{[r]}$ and $\psi^{[i]}$ have the same direction, which is perpendicular to the vector ζ.

To see this point, let us look at the simplest case: the two-dimensional tensor product tight framelet filter bank using $\mathbb{C}\mathrm{TF}_3$. By the definition in (2.2.3) with $s = 1$ and the requirement in (2.2.5), the tight framelet filter bank $\mathbb{C}\mathrm{TF}_3 = \{a; b^p, b^n\}$ is given by defining 2π-periodic functions $\widehat{a}, \widehat{b^p},$ and $\widehat{b^n}$:

$$\widehat{a} := \chi_{[-c,c];\varepsilon,\varepsilon}, \quad \widehat{b^p} := \chi_{[c,\pi];\varepsilon,\varepsilon}, \quad \text{and} \quad \widehat{b^n} := \chi_{[-\pi,-c];\varepsilon,\varepsilon}, \tag{2.2.6}$$

where the bump function χ is defined in (2.2.1). Then $\{a; b^p, b^n\}$ is a one-dimensional tight framelet filter bank such that a is real and symmetric about the origin with $\widehat{a}(0) = 1$. Define functions $\phi, \psi^p,$ and ψ^n by

$$\widehat{\phi}(\xi) := \prod_{j=1}^{\infty} \widehat{a}(2^{-j}\xi), \; \widehat{\psi^p}(\xi) := \widehat{b^p}(\xi/2)\widehat{\phi}(\xi/2), \text{ and } \widehat{\psi^n}(\xi) := \widehat{b^n}(\xi/2)\widehat{\phi}(\xi/2),$$

$$\xi \in \mathbb{R}.$$

Then $\{\phi; \psi^p, \psi^n\}$ is a tight frame for $L_2(\mathbb{R})$ such that ϕ is real-valued and symmetric about the origin. Since $\widehat{b^n}(\xi) = \overline{\widehat{b^p}(-\xi)}$, we have $b^n = \overline{b^p}$ and $\psi^n = \overline{\psi^p}$. Moreover, both functions ψ^p and ψ^n are complex-valued and enjoy the frequency separation:

$$\widehat{\psi^p}(\xi) \approx 0, \quad \xi \in (-\infty, 0] \quad \text{and} \quad \widehat{\psi^n}(\xi) \approx 0, \quad \xi \in [0, \infty). \tag{2.2.7}$$

The tensor product of complex tight frame $\{\phi; \psi^p, \psi^n\}$ in two dimensions are

$$\{\phi\otimes\phi\}\bigcup\{\phi\otimes\psi^p, \phi\otimes\psi^n, \psi^p\otimes\phi, \psi^n\otimes\phi, \psi^p\otimes\psi^p, \psi^p\otimes\psi^n, \psi^n\otimes\psi^p, \psi^n\otimes\psi^n\}. \tag{2.2.8}$$

By (2.2.7), for $g, h \in \{\psi^p, \psi^n\}$, $\widehat{g\otimes h} = \widehat{h}\otimes\widehat{h}$ concentrates in an area away from the origin of the frequency plane. As a consequence, both the real and imaginary parts of $g\otimes h$ exhibit good directions. For a complex-valued function $f : \mathbb{R}\to\mathbb{C}$, define

$$f^{[r]}(x) := \mathrm{Re}(f(x)), \quad f^{[i]}(x) := \mathrm{Im}(f(x)), \quad x\in\mathbb{R}.$$

Denote $f = f^{[r]} + if^{[i]}$ with both $f^{[r]}$ and $f^{[i]}$ real-valued functions on $\mathbb{R}$. Similarly, for a complex filter $u : \mathbb{Z}\to\mathbb{C}$, we can write $u = u^{[r]} + iu^{[i]}$ with both sequences $u^{[r]}$ and $u^{[i]}$ having real coefficients. Define real-valued functions $\psi^{p,[r]} := \mathrm{Re}(\psi^p)$, $\psi^{p,[i]} := \mathrm{Im}(\psi^p)$, $\psi^{n,[r]} := \mathrm{Re}(\psi^n)$, and $\psi^{n,[i]} := \mathrm{Im}(\psi^n)$. Correspondingly, define real filters $b^{p,[r]} := \mathrm{Re}(b^p)$, $b^{p,[i]} := \mathrm{Im}(b^p)$, $b^{n,[r]} := \mathrm{Re}(b^n)$, and $b^{n,[i]} := \mathrm{Im}(b^n)$. $\{\phi; \psi^{p,[r]}, \psi^{n,[r]}, \psi^{p,[i]}, \psi^{n,[i]}\}$ is a real tight frame in $L_2(\mathbb{R})$ with the underlying real tight framelet filter bank $\{a; b^{p,[r]}, b^{n,[r]}, b^{p,[i]}, b^{n,[i]}\}$. However, this real filter bank is not applied to generate the high-dimensional one by tensor product since it suffers the same shortcoming as general real wavelets or framelets. Instead, we first take the tensor product of the one-dimensional complex tight frame in two dimensions as in (2.2.8), then separate the real and imaginary parts to derive the directional real tight frame in $L_2(\mathbb{R}^2)$. More specifically, we have

$$\sqrt{2}\Big\{\tfrac{\sqrt{2}}{2}\phi\otimes\phi; \phi\otimes\psi^{p,[r]}, \phi\otimes\psi^{p,[i]}, \psi^{p,[r]}\otimes\phi, \psi^{p,[i]}\otimes\phi, \psi^{p,[r]}\otimes\psi^{p,[r]}-\psi^{p,[i]}\otimes\psi^{p,[i]},$$
$$\psi^{p,[r]}\otimes\psi^{p,[r]}+\psi^{p,[i]}\otimes\psi^{p,[i]}, \psi^{p,[r]}\otimes\psi^{p,[i]}-\psi^{p,[i]}\otimes\psi^{p,[r]}, \psi^{p,[r]}\otimes\psi^{p,[i]}+\psi^{p,[i]}\otimes\psi^{p,[r]}\Big\} \tag{2.2.9}$$

with the following underlying two-dimensional real tight framelet filter bank

$$\sqrt{2}\{\tfrac{\sqrt{2}}{2}a \otimes a; a \otimes b^{p,[r]}, a \otimes b^{p,[i]}, b^{p,[r]} \otimes a, b^{p,[i]} \otimes a, b^{p,[r]} \otimes b^{p,[r]} - b^{p,[i]} \otimes b^{p,[i]},$$
$$b^{p,[r]} \otimes b^{p,[r]} + b^{p,[i]} \otimes b^{p,[i]}, b^{p,[r]} \otimes b^{p,[i]} - b^{p,[i]} \otimes b^{p,[r]}, b^{p,[r]} \otimes b^{p,[i]} - b^{p,[i]} \otimes b^{p,[r]}\}.$$

Now one can check that the derived two-dimensional real tight frame exhibits four directions:

(1) $\phi \otimes \psi^{p,[r]}$ and $\phi \otimes \psi^{p,[i]}$ select the horizontal edges along $0°$;

(2) $\psi^{p,[r]} \otimes \phi$ and $\psi^{p,[i]} \otimes \phi$ select the vertical edges along $90°$;

(3) $\psi^{p,[r]} \otimes \psi^{p,[r]} \pm \psi^{p,[i]} \otimes \psi^{p,[i]}$ select the edges along $45°$;

(4) $\psi^{p,[r]} \otimes \psi^{p,[i]} \pm \psi^{p,[i]} \otimes \psi^{p,[r]}$ select the edges along $-45°$.

The directionality of tensor product complex tight framelet filter bank using $\mathbb{C}\mathrm{TF}_m$ with $m > 3$ can be analyzed similarly.

TP-$\mathbb{C}\mathrm{TF}_{2s+1}$ in d dimensions with $d \geqslant 3$ can be defined by taking d times the tensor product of $\mathbb{C}\mathrm{TF}_{2s+1}$. For simplicity, TP-$\mathbb{C}\mathrm{TF}_{2s+1}$ is also applied to stand for $\mathbb{C}\mathrm{TF}_{2s+1}$ in one dimension. Since TP-$\mathbb{C}\mathrm{TF}_{2s+1}$ is a tensor product filter bank in high dimensions, the discrete framelet transform using TP-$\mathbb{C}\mathrm{TF}_{2s+1}$ is essentially the same as the classical real discrete wavelet transform except for having more high-pass filters.

In two dimensions, there are $2s(s+1)$ directions for $4s(s+1)$ high-pass filters in TP-$\mathbb{C}\mathrm{TF}_{2s+1}$ with directions along $0°, \pm 45°,$ and $90°$ repeated $s-1$ times. Therefore, the two-dimensional TP-$\mathbb{C}\mathrm{TF}_{2s+1}$ offers $2s(s+1)-4(s-1) = 2s(s-1)+4 = \frac{1}{2}(n-1)(n-3)+4$ different directions with $n := 2s+1$. For example, TP-$\mathbb{C}\mathrm{TF}_3$ has four directions along $0°, \pm 45°$, and $90°$; TP-$\mathbb{C}\mathrm{TF}_5$ has eight directions along $0°, \pm 22.5°, \pm 45°, \pm 67.5°$, and $90°$. The particular example constructed in [19] corresponds to TP-$\mathbb{C}\mathrm{TF}_3$ here.

2.3 Tensor product complex tight framelets $\mathrm{TP}\text{-}\mathbb{C}\mathrm{TF}_{2s+2}$ with $s \in \mathbb{N}$

The directional selectivity of $\mathrm{TP}\text{-}\mathbb{C}\mathrm{TF}_{2s+1}$ can be further improved by splitting the low-pass filter a into two auxiliary low-pass filters a^p and a^n. Let $0 < c_1 < c_2 < \cdots < c_s < c_{s+1} := \pi$ and $\varepsilon_0, \varepsilon_1, \ldots, \varepsilon_s$ be positive numbers satisfying (2.2.2) with the additional condition

$$0 < \varepsilon_0 < c_1 - \varepsilon_1. \tag{2.3.1}$$

Define the two auxiliary filters a^p and a^n by

$$\widehat{a^p} := \chi_{[0,c_1];\varepsilon_0,\varepsilon_1} \quad \text{and} \quad \widehat{a^n} := \overline{\widehat{a^p}(-\cdot)}. \tag{2.3.2}$$

The high-pass filters $b^{1,p}, \ldots, b^{s,p}, b^{1,n}, \ldots, b^{s,n}$ are defined the same as in (2.2.3). Since

$$\begin{aligned} |\widehat{a}(\xi)|^2 &= |\widehat{a^p}(\xi)|^2 + |\widehat{a^n}(\xi)|^2, \\ \widehat{a}(\xi)\overline{\widehat{a}(\xi+\pi)} &= \widehat{a^p}(\xi)\overline{\widehat{a^p}(\xi+\pi)} + \widehat{a^n}(\xi)\overline{\widehat{a^n}(\xi+\pi)}, \end{aligned} \tag{2.3.3}$$

$\mathbb{C}\mathrm{TF}_{2s+2} := \{a^p, a^n; b^{1,p}, \ldots, b^{s,p}, b^{1,n}, \ldots, b^{s,n}\}$ is a (one-dimensional dyadic) tight framelet filter bank. Despite the low-pass filter a is real and symmetric about the origin, the two auxiliary filters a^p and a^n are complex and may not have any symmetry. They are one-sided in the frequency domain satisfying the relation $a^n = \overline{a^p}$ and (2.3.3). c_1, ε_0, and ε_1 are often set to be free parameters and the special choice in (2.2.4) is taken as well. For this particular case, both (2.2.5) and (2.3.1) must be satisfied. Techniques in (2.3.3) are often applied to split one filter into two one-sided auxiliary filters to improve the directional selectivity of high-dimensional filters.

The one-dimensional complex tight framelet filter bank is simply $\mathbb{C}\mathrm{TF}_{2s+2} :=$

$\{a^p, a^n; b^{1,p}, \dots, b^{s,p}, b^{1,n}, \dots, b^{s,n}\}$. Now the tensor product complex tight framelet filter bank $\text{TP-}\mathbb{C}\text{TF}_{2s+2}$ in d dimensions is defined to be

$$\text{TP-}\mathbb{C}\text{TF}_{2s+2} := \{\otimes^d a; \text{TP-}\mathbb{C}\text{TF -HP}_{2s+2}\},$$

where $\text{TP-}\mathbb{C}\text{TF -HP}_{2s+2}$ consists of total $(2s+2)^d - 2^d$ complex high-pass filters given by

$$\Big(\otimes^d \{a^p, a^n; b^{1,p}, \dots, b^{s,p}, b^{1,n}, \dots, b^{s,n}\}\Big) \backslash \Big(\otimes^d \{a^p, a^n\}\Big).$$

It is not difficult to see that the associated J-level discrete affine system is given by

$$\mathsf{DAS}_J(\text{TP-}\mathbb{C}\text{TF}_{2s+2}) = \mathsf{DAS}_J(\{\otimes^d a; \text{TP-}\mathbb{C}\text{TF -HP}_{2s+2}\}).$$

$\text{TP-}\mathbb{C}\text{TF}_{2s+2}$ is also used to stand for $\mathbb{C}\text{TF}_{2s+2}$ in one dimension for simplicity. The discrete framelet transform using $\text{TP-}\mathbb{C}\text{TF}_{2s+2}$ is essentially the same as the discrete framelet transform using filter bank $\otimes^d\{a^p, a^n; b^{1,p}, \dots, b^{s,p}, b^{1,n}, \dots, b^{s,n}\}$ with a slight modification as follows:

(1) the filter bank $\otimes^d\{a^p, a^n; b^{1,p}, \dots, b^{s,p}, b^{1,n}, \dots, b^{s,n}\}$ is first applied to the d-dimensional input data v;

(2) the outputs from $\otimes^d\{a^p, a^n\}$ are discarded;

(3) the low-pass filter $\otimes^d a$ is applied to the input data v, from which the output is used to replace the discarded outputs from step (2);

(4) steps (1) – (3) are repeated recursively by treating the output from step (3) as the new input data.

In two dimensions, due to $a^n = \overline{a^p}$ and $b^{\ell,n} = \overline{b^{\ell,p}}$, $\ell = 1, \dots, s$, there are $2s(s+2)$ directions for the $4s(s+2)$ high-pass filters in $\text{TP-}\mathbb{C}\text{TF -HP}_{2s+2}$ with the directions along $\pm 45^\circ$ degrees repeated $s-1$ times. Therefore, the two-dimensional tensor product complex tight framelet $\text{TP-}\mathbb{C}\text{TF}_{2s+2}$ offers $2s(s+2) - 2(s-1) = 2(s-1)(s+2)+6 = \frac{1}{2}(n-4)(n+2)+6$ different directions with $n := 2s+2$. For example, $\text{TP-}\mathbb{C}\text{TF}_4$ has six directions along $\pm 15^\circ$, $\pm 45^\circ$, and $\pm 75^\circ$, and $\text{TP-}\mathbb{C}\text{TF}_6$ has 14 directions.

2.4 Examples

This section presents several examples of tensor product complex tight framelets. These $\text{TP-}\mathbb{C}\text{TF}_m$ are characterized by their corresponding filter banks in the frequency domain. Despite the fact that there are many other choices, the parameters given here are tuned according to the best performance in image denoising for testing image *Barbara* at standard deviation $\sigma = 30$.

Example 1. This example is from [19]. For $\text{TP-}\mathbb{C}\text{TF}_3$, we apply (2.2.4) and set

$$c_1 = \tfrac{33}{32}, \; c_2 = \pi, \; \varepsilon_1 = \tfrac{69}{128}, \text{ and } \varepsilon_2 = \tfrac{51}{512}.$$

See Figure 2.1 for graphs of the one-dimensional complex tight framelet filter banks $\mathbb{C}\text{TF}_3$. See Figure 2.2 for the directionality of the two-dimensional tensor product complex tight framelet $\text{TP-}\mathbb{C}\text{TF}_3$ (more precisely, the generators in $\mathsf{DAS}_J(\text{TP-}\mathbb{C}\text{TF}_3)$). Please refer [19] for more details on this example.

Example 2. For $\text{TP-}\mathbb{C}\text{TF}_4$, we apply both (2.2.4) and (2.3.1), and set

$$c_0 = 0, \; c_1 = \tfrac{291}{256}, \; c_2 = \pi, \; \varepsilon_0 = \tfrac{35}{128}, \; \varepsilon_1 = \tfrac{27}{64}, \text{ and } \varepsilon_2 = \tfrac{1}{2}.$$

See Figure 2.1 for graphs of the one-dimensional complex tight framelet filter banks $\mathbb{C}\text{TF}_4$. See Figure 2.3 for the directionality of the two-dimensional ten-

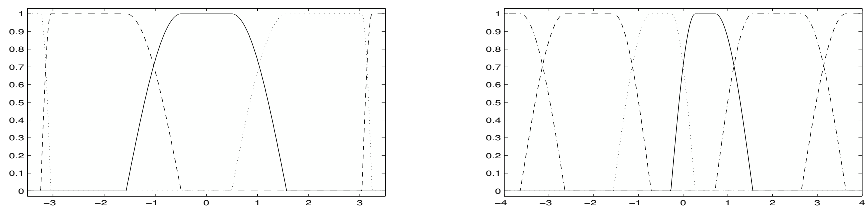

(a) $\mathbb{C}\mathrm{TF}_3$ (b) $\mathbb{C}\mathrm{TF}_4$

Figure 2.1: (a) $\mathbb{C}\mathrm{TF}_3 = \{a; b^p, b^n\}$ in the frequency domain. Solid line is for $\widehat{a}$, dotted line is for $\widehat{b^p}$, and dashed line is for $\widehat{b^n}$.
(b) $\mathbb{C}\mathrm{TF}_4 = \{a^p, a^n; b^p, b^n\}$ in the frequency domain. Solid line is for $\widehat{a^p}$, dotted line is for $\widehat{a^n}$, dotted-dashed line is for $\widehat{b^p}$, and dashed line is for $\widehat{b^n}$.

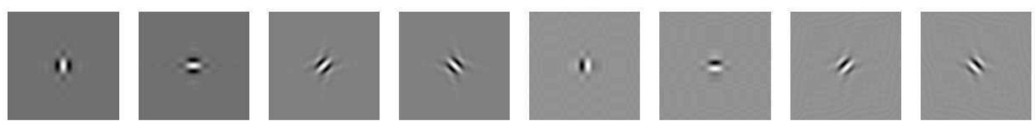

Figure 2.2: The real part (the first four) and the imaginary part (the last four) of the generators at level 5 in $\mathsf{DAS}_6(\mathrm{TP}\text{-}\mathbb{C}\mathrm{TF}_3)$.

sor product complex tight framelet $\mathrm{TP}\text{-}\mathbb{C}\mathrm{TF}_4$ (more precisely, the generators in $\mathsf{DAS}_J(\mathrm{TP}\text{-}\mathbb{C}\mathrm{TF}_4)$).

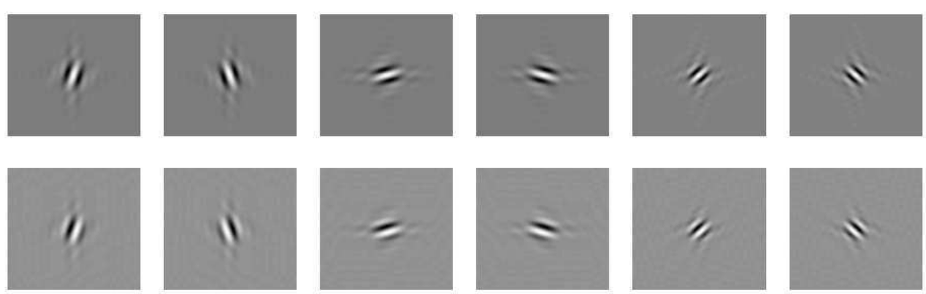

Figure 2.3: The first row shows the real part and the second row shows the imaginary part of the generators at level 5 in $\mathsf{DAS}_6(\mathrm{TP}\text{-}\mathbb{C}\mathrm{TF}_4)$.

Example 3. For $\mathrm{TP}\text{-}\mathbb{C}\mathrm{TF}_6$, we apply both (2.2.4) and (2.3.1), and set

$$c_0 = 0,\ c_1 = \tfrac{119}{128},\ c_2 = \tfrac{\pi}{2}+\tfrac{119}{256},\ c_3 = \pi,\ \varepsilon_0 = \tfrac{35}{128},\ \varepsilon_1 = \tfrac{81}{128},\ \varepsilon_2 = \tfrac{115}{256},\ \text{and } \varepsilon_3 = \tfrac{115}{256}.$$

See Figure 2.4 for graphs of the one-dimensional complex tight framelet filter banks $\mathbb{C}\mathrm{TF}_6$. See Figure 2.5 for the directionality of the two-dimensional tensor product complex tight framelet $\mathrm{TP}\text{-}\mathbb{C}\mathrm{TF}_6$ (more precisely, the generators in $\mathsf{DAS}_J(\mathrm{TP}\text{-}\mathbb{C}\mathrm{TF}_6)$).

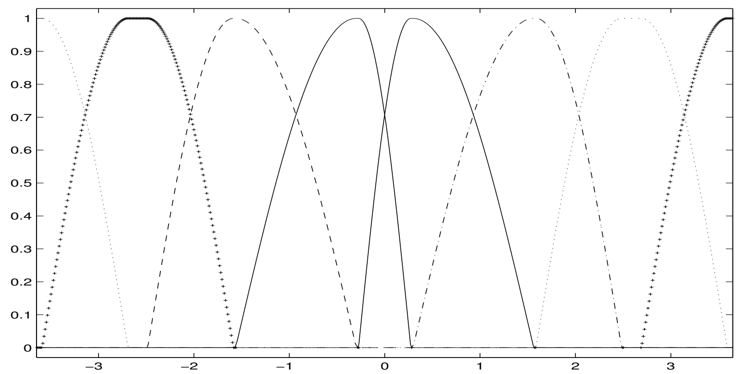

Figure 2.4: $\mathbb{C}\mathrm{TF}_6 = \{a^p, a^n; b^{1,p}, b^{2,p}, b^{1,n}, b^{2,n}\}$ in the frequency domain. Right solid line is for $\widehat{a^p}$ and left solid line is for $\widehat{a^n}$. Dotted-dashed line is for $\widehat{b^{1,p}}$ and dotted line is for $\widehat{b^{2,p}}$. Dashed line is for $\widehat{b^{1,n}}$ and the line with $+$ sign is for $\widehat{b^{2,n}}$.

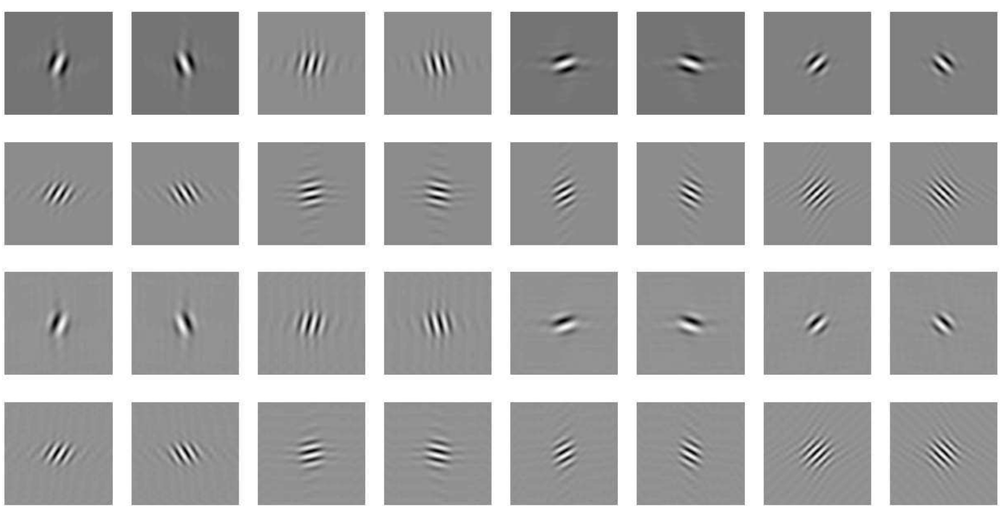

Figure 2.5: The first two rows show the real part and the last two rows show the imaginary part of the generators at level 5 in $\mathsf{DAS}_6(\mathrm{TP}\text{-}\mathbb{C}\mathrm{TF}_6)$. Among these 16 graphs, the directions along $\pm 45°$ are repeated once. Hence, there are total 14 directions in the discrete affine system $\mathsf{DAS}_J(\mathrm{TP}\text{-}\mathbb{C}\mathrm{TF}_6)$.

We now explain the directionality and oscillations for the graphs in Figure 2.5. The total six nonzero different vectors ζ's of the complex wavelets associated with the 12 high-pass filters in $\otimes\{a^p, a^n; b^{1,p}, b^{1,n}\}\backslash \otimes \{a^p, a^n\}$ have small norms (near the origin). Therefore, the graphs of the real and imaginary parts of these complex wavelet functions/filters exhibit six edge-like (i.e., fewer oscillation) directions in Figure 2.5. In addition, the corresponding vectors ζ's of the complex wavelet functions associated with all other 20 high-pass filters in $\mathrm{TP}\text{-}\mathbb{C}\mathrm{TF}$-HP$_6$ have larger norms (away from the origin) with total 10 different directions (with $\pm 45°$ repeated once). Therefore, the graphs of the real and imaginary parts of these complex wavelet functions/filters exhibit 10 texture-like (i.e., more oscillations) directions in Figure 2.5. The good performance of $\mathrm{TP}\text{-}\mathbb{C}\mathrm{TF}_6$ in applications is probably because $\mathrm{TP}\text{-}\mathbb{C}\mathrm{TF}_6$ has both edge-like (for selecting edges) and texture-like directional elements (for capturing textures).

Chapter 3

Directional Tensor Product Complex Tight Framelets with Low Redundancy

Though empirically higher redundancy of a tight frame often leads to better performance, the computational costs increase exponentially with respect to the redundancy rate and dimensions. These computational expenses and storage requirement restrict the usefulness of such tight frames and over-complete representations in multidimensional applications (in particular, for moderately high dimensions such as video processing).

Motivated by the directional tensor product complex tight framelets, this chapter covers the construction of tensor product complex tight framelets with low redundancy. We introduce the definition of redundancy rate and generalize the notion of dyadic tight framelet filter banks to tight framelet filter banks with mixed sampling factors. Finally, example of directional tensor product complex tight framelet with low redundancy are provided. The results in this chapter have been submitted to *Applied and Computational Harmonic Analysis* [25].

3.1 Redundancy rate

Let us explain by what we mean the redundancy rate of a transform or a system. Most data in d-dimensional applications has finite length. For given data v with finite length, we first extend it into a periodic sequence v^e on $\mathbb{Z}^d$, then perform the wavelet/framelet transform on the extended data v^e. This induces a linear transform on the original data v, which can be expressed in terms of a matrix $\mathcal{W}$. More precisely, we can arrange the d-dimensional data v properly so that it can be regarded as an $n \times 1$ column vector in $\mathbb{R}^n$, that is, $v \in \mathbb{R}^n$. By performing the linear transform $\mathcal{W}$ on v, we obtain another column vector $w := \mathcal{W}v \in \mathbb{R}^N$ of frame coefficients. If $\{a; b_1, \dots, b_s\}$ is a real orthonormal wavelet filter bank with $s = 2^d - 1$, then $N = n$ and $\mathcal{W}$ is a real $n \times n$ orthogonal matrix satisfying $\mathcal{W}^\mathsf{T}\mathcal{W} = \mathsf{I}_n$. If $\{a; b_1, \dots, b_s\}$ is a real tight framelet filter bank, then we must have $N > n$ and $\mathcal{W}$ is a real $N \times n$ matrix satisfying $\mathcal{W}^\mathsf{T}\mathcal{W} = \mathsf{I}_n$. The ratio N/n is called the redundancy rate of the linear transform $\mathcal{W}$ or its underlying tight frame, since it is the ratio of the frame coefficients number N to the original input data number n. Note that the redundancy rate N/n is independent of input data length n and it only depends on the number s of high-pass filters and the sampling factor (which is I_d here).

For the d-dimensional tensor product tight framelet filter bank TP-$\mathbb{C}$TF$_m$, if m is odd, there are one real low-pass filter and $(m-1)^d - 1$ complex high-pass filters. Consequently, its redundancy rate is no more than $\frac{m^d-1}{2^d-1}$ for any decomposition level $J \in \mathbb{N}$. If m is even, there are one real low-pass filter and $m^d - 2^d$ complex high-pass filters in the TP-$\mathbb{C}$TF$_m$. Therefore, its redundancy rate is no more than $\frac{m^d-2^d}{2^d-1}$ for any decomposition level $J \in \mathbb{N}$. For both the DT-$\mathbb{C}$WT and the TP-$\mathbb{C}$TF$_m$, one complex coefficient is counted as two in the calculation of redundancy rates. The TP-$\mathbb{C}$TF$_4$ has almost the same performance, directionality and redundancy rate as those of the DT-$\mathbb{C}$WT. The TP-$\mathbb{C}$TF$_6$ has superior performance than both TP-$\mathbb{C}$TF$_4$ and DT-$\mathbb{C}$WT in image denoising [24] and image inpainting [47], but it has higher redundancy rate $\frac{6^d-2^d}{2^d-1}$ in d dimensions. See Table 3.1 for a numerical illustration of redundancy rates.

d	1	2	3	4	5	6	7	8
UWT	4	10	22	46	94	190	383	766
UFT_2	7	25	79	241	727	2185	6559	19681
UFT_4	13	73	373	1873	9373	46873	234373	1171873
DT-$\mathbb{C}$WT	2	4	8	16	32	64	128	256
TP-$\mathbb{C}\mathrm{TF}_3$	2	$2\frac{2}{3}$	$3\frac{5}{7}$	$5\frac{1}{3}$	$7\frac{25}{31}$	$11\frac{5}{9}$	$17\frac{27}{127}$	$25\frac{37}{51}$
TP-$\mathbb{C}\mathrm{TF}_4$	2	4	8	16	32	64	128	256
TP-$\mathbb{C}\mathrm{TF}_5$	4	8	$17\frac{5}{7}$	$41\frac{3}{5}$	$100\frac{24}{31}$	248	$615\frac{19}{127}$	$1531\frac{73}{85}$
TP-$\mathbb{C}\mathrm{TF}_6$	4	$10\frac{2}{3}$	$29\frac{5}{7}$	$85\frac{1}{3}$	$249\frac{25}{31}$	$739\frac{5}{9}$	$2203\frac{27}{127}$	$6585\frac{37}{51}$
TP-$\mathbb{C}\mathrm{TF}_6^{\downarrow}$	2	$2\frac{2}{3}$	$3\frac{5}{7}$	$5\frac{1}{3}$	$7\frac{25}{31}$	$11\frac{5}{9}$	$17\frac{27}{127}$	$25\frac{37}{51}$

Table 3.1: Redundancy rates of various tight frames for different d dimensions.
UWT is the undecimated wavelet transform with decomposition level $J = 3$ with the tensor product of 1D orthonormal real wavelet filter bank $\{a; b\}$.
UFT_s is the undecimated framelet transform with decomposition level $J = 3$ with the tensor product of a 1D real tight framelet filter bank $\{a; b_1, \ldots, b_s\}$.
DT-$\mathbb{C}$WT is the dual tree complex wavelet transform.
TP-$\mathbb{C}\mathrm{TF}_m$ is the tensor product complex tight framelet with $m = 3, 4, 5, 6$. TP-$\mathbb{C}\mathrm{TF}_6^{\downarrow}$ is our proposed tensor product complex tight framelet with low redundancy.

The construction of TP-$\mathbb{C}\mathrm{TF}_m$ with $m \geqslant 3$ is modified in order to reduce the redundancy rate. For simplicity of presentation, we restrict our attention to one particular example: TP-$\mathbb{C}\mathrm{TF}_6$ with underlying one-dimensional complex tight framelet filter bank $\mathbb{C}\mathrm{TF}_6$. We hope the redundancy rate of TP-$\mathbb{C}\mathrm{TF}_6$ can be significantly reduced, while keep almost all the desirable properties of TP-$\mathbb{C}\mathrm{TF}_6$. Hence, the modified directional tensor product complex tight framelet is denoted by TP-$\mathbb{C}\mathrm{TF}_6^{\downarrow}$, where the superscript $\downarrow$ here means that TP-$\mathbb{C}\mathrm{TF}_6^{\downarrow}$ is a reduced version of TP-$\mathbb{C}\mathrm{TF}_6$.

There are also many nonseparable approaches beyond the tensor product (i.e., separable) to achieve directionality in high dimensions. The notation dD stands for d dimensions or d-dimensional. Some examples of such nonseparable transforms are 2D curvelets in [2], 2D contourlets in [5], the steerable pyramid in [48], 2D and

3D shearlets in [26, 29, 30, 33, 34], 3D surfacelets in [36], and directional tight framelets in [12, 18, 26], as well as quite a few more in the literature. The redundancy rates of such nonseparable transforms depend on the numbers of directions applied in each resolution level and the decomposition level $J \in \mathbb{N}$. Generally speaking, those nonseparable transforms often have much higher redundancy rates than those tensor product based transforms for reasonable performance in applications.

3.2 Tight framelet filter banks with mixed sampling factors

This section introduces tight framelet filter banks with mixed sampling factors and studies their properties. Our proposed $\mathrm{TP}\text{-}\mathbb{C}\mathrm{TF}_6^{\downarrow}$ is a particular case of such framelet filter banks.

3.2.1 Fast framelet transform using tight framelet filter banks with mixed sampling factors

To reduce the redundancy rate, higher sampling factors are applied to the high-pass filters in the $\mathrm{TP}\text{-}\mathbb{C}\mathrm{TF}_m$. To this end, let us generalize the definition of the (d-dimensional dyadic) tight framelet filter bank $\{a; b_1, \ldots, b_s\}$, which uses the uniform sampling matrix $2\mathsf{I}_d$, where I_d is the $d \times d$ identity matrix.

Let M be a $d \times d$ invertible integer matrix. For a sequence $u = \{u(k)\}_{k \in \mathbb{Z}^d} : \mathbb{Z}^d \to \mathbb{C}$, the downsampling sequence $u \downarrow \mathsf{M}$ and the upsampling sequence $u \uparrow \mathsf{M}$

with the sampling matrix M are defined by

$$[u\!\downarrow\!\mathsf{M}](k) := u(\mathsf{M}k),\ k \in \mathbb{Z}^d \quad \text{and} \quad [u\!\uparrow\!\mathsf{M}](k) := \begin{cases} u(\mathsf{M}^{-1}k), & \text{if } k \in \mathsf{M}\mathbb{Z}^d, \\ 0, & \text{if } k \in \mathbb{Z}^d\backslash[\mathsf{M}\mathbb{Z}^d]. \end{cases}$$

$|\det(\mathsf{M})|$ is called the sampling factor. We adopt the notation $u\,!\,\mathsf{M}$ to explicitly specify the sampling matrix M associated with the filter u. A (d-dimensional dyadic) tight framelet filter bank $\{a; b_1, \dots, b_s\}$ with uniform sampling matrix $2\mathsf{I}_d$ will be denoted more precisely as $\{a\,!\,2\mathsf{I}_d; b_1\,!\,2\mathsf{I}_d, \dots, b_s\,!\,2\mathsf{I}_d\}$ under this new notation.

For a filter $u \in l_1(\mathbb{Z}^d)$ and a $d \times d$ integer matrix M, the *subdivision operator* $\mathcal{S}_{u,\mathsf{M}} : l_\infty(\mathbb{Z}^d) \to l_\infty(\mathbb{Z}^d)$ and the *transition operator* $\mathcal{T}_{u,\mathsf{M}} : l_\infty(\mathbb{Z}^d) \to l_\infty(\mathbb{Z}^d)$ are defined to be

$$[\mathcal{S}_{u,\mathsf{M}}v](n) := |\det(\mathsf{M})| \sum_{k\in\mathbb{Z}^d} v(k)u(n-\mathsf{M}k), \qquad n \in \mathbb{Z}^d,$$
$$[\mathcal{T}_{u,\mathsf{M}}v](n) := |\det(\mathsf{M})| \sum_{k\in\mathbb{Z}^d} v(k)\overline{u(k-\mathsf{M}n)}, \qquad n \in \mathbb{Z}^d.$$

Define $\Omega_\mathsf{M} := (\mathsf{M}^{-\mathsf{T}}\mathbb{Z}^d) \cap [0,1)^d$. In terms of Fourier series, we have

$$\begin{aligned} \widehat{\mathcal{S}_{u,\mathsf{M}}v}(\xi) &= |\det(\mathsf{M})|\widehat{v}(\mathsf{M}^\mathsf{T}\xi)\widehat{u}(\xi), \\ \widehat{\mathcal{T}_{u,\mathsf{M}}v}(\xi) &= \sum_{\omega\in\Omega_\mathsf{M}} \widehat{v}(\mathsf{M}^{-\mathsf{T}}\xi+2\pi\omega)\overline{\widehat{u}(\mathsf{M}^{-\mathsf{T}}\xi+2\pi\omega)}. \end{aligned} \tag{3.2.1}$$

Define the conjugate sequence $u^\star$ of u by $u^\star(k) := \overline{u(-k)},\ k \in \mathbb{Z}^d$. Note that $\widehat{u^\star}(\xi) = \overline{\widehat{u}(\xi)}$. Then

$$\mathcal{S}_{u,\mathsf{M}}v = |\det(\mathsf{M})|(v\!\uparrow\!\mathsf{M}) * u \quad \text{and} \quad \mathcal{T}_{u,\mathsf{M}}v = |\det(\mathsf{M})|(v * u^\star)\!\downarrow\!\mathsf{M},$$

where $v * u := \sum_{k\in\mathbb{Z}^d} v(k)u(\cdot - k)$ is the convolution of v and u.

Let $a, b_1, \dots, b_s \in l_1(\mathbb{Z}^d)$ and $\mathsf{M}, \mathsf{M}_1, \dots, \mathsf{M}_s$ be $d\times d$ invertible integer matrices.

For $J \in \mathbb{N}$ and given data $v_0 \in l_\infty(\mathbb{Z}^d)$, the J-level discrete framelet decomposition (or forward transform) employing the filter bank $\{a\,!\,\mathsf{M}; b_1\,!\,\mathsf{M}_1, \dots, b_s\,!\,\mathsf{M}_s\}$ is

$$v_j := |\det(\mathsf{M})|^{-1/2}\mathcal{T}_{a,\mathsf{M}}v_{j-1} \quad \text{and} \quad w_{\ell,j} := |\det(\mathsf{M}_\ell)|^{-1/2}\mathcal{T}_{b_\ell,\mathsf{M}_\ell}v_{j-1}, \quad \ell = 1, \dots, s,\ j = 1, \dots, J, \tag{3.2.2}$$

where v_j are sequences of low-pass coefficients and all $w_{\ell,j}$ are sequences of high-pass coefficients of the input signal v_0. The J-level discrete framelet reconstruction (or backward transform) employing the filter bank $\{a\,!\,\mathsf{M}; b_1\,!\,\mathsf{M}_1, \dots, b_s\,!\,\mathsf{M}_s\}$ can be described by

$$\mathring{v}_{j-1} := |\det(\mathsf{M})|^{-1/2}\mathcal{S}_{a,\mathsf{M}}\mathring{v}_j + \sum_{\ell=1}^{s} |\det(\mathsf{M}_\ell)|^{-1/2}\mathcal{S}_{b_\ell,\mathsf{M}_\ell}\mathring{w}_{\ell,j}, \quad j = J, \dots, 1, \tag{3.2.3}$$

where $\mathring{v}_0$ is a reconstructed sequence on $\mathbb{Z}^d$. The property of perfect reconstruction requires that the reconstructed sequence $\mathring{v}_0$ be exactly the same as the original input data v_0 if $\mathring{v}_J = v_J$ and $\mathring{w}_{\ell,j} = w_{\ell,j}$ for $j = 1, \dots, J$ and $\ell = 1, \dots, s$.

Using [19, Theorem 2.1], we have the following result on the perfect reconstruction for the filter bank $\{a\,!\,\mathsf{M}; b_1\,!\,\mathsf{M}_1, \dots, b_s\,!\,\mathsf{M}_s\}$.

Theorem 2. *Let $a, b_1, \dots, b_s \in l_1(\mathbb{Z}^d)$ and let $\mathsf{M}, \mathsf{M}_1, \dots, \mathsf{M}_s$ be $d \times d$ invertible integer matrices. Then the following statements are equivalent:*

(1) For every $J \in \mathbb{N}$, the J-level fast framelet transform employing the filter bank $\{a\,!\,\mathsf{M}; b_1\,!\,\mathsf{M}_1, \dots, b_s\,!\,\mathsf{M}_s\}$ has perfect reconstruction.

(2) The one-level discrete framelet transform employing the filter bank $\{a\,!\,\mathsf{M}; b_1\,!\,\mathsf{M}_1, \dots, b_s\,!\,\mathsf{M}_s\}$ has perfect reconstruction, that is,

$$v = |\det(\mathsf{M})|^{-1}\mathcal{S}_{a,\mathsf{M}}\mathcal{T}_{a,\mathsf{M}}v + \sum_{\ell=1}^{s} |\det(\mathsf{M}_\ell)|^{-1}\mathcal{S}_{b_\ell,\mathsf{M}_\ell}\mathcal{T}_{b_\ell,\mathsf{M}_\ell}v, \quad v \in l_\infty(\mathbb{Z}^d). \tag{3.2.4}$$

(3) The filter bank $\{a\,!\,\mathsf{M}; b_1\,!\,\mathsf{M}_1, \ldots, b_s\,!\,\mathsf{M}_s\}$ is a tight framelet filter bank with mixed sampling factors, that is, the following perfect reconstruction conditions hold:

$$|\widehat{a}(\xi)|^2 + |\widehat{b_1}(\xi)|^2 + \cdots + |\widehat{b_s}(\xi)|^2 = 1, \tag{3.2.5}$$

$$\chi_{\mathsf{M}^{-\mathsf{T}}\mathbb{Z}^d}(\omega)\widehat{a}(\xi)\overline{\widehat{a}(\xi+2\pi\omega)} + \sum_{\ell=1}^{s} \chi_{\mathsf{M}_\ell^{-\mathsf{T}}\mathbb{Z}^d}(\omega)\widehat{b_\ell}(\xi)\overline{\widehat{b_\ell}(\xi+2\pi\omega)} = 0, \tag{3.2.6}$$

for almost every $\xi \in \mathbb{R}^d$ and all $\omega \in [\Omega_{\mathsf{M}} \cup \cup_{\ell=1}^{s}\Omega_{\mathsf{M}_\ell}]\backslash\{0\}$, where $\Omega_{\mathsf{M}_\ell} := (\mathsf{M}_\ell^{-\mathsf{T}}\mathbb{Z}^d) \cap [0,1)^d$ and

$$\chi_{\mathsf{M}_\ell^{-\mathsf{T}}\mathbb{Z}^d}(\omega) = \begin{cases} 1, & \text{if } \omega \in \mathsf{M}_\ell^{-\mathsf{T}}\mathbb{Z}^d, \\ 0, & \text{if } \omega \notin \mathsf{M}_\ell^{-\mathsf{T}}\mathbb{Z}^d. \end{cases}$$

Proof. The equivalence between item (1) and item (2) is straightforward. By (3.2.1), the Fourier series of the sequence $\mathcal{S}_{b_\ell,\mathsf{M}_\ell}\mathcal{T}_{b_\ell,\mathsf{M}_\ell}v$ is

$$|\det(\mathsf{M}_\ell)| \sum_{\omega_\ell\in\Omega_{\mathsf{M}_\ell}} \widehat{v}(\xi+2\pi\omega_\ell)\widehat{b_\ell}(\xi)\overline{\widehat{b_\ell}(\xi+2\pi\omega_\ell)}.$$

Consequently, we see that (3.2.4) holds if and only if

$$\widehat{v}(\xi) = \sum_{\omega_0\in\Omega_{\mathsf{M}}} \widehat{v}(\xi+2\pi\omega_0)\widehat{a}(\xi)\overline{\widehat{a}(\xi+2\pi\omega_0)} + \sum_{\ell=1}^{s}\sum_{\omega_\ell\in\Omega_{\mathsf{M}_\ell}} \widehat{v}(\xi+2\pi\omega_\ell)\widehat{b_\ell}(\xi)\overline{\widehat{b_\ell}(\xi+2\pi\omega_\ell)}$$

$$= \sum_{\omega\in\Omega_{\mathsf{M}}\cup\cup_{\ell=1}^{s}\Omega_{\mathsf{M}_\ell}} \widehat{v}(\xi+2\pi\omega)\left(\chi_{\mathsf{M}^{-\mathsf{T}}\mathbb{Z}^d}(\omega)\widehat{a}(\xi)\overline{\widehat{a}(\xi+2\pi\omega)} + \sum_{\ell=1}^{s}\chi_{\mathsf{M}_\ell^{-\mathsf{T}}\mathbb{Z}^d}(\omega)\widehat{b_\ell}(\xi)\overline{\widehat{b_\ell}(\xi+2\pi\omega)}\right).$$

Now using the above identity and employing a similar argument as in the proof of [19, Theorem 2.1], we can deduce that item (2) is equivalent to item (3). □

3.2.2 Discrete affine systems of tight framelet filter banks with mixed sampling factors

To understand the performance and properties of the J-level fast framelet transform using a tight framelet filter bank $\{a\,!\,\mathsf{M}; b_1\,!\,\mathsf{M}_1, \ldots, b_s\,!\,\mathsf{M}_s\}$, it is important to look at the J-level discrete affine system associated with $\{a\,!\,\mathsf{M}; b_1\,!\,\mathsf{M}_1, \ldots, b_s\,!\,\mathsf{M}_s\}$.

Let $a, b_1, \ldots, b_s \in l_1(\mathbb{Z}^d)$. Note that $l_1(\mathbb{Z}^d) \subseteq l_2(\mathbb{Z}^d)$ and $l_2(\mathbb{Z}^d)$ is a Hilbert space equipped with the inner product $\langle u, v\rangle := \sum_{k\in\mathbb{Z}^d} u(k)\overline{v(k)}$ for $u, v \in l_2(\mathbb{Z}^d)$. Following Chapter 2, the multilevel filters a_j and $b_{\ell,j}$ with $j \in \mathbb{N}$ and $\ell = 1, \ldots, s$ are defined to be

$$\widehat{a_j}(\xi) := \widehat{a}(\xi)\widehat{a}(\mathsf{M}^\mathsf{T}\xi)\cdots\widehat{a}((\mathsf{M}^\mathsf{T})^{j-2}\xi)\widehat{a}((\mathsf{M}^\mathsf{T})^{j-1}\xi), \tag{3.2.7}$$

$$\widehat{b_{\ell,j}}(\xi) := \widehat{a_{j-1}}(\xi)\widehat{b_\ell}((\mathsf{M}^\mathsf{T})^{j-1}\xi) = \widehat{a}(\xi)\widehat{a}(\mathsf{M}^\mathsf{T}\xi)\cdots\widehat{a}((\mathsf{M}^\mathsf{T})^{j-2}\xi)\widehat{b_\ell}((\mathsf{M}^\mathsf{T})^{j-1}\xi). \tag{3.2.8}$$

In particular, $a_1 = a$ and $b_{\ell,1} = b_\ell$. We also use the convention $a_0 = \boldsymbol{\delta}$. Since $a, b_1, \ldots, b_s \in l_1(\mathbb{Z}^d)$, it is straightforward to see that all $a_j, b_{\ell,j}$ are well-defined filters in $l_1(\mathbb{Z}^d) \subseteq l_2(\mathbb{Z}^d)$. For $j \in \mathbb{N}$ and $k \in \mathbb{Z}^d$, we define the shifts to be

$$\begin{aligned} a_{j;k} &:= |\det(\mathsf{M})|^{j/2} a_j(\cdot - \mathsf{M}^j k), \\ b_{\ell,j;k} &:= |\det(\mathsf{M})|^{(j-1)/2} |\det(\mathsf{M}_\ell)|^{1/2} b_{\ell,j}(\cdot - \mathsf{M}^{j-1}\mathsf{M}_\ell k). \end{aligned} \tag{3.2.9}$$

Then J-level discrete affine system associated with mixed sampling factors filter bank $\{a\,!\,\mathsf{M}; b_1\,!\,\mathsf{M}_1, \ldots, b_s\,!\,\mathsf{M}_s\}$ is defined to be

$$\begin{aligned} &\mathrm{DAS}_J(\{a\,!\,\mathsf{M}; b_1\,!\,\mathsf{M}_1, \ldots, b_s\,!\,\mathsf{M}_s\}) := \\ &\qquad \{a_{J;k} \;:\; k \in \mathbb{Z}^d\} \bigcup \{b_{\ell,j;k} \;:\; k \in \mathbb{Z}^d, \ell = 1, \ldots, s, j = 1, \ldots, J\}. \end{aligned} \tag{3.2.10}$$

Under the framework of the Hilbert space $l_2(\mathbb{Z}^d)$, the J-level fast framelet transform using the tight framelet filter bank $\{a\,!\,\mathsf{M}; b_1\,!\,\mathsf{M}_1, \ldots, b_s\,!\,\mathsf{M}_s\}$ is exactly to compute the following representation:

$$\begin{aligned} v &= \sum_{u \in \mathrm{DAS}_J(\{a\,!\,\mathsf{M}; b_1\,!\,\mathsf{M}_1,\ldots,b_s\,!\,\mathsf{M}_s\})} \langle v, u\rangle u \\ &= \sum_{k\in\mathbb{Z}^d} \langle v, a_{J;k}\rangle a_{J;k} + \sum_{j=1}^{J}\sum_{\ell=1}^{s}\sum_{k\in\mathbb{Z}^d} \langle v, b_{\ell,j;k}\rangle b_{\ell,j;k}, \quad v \in l_2(\mathbb{Z}^d), \end{aligned} \tag{3.2.11}$$

where the series converges unconditionally in $l_2(\mathbb{Z}^d)$.

Similar to Theorem 1, we have the following result on the discrete affine system associated with a mixed sampling factor filter bank.

Theorem 3. *Let $a, b_1, \ldots, b_s \in l_1(\mathbb{Z}^d)$ and $\mathsf{M}, \mathsf{M}_1, \ldots, \mathsf{M}_s$ be $d \times d$ invertible integer matrices. For $J \in \mathbb{N}$, define $\mathrm{DAS}_J(\{a\,!\,\mathsf{M}; b_1\,!\,\mathsf{M}_1, \ldots, b_s\,!\,\mathsf{M}_s\})$ as in (3.2.10) with a_j and $b_{\ell,j}$ being given in (3.2.7) and (3.2.8), respectively. Then the following statements are equivalent:*

(1) $\{a\,!\,\mathsf{M}; b_1\,!\,\mathsf{M}_1, \ldots, b_s\,!\,\mathsf{M}_s\}$ is a tight framelet filter bank with mixed sampling factors.

(2) The following identity holds:

$$v = \sum_{k\in\mathbb{Z}^d} \langle v, a_{1;k}\rangle a_{1;k} + \sum_{\ell=1}^{s}\sum_{k\in\mathbb{Z}^d} \langle v, b_{\ell,1;k}\rangle b_{\ell,1;k}, \quad v \in l_2(\mathbb{Z}^d). \tag{3.2.12}$$

(3) $\mathrm{DAS}_1(\{a\,!\,\mathsf{M}; b_1\,!\,\mathsf{M}_1, \ldots, b_s\,!\,\mathsf{M}_s\})$ is a (normalized) tight frame for $l_2(\mathbb{Z}^d)$, that is,

$$\|v\|^2_{l_2(\mathbb{Z}^d)} = \sum_{k\in\mathbb{Z}^d} |\langle v, a_{1;k}\rangle|^2 + \sum_{\ell=1}^{s}\sum_{k\in\mathbb{Z}^d} |\langle v, b_{\ell,1;k}\rangle|^2, \quad v \in l_2(\mathbb{Z}^d). \tag{3.2.13}$$

(4) For every $j \in \mathbb{N}$, the following identity holds:

$$\sum_{k\in\mathbb{Z}^d} \langle v, a_{j-1;k}\rangle a_{j-1;k} = \sum_{k\in\mathbb{Z}^d} \langle v, a_{j;k}\rangle a_{j;k} + \sum_{\ell=1}^{s}\sum_{k\in\mathbb{Z}^d} \langle v, b_{\ell,j;k}\rangle b_{\ell,j;k}, \quad v \in l_2(\mathbb{Z}^d),$$

where by convention $a_0 := \boldsymbol{\delta}$ and $a_{0;k} := \boldsymbol{\delta}(\cdot - k)$ for $k \in \mathbb{Z}^d$.

(5) For every $J \in \mathbb{N}$, the identity in (3.2.11) holds.

(6) For every $J \in \mathbb{N}$, $\mathrm{DAS}_J(\{a\,!\,\mathsf{M}; b_1\,!\,\mathsf{M}_1, \dots, b_s\,!\,\mathsf{M}_s\})$ is a (normalized) tight frame for $l_2(\mathbb{Z}^d)$, that is,

$$\|v\|^2_{l_2(\mathbb{Z}^d)} = \sum_{k\in\mathbb{Z}^d} |\langle v, a_{J;k}\rangle|^2 + \sum_{j=1}^{J}\sum_{\ell=1}^{s}\sum_{k\in\mathbb{Z}^d} |\langle v, b_{\ell,j;k}\rangle|^2, \quad v \in l_2(\mathbb{Z}^d).$$

Proof. Similar to Theorem 1, we only prove (2)$\Longrightarrow$(4). By the definition of $b_{\ell,j}$ in (3.2.8) and $b_{\ell,1} = b_\ell$,

$$\begin{aligned} b_{\ell,j} &= a_{j-1} * (b_\ell \uparrow \mathsf{M}^{j-1}) = a_{j-1} * (b_{\ell,1} \uparrow \mathsf{M}^{j-1}) \\ &= \sum_{n\in\mathbb{Z}^d} a_{j-1}(\cdot - n)(b_{\ell,1}\uparrow \mathsf{M}^{j-1})(n) = \sum_{m\in\mathbb{Z}^d} a_{j-1}(\cdot - \mathsf{M}^{j-1}m) b_{\ell,1}(m). \end{aligned}$$

Therefore, by the definition of $b_{\ell,j;k}$ in (3.2.9),

$$\begin{aligned} b_{\ell,j;k} &= |\det(\mathsf{M})|^{(j-1)/2} |\det(\mathsf{M}_\ell)|^{1/2} b_{\ell,j}(\cdot - \mathsf{M}^{j-1}\mathsf{M}_\ell k) \\ &= |\det(\mathsf{M})|^{(j-1)/2} |\det(\mathsf{M}_\ell)|^{1/2} \sum_{m\in\mathbb{Z}^d} a_{j-1}(\cdot - \mathsf{M}^{j-1}\mathsf{M}_\ell k - \mathsf{M}^{j-1}m) b_{\ell,1}(m) \\ &= |\det(\mathsf{M})|^{(j-1)/2} |\det(\mathsf{M}_\ell)|^{1/2} \sum_{m\in\mathbb{Z}^d} a_{j-1}(\cdot - \mathsf{M}^{j-1}m) b_{\ell,1}(m - \mathsf{M}_\ell k) \\ &= \sum_{m\in\mathbb{Z}^d} a_{j-1;m} b_{\ell,1;k}(m). \end{aligned}$$

Consequently,

$$\langle v, b_{\ell,j;k}\rangle = \sum_{m\in\mathbb{Z}^d} \langle v, a_{j-1;m}\rangle \overline{b_{\ell,1;k}(m)} = \langle \langle v, a_{j-1;\cdot}\rangle, b_{\ell,1;k}(\cdot)\rangle. \tag{3.2.14}$$

From the above two identities,

$$\sum_{k\in\mathbb{Z}^d} \langle v, b_{\ell,j;k}\rangle b_{\ell,j;k} = \sum_{m\in\mathbb{Z}^d} a_{j-1;m} \left(\sum_{k\in\mathbb{Z}^d} \langle\langle v, a_{j-1;\cdot}\rangle, b_{\ell,1;k}\rangle b_{\ell,1;k}(m) \right).$$

The same argument can be applied to $a_{j;k}$ and the above identity still holds by replacing $b_{\ell,j;k}$ and $b_{\ell,1;k}$ with $a_{j;k}$ and $a_{1;k}$, respectively. Therefore,

$$\begin{aligned}&\sum_{k\in\mathbb{Z}^d}\langle v, a_{j;k}\rangle a_{j;k}+\sum_{\ell=1}^{s}\sum_{k\in\mathbb{Z}^d}\langle v, b_{\ell,j;k}\rangle b_{\ell,j;k}\\ &=\sum_{m\in\mathbb{Z}^d} a_{j-1;m}\left(\sum_{k\in\mathbb{Z}^d}\langle\langle v, a_{j-1;\cdot}\rangle, a_{1;k}\rangle a_{1;k}(m)+\sum_{\ell=1}^{s}\sum_{k\in\mathbb{Z}^d}\langle\langle v, a_{j-1;\cdot}\rangle, b_{\ell,1;k}\rangle b_{\ell,1;k}(m)\right)\\ &=\sum_{m\in\mathbb{Z}^d}\langle v, a_{j-1;m}\rangle a_{j-1;m},\end{aligned}$$

where (3.2.12) in item (2) is applied in the last identity. This proves (2)$\Longrightarrow$(4). $\square$

The coefficients in the representation in (3.2.11) using a J-level discrete affine system can be exactly computed through the J-level fast framelet decomposition in (3.2.2). In fact, since $\widehat{a_{j-1}}(\xi)=\widehat{a}(\xi)\cdots\widehat{a}((\mathsf{M}^{\mathsf{T}})^{j-2}\xi)$ and $\mathcal{T}_{u,\mathsf{M}}v=|\det(\mathsf{M})|(v*u^{\star})\downarrow\mathsf{M}$, by [19, Lemma 4.3],

$$\begin{aligned}\langle v, a_{j-1;k}\rangle &= |\det(\mathsf{M})|^{(j-1)/2}\langle v, a_{j-1}(\cdot-\mathsf{M}^{j-1}k)\rangle = |\det(\mathsf{M})|^{(1-j)/2}[\mathcal{T}_{a_{j-1},\mathsf{M}^{j-1}}v](k)\\ &= |\det(\mathsf{M})|^{(1-j)/2}[\mathcal{T}_{a,\mathsf{M}}^{j-1}v](k)=v_{j-1}(k),\end{aligned}$$

where v_{j-1} is exactly the same sequence as obtained in the fast framelet decomposition in (3.2.2) with $v_0 := v$. Similarly, by (3.2.14) and the above identity,

$$\begin{aligned}\langle v, b_{\ell,j;k}\rangle &= \langle\langle v, a_{j-1;\cdot}\rangle, b_{\ell,1;k}\rangle = |\det(\mathsf{M}_\ell)|^{1/2}\langle v_{j-1}, b_\ell(\cdot-\mathsf{M}_\ell k)\rangle\\ &= |\det(\mathsf{M}_\ell)|^{1/2}\sum_{m\in\mathbb{Z}^d} v_{j-1}(m)\overline{b_\ell(m-\mathsf{M}_\ell k)} = |\det(\mathsf{M}_\ell)|^{-1/2}[\mathcal{T}_{b_\ell,\mathsf{M}_\ell}v_{j-1}](k)\\ &= w_{\ell,j}(k).\end{aligned}$$

This establishes the connection between the representation in (3.2.11) under the J-level discrete affine system and the J-level fast/discrete framelet transform in (3.2.2) and (3.2.3).

3.2.3 Connections to tight frames in $L_2(\mathbb{R}^d)$

Following the general theory on frequency-based framelets in [14, 18], this subsection discusses the natural connections between the tight framelet filter bank $\{a\,!\,\mathsf{M}; b_1\,!\,\mathsf{M}_1, \dots, b_s\,!\,\mathsf{M}_s\}$ and the tight frame in $L_2(\mathbb{R}^d)$.

For a function $f : \mathbb{R}^d \to \mathbb{C}$ and a $d \times d$ real matrix U, following [18], we adopt the notation:

$$f_{\mathsf{U};k,n}(x) := f_{[\![\mathsf{U};k,n]\!]}(x) := [\![\mathsf{U}; k, n]\!] f(x) := |\det(\mathsf{U})|^{1/2} e^{-in\cdot \mathsf{U}x} f(\mathsf{U}x - k), \quad x, k, n \in \mathbb{R}^d.$$

In particular, $f_{\mathsf{U};k} := f_{\mathsf{U};k,0} = |\det \mathsf{U}|^{1/2} f(\mathsf{U}\cdot -k)$. For $f \in L_1(\mathbb{R}^d)$, its Fourier transform is defined to be $\widehat{f}(\xi) := \int_{\mathbb{R}^d} f(x) e^{-ix\cdot\xi} dx$ for $\xi \in \mathbb{R}^d$. Note that $\widehat{f_{\mathsf{U};k}} = \widehat{f}_{\mathsf{U}^{-\mathsf{T}};0,k}$.

The following result is based on the general theory developed in [14, 18] on frequency-based framelets.

Theorem 4. *Let $a, b_1, \dots, b_s \in l_1(\mathbb{Z}^d)$ and $\mathsf{M}, \mathsf{M}_1, \dots, \mathsf{M}_s$ be $d\times d$ invertible integer matrices. Suppose that all the eigenvalues of M are greater than one in modulus and there exist positive numbers ε, C, τ such that $|1-\widehat{a}(\xi)| \leqslant C\|\xi\|^{\tau},\ \xi \in [-\varepsilon, \varepsilon]^d$. Define*

$$\widehat{\phi}(\xi) := \prod_{j=1}^{\infty} \widehat{a}((\mathsf{M}^{\mathsf{T}})^{-j}\xi) \quad \text{and} \quad \widehat{\psi^{\ell}}(\xi) := \widehat{b_{\ell}}(\mathsf{M}^{-\mathsf{T}}\xi)\widehat{\phi}(\mathsf{M}^{-\mathsf{T}}\xi), \quad \xi \in \mathbb{R}^d,\ \ell = 1, \dots, s. \tag{3.2.15}$$

If $\{a\,!\,\mathsf{M}; b_1\,!\,\mathsf{M}_1, \dots, b_s\,!\,\mathsf{M}_s\}$ is a tight framelet filter bank, then $\{\phi\,!\,\mathsf{M}; \psi^1\,!\,\mathsf{M}_1, \dots, \psi^s\,!\,\mathsf{M}_s\}$ is a tight framelet in $L_2(\mathbb{R}^d)$, that is, $\phi, \psi^1, \dots, \psi^s \in L_2(\mathbb{R}^d)$ and $\mathsf{AS}_0(\{\phi\,!\,\mathsf{M}; \psi^1\,!\,\mathsf{M}_1, \dots, \psi^s\,!\,\mathsf{M}_s\})$ is a (normalized) tight frame in $L_2(\mathbb{R}^d)$:

$$\|f\|^2_{L_2(\mathbb{R}^d)} = \sum_{k\in\mathbb{Z}^d} |\langle f, \phi(\cdot - k)\rangle|^2 + \sum_{j=0}^{\infty}\sum_{\ell=1}^{s}\sum_{k\in\mathbb{Z}^d} |\langle f, |\det(\mathsf{M}^{-1}\mathsf{M}_\ell)|^{1/2}\psi^\ell_{\mathsf{M}^j;\mathsf{M}^{-1}\mathsf{M}_\ell k}\rangle|^2, \quad f \in L_2(\mathbb{R}^d), \tag{3.2.16}$$

where

$$\begin{aligned} &\mathsf{AS}_0(\{\phi\,!\,\mathsf{M}; \psi^1\,!\,\mathsf{M}_1, \ldots, \psi^s\,!\,\mathsf{M}_s\}) := \{\phi(\cdot - k) \;:\; k \in \mathbb{Z}^d\} \\ &\quad \bigcup \{|\det(\mathsf{M}^{-1}\mathsf{M}_\ell)|^{1/2}\psi^\ell_{\mathsf{M}^j;\mathsf{M}^{-1}\mathsf{M}_\ell k} \;:\; k\in\mathbb{Z}^d, \ell = 1,\ldots,s, j\in\mathbb{N}\cup\{0\}\}. \end{aligned} \tag{3.2.17}$$

The converse direction also holds provided in addition that $\sum_{k\in\mathbb{Z}^d} |\widehat{\phi}(\xi + 2\pi k)|^2 \ne 0$ *for almost every* $\xi \in \mathbb{R}^d$.

Proof. By the same argument as in [18, Theorem 13] and [14, Theorem 6], (3.2.16) holds for all $f \in L_2(\mathbb{R}^d)$ and $\phi, \psi^1, \ldots, \psi^s \in L_2(\mathbb{R}^d)$ if and only if

$$\lim_{j\to+\infty} \sum_{k\in\mathbb{Z}^d} |\langle f, \phi_{\mathsf{M}^j;k}\rangle|^2 = \|f\|^2_{L_2(\mathbb{R}^d)} \tag{3.2.18}$$

and

$$\begin{aligned} \sum_{k\in\mathbb{Z}^d} |\langle f, \phi_{\mathsf{M};k}\rangle|^2 = &\sum_{k\in\mathbb{Z}^d} |\langle f, \phi(\cdot - k)\rangle|^2 + \\ &\sum_{\ell=1}^{s}\sum_{k\in\mathbb{Z}^d} |\langle f, |\det(\mathsf{M}^{-1}\mathsf{M}_\ell)|^{1/2}\psi^\ell(\cdot - \mathsf{M}^{-1}\mathsf{M}_\ell k)\rangle|^2 \end{aligned} \tag{3.2.19}$$

for all $f \in L_2(\mathbb{R}^d)$ such that $\widehat{f}$ is a compactly supported C^∞ function.

By our assumption on M and $\widehat{a}$, $\widehat{\phi}$ is a well-defined bounded function. By the similar argument as in [14, Lemma 4], we see that (3.2.18) is satisfied, since $\lim_{j\to+\infty} \widehat{\phi}((\mathsf{M}^\mathsf{T})^{-j}\xi) = 1$.

Define $\mathsf{N} := \mathsf{M}^{-\mathsf{T}}$ and $\mathsf{N}_\ell := \mathsf{M}_\ell^{-\mathsf{T}}$. Note that $\psi^\ell(\cdot - \mathsf{M}^{-1}\mathsf{M}_\ell k) = \eta^\ell(\mathsf{M}_\ell^{-1}\mathsf{M}\cdot -k)$ with $\eta^\ell := \psi^\ell(\mathsf{M}^{-1}\mathsf{M}_\ell\cdot)$ and $\widehat{\eta^\ell}(\xi) = |\det(\mathsf{M}_\ell^{-1}\mathsf{M})|\widehat{\psi^\ell}(\mathsf{N}^{-1}\mathsf{N}_\ell\xi)$. By [18, Lemma 10], we have

$$\sum_{k\in\mathbb{Z}^d}|\langle f,|\det(\mathsf{M}^{-1}\mathsf{M}_\ell)|^{1/2}\psi^\ell(\cdot-\mathsf{M}^{-1}\mathsf{M}_\ell k)\rangle|^2=|\det(\mathsf{M}^{-1}\mathsf{M}_\ell)|^2\sum_{k\in\mathbb{Z}^d}|\langle f,\eta^\ell_{\mathsf{M}_\ell^{-1}\mathsf{M};k}\rangle|^2$$

$$=(2\pi)^{-2d}|\det(\mathsf{M}^{-1}\mathsf{M}_\ell)|^2\sum_{k\in\mathbb{Z}^d}|\langle\widehat{f},\widehat{\eta^\ell}_{\mathsf{N}_\ell^{-1}\mathsf{N};0,k}\rangle|^2$$

$$=(2\pi)^{-d}\int_{\mathbb{R}^d}\sum_{k\in\mathbb{Z}^d}\widehat{f}(\xi)\overline{\widehat{f}(\xi+2\pi\mathsf{N}^{-1}\mathsf{N}_\ell k)}\overline{\widehat{\psi^\ell}(\xi)}\widehat{\psi^\ell}(\xi+2\pi\mathsf{N}^{-1}\mathsf{N}_\ell k)d\xi$$

$$=(2\pi)^{-d}\int_{\mathbb{R}^d}\sum_{k\in\mathbb{Z}^d}\widehat{f}(\xi)\overline{\widehat{f}(\xi+2\pi\mathsf{N}^{-1}\mathsf{N}_\ell k)\widehat{b_\ell}(\mathsf{N}\xi)}\widehat{b_\ell}(\mathsf{N}\xi+2\pi\mathsf{N}_\ell k)\overline{\widehat{\phi}(\mathsf{N}\xi)}\widehat{\phi}(\mathsf{N}\xi+2\pi\mathsf{N}_\ell k)d\xi$$

$$=(2\pi)^{-d}\int_{\mathbb{R}^d}\widehat{f}(\xi)\overline{\widehat{\phi}(\mathsf{N}\xi)}\sum_{\omega_\ell\in\Omega_{\mathsf{M}_\ell}}\overline{\widehat{b_\ell}(\mathsf{N}\xi)}\widehat{b_\ell}(\mathsf{N}\xi+2\pi\omega_\ell)$$

$$\sum_{k\in\mathbb{Z}^d}\overline{\widehat{f}(\xi+2\pi\mathsf{N}^{-1}\omega_\ell+2\pi\mathsf{N}^{-1}k)}\widehat{\phi}(\mathsf{N}\xi+2\pi\omega_\ell+2\pi k)d\xi,$$

where we used (3.2.15) in the last second identity and the fact that $\mathbb{Z}^d=\mathsf{M}_\ell^{\mathsf{T}}\Omega_{\mathsf{M}_\ell}+\mathsf{M}_\ell^{\mathsf{T}}\mathbb{Z}^d$. Similarly, by [18, Lemma 10] we have

$$\sum_{k\in\mathbb{Z}^d}|\langle f,\phi(\cdot-k)\rangle|^2$$

$$=(2\pi)^{-d}\int_{\mathbb{R}^d}\sum_{k\in\mathbb{Z}^d}\widehat{f}(\xi)\overline{\widehat{f}(\xi+2\pi k)}\overline{\widehat{a}(\mathsf{N}\xi)}\widehat{a}(\mathsf{N}\xi+2\pi\mathsf{N}k)\overline{\widehat{\phi}(\mathsf{N}\xi)}\widehat{\phi}(\mathsf{N}\xi+2\pi\mathsf{N}k)d\xi$$

$$=(2\pi)^{-d}\int_{\mathbb{R}^d}\widehat{f}(\xi)\overline{\widehat{\phi}(\mathsf{N}\xi)}\sum_{\omega_0\in\Omega_{\mathsf{M}}}\overline{\widehat{a}(\mathsf{N}\xi)}\widehat{a}(\mathsf{N}\xi+2\pi\omega_0)$$

$$\sum_{k\in\mathbb{Z}^d}\overline{\widehat{f}(\xi+2\pi\mathsf{N}^{-1}\omega_0+2\pi\mathsf{N}^{-1}k)}\widehat{\phi}(\mathsf{N}\xi+2\pi\omega_0+2\pi k)d\xi$$

and

$$\sum_{k\in\mathbb{Z}^d}|\langle f,\phi_{\mathsf{M};k}\rangle|^2=(2\pi)^{-d}\int_{\mathbb{R}^d}\widehat{f}(\xi)\overline{\widehat{\phi}(\mathsf{N}\xi)}\sum_{k\in\mathbb{Z}^d}\overline{\widehat{f}(\xi+2\pi\mathsf{N}^{-1}k)}\widehat{\phi}(\mathsf{N}\xi+2\pi k)d\xi.$$

By the similar argument as in [14, Lemma 5], we can conclude that (3.2.19) holds if and only if

$$\overline{\widehat{\phi}(\xi)}\widehat{\phi}(\xi+2\pi\omega+2\pi k)\Big(\chi_{\mathsf{M}^{-\mathsf{T}}\mathbb{Z}^d}(\omega)\overline{\widehat{a}(\xi)}\widehat{a}(\xi+2\pi\omega)+\sum_{\ell=1}^{s}\chi_{\mathsf{M}_\ell^{-\mathsf{T}}\mathbb{Z}^d}(\omega)\overline{\widehat{b_\ell}(\xi)}\widehat{b_\ell}(\xi+2\pi\omega)\Big)$$
$$=\boldsymbol{\delta}(\omega)\overline{\widehat{\phi}(\xi)}\widehat{\phi}(\xi+2\pi k), \quad a.e.\, \xi\in\mathbb{R}^d \tag{3.2.20}$$

for all $\omega \in \Omega_{\mathsf{M}} \cup \cup_{\ell=1}^{s}\Omega_{\mathsf{M}_\ell}$ and for all $k \in \mathbb{Z}^d$. If $\{a\,!\,\mathsf{M}; b_1\,!\,\mathsf{M}_1,\dots,b_s\,!\,\mathsf{M}_s\}$ is a tight framelet filter bank, by (3.2.5) and (3.2.6), it is obvious that (3.2.20) is satisfied and therefore, $\{\phi\,!\,\mathsf{M}; \psi^1\,!\,\mathsf{M}_1,\dots,\psi^s\,!\,\mathsf{M}_s\}$ is a tight framelet for $L_2(\mathbb{R}^d)$.

If $\sum_{k\in\mathbb{Z}^d}|\widehat{\phi}(\xi+2\pi k)|^2 \neq 0$ for almost every $\xi\in\mathbb{R}^d$, then it is easy to deduce that (3.2.20) is equivalent to (3.2.5) and (3.2.6). This proves the converse direction.

□

Since $\mathsf{M}^{-1}\mathsf{M}_\ell\mathbb{Z}^d = \mathbb{Z}^d$ may not hold any more for all $\ell = 1,\dots,s$, the system $\mathsf{AS}_0(\{\phi\,!\,\mathsf{M}; \psi^1\,!\,\mathsf{M}_1,\dots,\psi^s\,!\,\mathsf{M}_s\})$ in (3.2.17) is not covered by the current theory of wavelet/multiresolution analysis.

3.3 One-dimensional complex tight framelets with low redundancy

Built on the tight framelet filter banks with mixed sampling factors, this subsection builds a one-dimensional tight framelet filter bank $\mathbb{C}\mathrm{TF}_6^{\downarrow}$, which consists of one real low-pass filter a, two auxiliary complex filters a^p and a^n, and four complex high-pass filters $b^{1,p}, b^{2,p}, b^{1,n}$ and $b^{2,n}$ such that

(1) $a^n = \overline{a^p}$, $b^{1,n} = \overline{b^{1,p}}$, and $b^{2,n} = \overline{b^{2,p}}$;

(2) both $\mathbb{C}\mathrm{TF}_6^{\downarrow} := \{a^p\,!\,4, a^n\,!\,4; b^{1,p}\,!\,4, b^{2,p}\,!\,4, b^{1,n}\,!\,4, b^{2,n}\,!\,4\}$ and $\{a\,!\,2; b^{1,p}\,!\,4, b^{2,p}\,!\,4, b^{1,n}\,!\,4, b^{2,n}\,!\,4\}$ are tight framelet filter banks;

(3) all the filters $a^p, a^n, b^{1,p}, b^{2,p}, b^{1,n},$ and $b^{2,n}$ have good frequency separation.

As discussed in Chapter 2, the directionality of the tensor product complex tight framelet TP-$\mathbb{C}\mathrm{TF}_6^{\downarrow}$ largely depends on the frequency separation of all the high-pass filters in the J-level discrete affine system $\mathrm{DAS}_J(\{a\,!\,2; b^{1,p}\,!\,4, b^{2,p}\,!\,4, b^{1,n}\,!\,4, b^{2,n}\,!\,4\})$ as well as the frequency separation of the two auxiliary filters a^p and a^n. For $\ell = 1, 2$ and $j \in \mathbb{N}$, define

$$\widehat{a_j}(\xi) := \widehat{a}(\xi)\widehat{a}(2\xi)\cdots\widehat{a}(2^{j-2}\xi)\widehat{a}(2^{j-1}\xi),$$

$$\widehat{b^p_{\ell,j}} := \widehat{a_{j-1}}(\xi)\widehat{b^p_\ell}(2^{j-1}\xi) = \widehat{a}(\xi)\widehat{a}(2\xi)\cdots\widehat{a}(2^{j-2}\xi)\widehat{b^p_\ell}(2^{j-1}\xi), \tag{3.3.1}$$

$$\widehat{b^n_{\ell,j}} := \widehat{a_{j-1}}(\xi)\widehat{b^n_\ell}(2^{j-1}\xi) = \widehat{a}(\xi)\widehat{a}(2\xi)\cdots\widehat{a}(2^{j-2}\xi)\widehat{b^n_\ell}(2^{j-1}\xi). \tag{3.3.2}$$

Note that $a_1 = a, b^p_{\ell,1} = b^p_\ell$ and $b^n_{\ell,1} = b^n_\ell$. We also define

$$a_{j;k} := 2^{j/2}a_j(\cdot - 2^j k),\ b^p_{\ell,j;k} := 2^{(j+1)/2}b^p_{\ell,j}(\cdot - 2^{j+1}k),\ b^n_{\ell,j;k} := 2^{(j+1)/2}b^n_{\ell,j}(\cdot - 2^{j+1}k),$$

for $\ell = 1, 2,\ j \in \mathbb{N}$, and $k \in \mathbb{Z}$. Then the associated one-dimensional J-level discrete affine system is given by

$$\mathrm{DAS}_J(\{a\,!\,2; b^p_1\,!\,4, b^p_2\,!\,4, b^n_1\,!\,4, b^n_2\,!\,4\}) := \{a_{J;k}\ :\ k \in \mathbb{Z}\} \bigcup \{b^p_{\ell,j;k}, b^n_{\ell,j;k}\ :\ k \in \mathbb{Z},\ \ell = 1, 2,\ j = 1, \dots, J\}.$$

A detailed construction of $\mathbb{C}\mathrm{TF}_6^{\downarrow}$ is given in the following result by defining the filters a and $b^{1,p}, b^{2,p}, b^{1,n}, b^{2,n}$ as in (2.2.3) with $s = 2$ and a^p, a^n as in (2.3.2).

For a filter u, we say that u has the ideal frequency separation if either $\widehat{u}(\xi) = 0$ for all $\xi \in [-\pi, 0]$ or $\widehat{u}(\xi) = 0$ for all $\xi \in [0, \pi]$. The following result describes the frequency separation of tight framelet filter banks with mixed sampling factors.

Theorem 5. *Let* $0 < c_0 < c_1 < c_2 < \pi$ *and* $\varepsilon_0, \varepsilon_1, \varepsilon_2, \varepsilon_3$ *be positive real numbers. The filters* a, a^p, b^p_1, b^p_2 *are constructed by defining their* 2π*-periodic Fourier series* *on the basic interval* $[-\pi,\pi)$ *as follows:*

$$\widehat{a} := \chi_{[-c_1,c_1];\varepsilon_1,\varepsilon_1}, \ \ \widehat{a^p} := \chi_{[0,c_1];\varepsilon_0,\varepsilon_1}, \ \ \widehat{b_1^p} := \chi_{[c_1,c_2];\varepsilon_1,\varepsilon_2}, \ \ \textit{and} \ \widehat{b_2^p} := \chi_{[c_2,\pi];\varepsilon_2,\varepsilon_3}.$$

Define

$$a^n := \overline{a^p}, \quad b_1^n := \overline{b_1^p}, \quad b_2^n := \overline{b_2^p}. \tag{3.3.3}$$

If the following conditions are satisfied,

$$\begin{aligned} &\varepsilon_0+\varepsilon_1 \leqslant c_1 \leqslant \tfrac{\pi}{2}-\varepsilon_0-\varepsilon_1, \quad \tfrac{\pi}{2}+\varepsilon_2+\varepsilon_3 \leqslant c_2 \leqslant \pi-\varepsilon_2-\varepsilon_3, \\ &\varepsilon_1+\varepsilon_2 \leqslant c_2-c_1 \leqslant \tfrac{\pi}{2}-\varepsilon_1-\varepsilon_2, \end{aligned} \tag{3.3.4}$$

then both $\{a^p\,!\,4, a^n\,!\,4; b_1^p\,!\,4, b_2^p\,!\,4, b_1^n\,!\,4, b_2^n\,!\,4\}$ *and* $\{a\,!\,2; b_1^p\,!\,4, b_2^p\,!\,4, b_1^n\,!\,4, b_2^n\,!\,4\}$ *are tight framelet filter banks. If both* (3.3.4) *and the following additional conditions are satisfied:*

$$\tfrac{1}{2}c_2+\tfrac{1}{2}\varepsilon_2+c_1+\varepsilon_1 \leqslant \pi \quad \textit{and} \quad c_1+\varepsilon_1+\tfrac{1}{2}\varepsilon_3 \leqslant \tfrac{\pi}{2}, \tag{3.3.5}$$

then all the high-pass filters $b^p_{1,j;k}, b^p_{2,j;k}, b^n_{1,j;k}, b^n_{2,j;k},\ k\in\mathbb{Z}$ *at all scale levels* $j \geqslant 2$ *in the* J*-level discrete affine system* $\mathrm{DAS}_J(\{a\,!\,2; b_1^p\,!\,4, b_2^p\,!\,4, b_1^n\,!\,4, b_2^n\,!\,4\})$ *have the ideal frequency separation for any* $J \geqslant 2$*, more precisely,*

$$\begin{aligned} \widehat{b^p_{\ell,j}}(\xi)=0, \quad \xi\in[-\pi,0] \quad \textit{and} \quad \widehat{b^n_{\ell,j}}(\xi)=0, \quad \xi\in[0,\pi] \\ j\geqslant 2 \quad \textit{and} \quad \ell=1,2, \end{aligned} \tag{3.3.6}$$

where $\widehat{b^p_{\ell,j}}$ *and* $\widehat{b^n_{\ell,j}}$ *are defined in* (3.3.1) *and* (3.3.2)*, respectively.*

Proof. By Theorem 2, $\{a\,!\,2; b_1^p\,!\,4, b_2^p\,!\,4, b_1^n\,!\,4, b_2^n\,!\,4\}$ is a tight framelet filter bank if and only if

$$|\widehat{a}(\xi)|^2+|\widehat{b_1^p}(\xi)|^2+|\widehat{b_2^p}(\xi)|^2+|\widehat{b_1^n}(\xi)|^2+|\widehat{b_2^n}(\xi)|^2=1, \tag{3.3.7}$$

$$\widehat{a}(\xi)\overline{\widehat{a}(\xi+\pi)} + \sum_{\ell=1}^{2}\left(\widehat{b_\ell^p}(\xi)\overline{\widehat{b_\ell^p}(\xi+\pi)} + \widehat{b_\ell^n}(\xi)\overline{\widehat{b_\ell^n}(\xi+\pi)}\right) = 0, \tag{3.3.8}$$

$$\sum_{\ell=1}^{2}\left(\widehat{b_\ell^p}(\xi)\overline{\widehat{b_\ell^p}(\xi+\tfrac{\pi}{2})} + \widehat{b_\ell^n}(\xi)\overline{\widehat{b_\ell^n}(\xi+\tfrac{\pi}{2})}\right) = 0, \tag{3.3.9}$$

$$\sum_{\ell=1}^{2}\left(\widehat{b_\ell^p}(\xi)\overline{\widehat{b_\ell^p}(\xi+\tfrac{3\pi}{2})} + \widehat{b_\ell^n}(\xi)\overline{\widehat{b_\ell^n}(\xi+\tfrac{3\pi}{2})}\right) = 0. \tag{3.3.10}$$

By the definition of the bump function, it is easy to check that the identity (3.3.7) holds. By (3.3.4), we see that for $\xi \in \mathbb{R}$, $\gamma = 1, 2, 3$, and $u \in \{b_1^p, b_2^p, b_1^n, b_2^n\}$:

$$\widehat{a}(\xi)\widehat{a}(\xi+\pi) = 0, \quad \widehat{a^p}(\xi)\widehat{a^p}(\xi+\tfrac{\gamma\pi}{2}) = 0, \quad \widehat{a^n}(\xi)\widehat{a^n}(\xi+\tfrac{\gamma\pi}{2}) = 0, \tag{3.3.11}$$

$$\widehat{u}(\xi)\widehat{u}(\xi+\tfrac{\gamma\pi}{2}) = 0. \tag{3.3.12}$$

Therefore, all the identities (3.3.8) – (3.3.10) hold and $\{a\,!\,2; b_1^p\,!\,4, b_2^p\,!\,4, b_1^n\,!\,4, b_2^n\,!\,4\}$ is a tight framelet filter bank.

By Theorem 2, $\{a^p\,!\,4, a^n\,!\,4; b_1^p\,!\,4, b_2^p\,!\,4, b_1^n\,!\,4, b_2^n\,!\,4\}$ is a tight framelet filter bank if and only if

$$|\widehat{a^p}(\xi)|^2 + |\widehat{a^n}(\xi)|^2 + |\widehat{b_1^p}(\xi)|^2 + |\widehat{b_2^p}(\xi)|^2 + |\widehat{b_1^n}(\xi)|^2 + |\widehat{b_2^n}(\xi)|^2 = 1 \tag{3.3.13}$$

and for all $\gamma = 1, 2, 3$,

$$\widehat{a^p}(\xi)\overline{\widehat{a^p}(\xi+\tfrac{\gamma\pi}{2})} + \widehat{a^n}(\xi)\overline{\widehat{a^n}(\xi+\tfrac{\gamma\pi}{2})} + \sum_{\ell=1}^{2}\left(\widehat{b_\ell^p}(\xi)\overline{\widehat{b_\ell^p}(\xi+\tfrac{\gamma\pi}{2})} + \widehat{b_\ell^n}(\xi)\overline{\widehat{b_\ell^n}(\xi+\tfrac{\gamma\pi}{2})}\right) = 0. \tag{3.3.14}$$

By the definition of the bump function, it is easy to check that the identity (3.3.13) holds. It also follows directly from (3.3.11) and (3.3.12) that (3.3.14) holds. Hence, $\{a^p\,!\,4, a^n\,!\,4; b_1^p\,!\,4, b_2^p\,!\,4, b_1^n\,!\,4, b_2^n\,!\,4\}$ is a tight framelet filter bank.

Using (3.3.4) and (3.3.5), by calculation we can directly check that the ideal frequency separation (3.3.6) holds. □

3.4 Tensor product of $\mathbb{C}\mathrm{TF}_6^{\downarrow}$

This section discusses the tensor product tight framelet filter bank $\mathrm{TP}\text{-}\mathbb{C}\mathrm{TF}_6^{\downarrow}$ derived from the one-dimensional tight framelet filter banks in Theorem 5. Define $\mathrm{TP}\text{-}\mathbb{C}\mathrm{TF}\,\textbf{-HP}_6^{\downarrow}$ to be the set including all $6^d - 2^d$ complex high-pass filters as follows:

$$\mathrm{TP}\text{-}\mathbb{C}\mathrm{TF}\,\textbf{-HP}_6^{\downarrow} := \left(\otimes^d \{a^p, a^n; b^{1,p}, b^{2,p}, b^{1,n}, b^{2,n}\}\right) \setminus \left(\otimes^d \{a^p, a^n\}\right).$$

Then the directional tensor product complex tight framelet filter bank $\mathrm{TP}\text{-}\mathbb{C}\mathrm{TF}_6^{\downarrow}$ in d dimensions is defined to be

$$\mathrm{TP}\text{-}\mathbb{C}\mathrm{TF}_6^{\downarrow} := \{\otimes^d a \,!\, 2\mathsf{I}_d\ ;\ u \,!\, 4\mathsf{I}_d \text{ with } u \in \mathrm{TP}\text{-}\mathbb{C}\mathrm{TF}\,\textbf{-HP}_6^{\downarrow}\}.$$

Note that the low-pass filter $\otimes^d a$ is real and due to the relations in (3.3.3), $\overline{u} \in \mathrm{TP}\text{-}\mathbb{C}\mathrm{TF}\,\textbf{-HP}_6^{\downarrow}$ if $u \in \mathrm{TP}\text{-}\mathbb{C}\mathrm{TF}\,\textbf{-HP}_6^{\downarrow}$. Therefore, the tight framelet filter bank $\mathrm{TP}\text{-}\mathbb{C}\mathrm{TF}_6^{\downarrow}$ can always be rewritten as

$$\mathrm{TP}\text{-}\mathbb{C}\mathrm{TF}_6^{\downarrow} = \{\otimes^d a \,!\, 2\mathsf{I}_d\ ;\ u \,!\, 4\mathsf{I}_d, \overline{u} \,!\, 4\mathsf{I}_d \text{ with } u \in \mathrm{TP}\text{-}\mathbb{C}\mathrm{TF}\,\textbf{-CHP}_6^{\downarrow}\},$$

where $\mathrm{TP}\text{-}\mathbb{C}\mathrm{TF}\,\textbf{-CHP}_6^{\downarrow}$ is a subset of $\mathrm{TP}\text{-}\mathbb{C}\mathrm{TF}\,\textbf{-HP}_6^{\downarrow}$ with exactly $\frac{6^d-2^d}{2}$ filters. Consequently, the complex tight framelet filter bank $\mathrm{TP}\text{-}\mathbb{C}\mathrm{TF}_6^{\downarrow}$ is essentially equivalent to the following real tight framelet filter bank:

$$\{\otimes^d a\ ;\ \sqrt{2}\,\mathrm{Re}(u), \sqrt{2}\,\mathrm{Im}(u) \text{ with } u \in \mathrm{TP}\text{-}\mathbb{C}\mathrm{TF}\,\textbf{-CHP}_6^{\downarrow}\}. \tag{3.4.1}$$

Therefore, we essentially only have total $(6^d - 2^d)/2$ number of complex high-pass filters in $\mathrm{TP}\text{-}\mathbb{C}\mathrm{TF}\,\textbf{-HP}_6^{\downarrow}$. Thus, the number of real coefficients (by identifying one complex number with two real numbers: its real and imaginary parts) produced by all the complex filters in $\mathrm{TP}\text{-}\mathbb{C}\mathrm{TF}_6^{\downarrow}$ is the same as those produced by the real tight framelet filter bank in (3.4.1). That is, $\text{TP-}\mathbb{C}\text{TF}$ -HP$_6^{\downarrow}$ produces exactly the same set of real coefficients as the $6^d - 2^d$ real filters in (3.4.1) do. Note that the sampling matrix is $4\mathsf{I}_d$ for all high-pass filters in $\otimes^d\{a^p, a^n; b_1^p, b_2^p, b_1^n, b_2^n\}$, while we only perform sampling by $2\mathsf{I}_d$ on the low-pass filter $\otimes^d a$. Consequently, regardless of the decomposition level, the redundancy rate of the fast framelet transform employing $\text{TP-}\mathbb{C}\text{TF}_6^{\downarrow}$ in d dimensions is no more than

$$\frac{6^d - 2^d}{4^d} \sum_{j=0}^{\infty} \frac{1}{2^{jd}} = \frac{3^d - 1}{2^d - 1}.$$

For example, the redundancy rates of $\text{TP-}\mathbb{C}\text{TF}_6^{\downarrow}$ are $2, 2\frac{2}{3}, 3\frac{5}{7}, 5\frac{1}{3}$ and $7\frac{25}{31}$ for $d = 1, \ldots, 5$, respectively. See Table 3.1 for more details on the redundancy rates of $\text{TP-}\mathbb{C}\text{TF}_6^{\downarrow}$. Note that the redundancy rate of the original $\text{TP-}\mathbb{C}\text{TF}_6$ is 2^d times that of the $\text{TP-}\mathbb{C}\text{TF}_6^{\downarrow}$ in d dimensions.

3.5 Example

This section presents one example of tensor product complex tight framelets with low redundancy rate.

Example 4. For the directional tensor product complex tight framelet $\text{TP-}\mathbb{C}\text{TF}_6^{\downarrow}$ with low redundancy, the parameters in Theorem 5 are set to be

$$\varepsilon_0 = 0.125, \quad \varepsilon_1 = 0.3, \quad \varepsilon_2 = 0.35, \quad \varepsilon_3 = 0.0778, \quad c_1 = \tfrac{\pi}{2} - 0.425, \quad c_2 = 2.0. \tag{3.5.1}$$

Note that the above parameters satisfy the conditions in both (3.3.4) and (3.3.5). To have some ideas about the filters in $\mathbb{C}\text{TF}_6^{\downarrow}$, see Figure 3.1 for the frequency response of the filters in $\mathbb{C}\text{TF}_6^{\downarrow}$. For the directionality of $\text{TP-}\mathbb{C}\text{TF}_6^{\downarrow}$ in two dimensions, see Figure 3.2 for some elements of $\text{DAS}_J(\text{TP-}\mathbb{C}\text{TF}_6^{\downarrow})$ with $J = 5$.

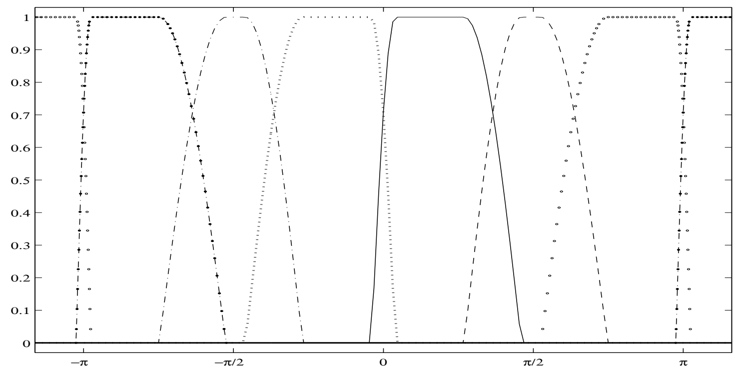

Figure 3.1: The one-dimensional tight framelet filter bank $\mathbb{C}\mathrm{TF}_6^{\downarrow} = \{a^p \,!\, 4, a^n \,!\, 4; b_1^p \,!\, 4, b_2^p \,!\, 4, b_1^n \,!\, 4, b_2^n \,!\, 4\}$ in Theorem 5 with parameters in (3.5.1). Solid line for $\widehat{a^p}$, dotted line for $\widehat{a^n}$, dashed line for $\widehat{b_1^p}$, dash-dotted line for $\widehat{b_1^n}$, circled line for $\widehat{b_2^p}$, and circle-dotted line for $\widehat{b_2^n}$.

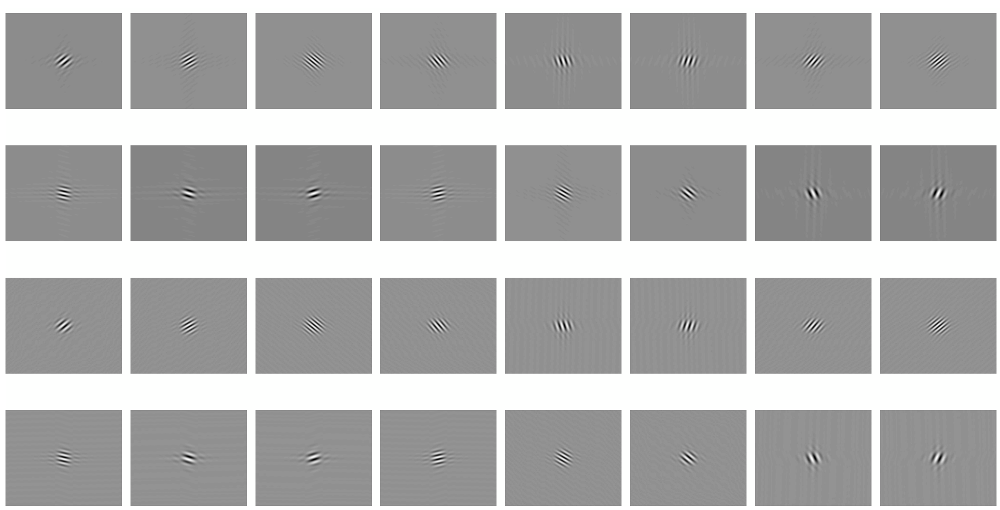

Figure 3.2: The first two rows show the real part and the last two rows show the imaginary part of the 2D high-pass filters at the level 4 in $\mathrm{DAS}_5(\mathrm{TP}\text{-}\mathbb{C}\mathrm{TF}_6^{\downarrow})$ in two dimensions. Among these 16 graphs for the first two rows or the last two rows, the directions along $\pm 45°$ are repeated once. Hence, there are 14 directions in the 2D discrete affine system $\mathrm{DAS}_5(\mathrm{TP}\text{-}\mathbb{C}\mathrm{TF}_6^{\downarrow})$.

Chapter 4

Compactly Supported Tensor Product Complex Tight Framelets $\mathrm{TP}\text{-}\mathbb{C}\mathrm{TF}_3$

Despite several desirable properties, the directional complex tight framelets constructed in Chapter 2 and Chapter 3 are bandlimited and they do not have compact support in the time domain. Compactly supported wavelets and framelets are of great interest and importance due to their good space-frequency localization and computational efficiency. It remains an unsolved problem whether there exist compactly supported tensor product complex tight framelets with directionality. This chapter satisfactorily answers this question by studying and constructing compactly supported tensor product complex tight framelet filter banks with directionality. Several concrete examples will be provided. The results in this chapter have been accepted by *SIAM Journal on Mathematical Analysis* [23] for publication.

4.1 Preliminaries

This chapter only discusses the two-dimensional $\mathrm{TP}\text{-}\mathbb{C}\mathrm{TF}_3$ with two high-pass filter in its underlying one-dimensional filter bank. It plays a fundamental role for the construction of compactly supported $\mathrm{TP}\text{-}\mathbb{C}\mathrm{TF}_4$ and $\mathrm{TP}\text{-}\mathbb{C}\mathrm{TF}_6$ with increasing directionality.

The tight framelet filter bank $\mathbb{C}\mathrm{TF}_3 = \{a; b^p, b^n\}$ constructed in (2.2.6) (see [19, 24] for more detail) are bandlimited. Due to the short support length of $\widehat{a}, \widehat{b^p},$ and $\widehat{b^n}$, one can observe that the equation (1.2.2) in the definition holds. More precisely, (2.2.6) induces

$$\widehat{a}(\xi)\overline{\widehat{a}(\xi+\pi)} = 0, \quad \widehat{b^p}(\xi)\overline{\widehat{b^p}(\xi+\pi)} = 0, \quad \widehat{b^n}(\xi)\overline{\widehat{b^n}(\xi+\pi)} = 0, \tag{4.1.1}$$

which straightforwardly imply

$$\widehat{a}(\xi)\overline{\widehat{a}(\xi+\pi)} + \widehat{b^p}(\xi)\overline{\widehat{b^p}(\xi+\pi)} + \widehat{b^n}(\xi)\overline{\widehat{b^n}(\xi+\pi)} = 0. \tag{4.1.2}$$

Therefore, taking advantages of short supports of $\widehat{a}, \widehat{b^p}$, and $\widehat{b^n}$, the bandlimited tight framelet filter bank $\mathbb{C}\mathrm{TF}_3$ only has to satisfy the following partition of unity:

$$|\widehat{a}(\xi)|^2 + |\widehat{b^p}(\xi)|^2 + |\widehat{b^n}(\xi)|^2 = 1.$$

If we require all filters $a, b^p, b^n \in l_0(\mathbb{Z})$ to have finite support, then $\widehat{a}, \widehat{b^p},$ and $\widehat{b^n}$ are 2π-periodic trigonometric polynomials. Consequently, the identities in (4.1.1) cannot be true and the condition in (4.1.2) can not be ignored for constructing a finitely supported tight framelet filter bank $\mathbb{C}\mathrm{TF}_3$. As we discussed before, the directionality of the above bandlimited tight framelet using $\mathbb{C}\mathrm{TF}_3$ largely relies on the frequency separation of ψ^p and ψ^n in (2.2.7). However, if ψ^p and ψ^n have are compactly supported and not identically zero, the frequency separation in (2.2.7) cannot hold neither. These restrictions make the construction of directional compactly supported $\mathbb{C}\mathrm{TF}_3$ much more difficult than that of bandlimited one.

Directionality of wavelets or framelets in high dimensions has close relation to the frequency separation of their associated one-dimensional filter banks. By $\widehat{\psi^p}(2\xi) = \widehat{b^p}(\xi)\widehat{\phi}(\xi)$ and $\widehat{\psi^n}(2\xi) = \widehat{b^n}(\xi)\widehat{\phi}(\xi)$, since generally $\widehat{\phi} \approx \chi_{[-\pi,\pi]}$, to satisfy the condition in (2.2.7), $\widehat{b^p}$ should be relatively small on the negative interval $[-\pi, 0)$ so that $\widehat{b^p}$ concentrates largely on the positive interval $[0, \pi)$, while $\widehat{b^n}$ should be relatively small on the positive interval $[0, \pi)$ so that $\widehat{b^n}$ concentrates largely on the negative interval $[-\pi, 0)$. A natural quantity to measure frequency separation (and therefore, the directionality of tensor product tight framelets) is

$$B_{b^p,b^n}(\xi) := |\widehat{b^p}(\xi+\pi)|^2 + |\widehat{b^n}(\xi)|^2, \qquad \xi \in [0, \pi].$$

The smaller the quantity B_{b^p,b^n} over the interval $[0, \pi]$, the better the frequency separation of the two high-pass filters b^p and b^n. If we can construct a tight framelet filter bank $\{a; b^p, b^n\}$ such that the integration of $B_{b^p,b^n}(\xi)$ over $[0, \pi]$ is relatively small, then the resulting tensor product tight framelet filter bank $\otimes\{a; b^p, b^n\}$ and its associated real tight frame will have strong directions along $0°$ (horizontal), $\pm 45°$, and $90°$ (vertical) in two dimensions.

4.2 Lower bound for frequency separation of $\mathbb{C}\mathrm{TF}_3$

This section addresses a sharp theoretical lower bound for the best possible frequency separation of $\mathbb{C}\mathrm{TF}_3 = \{a; b^p, b^n\}$, shows that the frequency separation function $A(\xi)$ in (4.2.2) is often small for many known low-pass filters, and finally shows that all real tight framelet filter banks cannot have good frequency separation.

Theorem 6. *Let $a, b^p, b^n \in l_2(\mathbb{Z})$ such that $\{a; b^p, b^n\}$ is a tight framelet filter bank. Then*

$$|\widehat{b^p}(\xi+\pi)|^2 + |\widehat{b^n}(\xi)|^2 \geqslant A(\xi), \quad a.e.\ \xi \in [0, \pi], \tag{4.2.1}$$

where the frequency separation function $A(\xi)$ associated with the low-pass filter a is defined to be

$$A(\xi) = \frac{2 - |\widehat{a}(\xi)|^2 - |\widehat{a}(\xi+\pi)|^2 - \sqrt{C(\xi)}}{2} \tag{4.2.2}$$

with

$$C(\xi) := 4\big(1 - |\widehat{a}(\xi)|^2 - |\widehat{a}(\xi+\pi)|^2\big) + (|\widehat{a}(\xi)|^2 - |\widehat{a}(\xi+\pi)|^2)^2. \qquad (4.2.3)$$

Moreover, the inequality in (4.2.1) is sharp in the sense that there exist $\mathring{b}^p, \mathring{b}^n \in l_2(\mathbb{Z})$ *such that* $\{a; \mathring{b}^p, \mathring{b}^n\}$ *is a tight framelet filter bank satisfying* $|\widehat{\mathring{b}^p}(\xi+\pi)|^2 + |\widehat{\mathring{b}^n}(\xi)|^2 = A(\xi)$ *a.e.* $\xi \in [0,\pi]$. *If in addition the filter* a *is real, that is,* $\widehat{a}(\xi) = \overline{\widehat{a}(-\xi)}$ *a.e.* $\xi \in \mathbb{R}$, *then the tight framelet filter bank* $\{a; \mathring{b}^p, \mathring{b}^n\}$ *can satisfy the additional property:* $\widehat{\mathring{b}^n}(\xi) = \overline{\widehat{\mathring{b}^p}(-\xi)}$ *a.e.* $\xi \in \mathbb{R}$, *that is,* $\mathring{b}^n = \overline{\mathring{b}^p}$.

Proof. Since $\{a; b^p, b^n\}$ is a tight framelet filter bank, by definition

$$\begin{bmatrix} \widehat{b^p}(\xi) & \widehat{b^n}(\xi) \\ \widehat{b^p}(\xi+\pi) & \widehat{b^n}(\xi+\pi) \end{bmatrix} \begin{bmatrix} \overline{\widehat{b^p}(\xi)} & \overline{\widehat{b^p}(\xi+\pi)} \\ \overline{\widehat{b^n}(\xi)} & \overline{\widehat{b^n}(\xi+\pi)} \end{bmatrix} = \begin{bmatrix} 1-|\widehat{a}(\xi)|^2 & -\widehat{a}(\xi)\overline{\widehat{a}(\xi+\pi)} \\ -\widehat{a}(\xi+\pi)\overline{\widehat{a}(\xi)} & 1-|\widehat{a}(\xi+\pi)|^2 \end{bmatrix}. \qquad (4.2.4)$$

Since the determinant of the matrix on the right-hand side of (4.2.4) is $1-|\widehat{a}(\xi)|^2 - |\widehat{a}(\xi+\pi)|^2$, it follows directly from (4.2.4) that we must have $1-|\widehat{a}(\xi)|^2 - |\widehat{a}(\xi+\pi)|^2 \geqslant 0$, for almost every $\xi \in \mathbb{R}$.

Note that from (4.2.4), $\{a; b^p, b^n\}$ is a tight framelet filter bank if and only if for almost every $\xi \in [0,\pi]$, the following three equations hold:

$$|\widehat{a}(\xi)|^2 + |\widehat{b^p}(\xi)|^2 + |\widehat{b^n}(\xi)|^2 = 1, \qquad (4.2.5)$$

$$|\widehat{a}(\xi+\pi)|^2 + |\widehat{b^p}(\xi+\pi)|^2 + |\widehat{b^n}(\xi+\pi)|^2 = 1, \qquad (4.2.6)$$

$$\widehat{a}(\xi)\overline{\widehat{a}(\xi+\pi)} + \widehat{b^p}(\xi)\overline{\widehat{b^p}(\xi+\pi)} + \widehat{b^n}(\xi)\overline{\widehat{b^n}(\xi+\pi)} = 0. \qquad (4.2.7)$$

In the rest of the proof, we always assume $\xi \in [0,\pi]$. Note that (4.2.5) and (4.2.6) imply

$$\begin{aligned} |\widehat{b^p}(\xi)| &= \sqrt{1-|\widehat{a}(\xi)|^2 - |\widehat{b^n}(\xi)|^2}, \\ |\widehat{b^n}(\xi+\pi)| &= \sqrt{1-|\widehat{a}(\xi+\pi)|^2 - |\widehat{b^p}(\xi+\pi)|^2}. \end{aligned} \qquad (4.2.8)$$

Using (4.2.8), we deduce from (4.2.7) that

$$
\begin{aligned}
&|\widehat{a}(\xi)\widehat{a}(\xi+\pi)|^2 \leqslant \Big(|\widehat{b^p}(\xi)\widehat{b^p}(\xi+\pi)| + |\widehat{b^n}(\xi)\widehat{b^n}(\xi+\pi)|\Big)^2 \\
&= \Big(|\widehat{b^p}(\xi+\pi)|\sqrt{1-|\widehat{a}(\xi)|^2-|\widehat{b^n}(\xi)|^2} + |\widehat{b^n}(\xi)|\sqrt{1-|\widehat{a}(\xi+\pi)|^2-|\widehat{b^p}(\xi+\pi)|^2}\Big)^2 \\
&\leqslant \Big(|\widehat{b^p}(\xi+\pi)|^2+|\widehat{b^n}(\xi)|^2\Big)\Big(2-|\widehat{a}(\xi)|^2-|\widehat{a}(\xi+\pi)|^2-(|\widehat{b^p}(\xi+\pi)|^2+|\widehat{b^n}(\xi)|^2)\Big),
\end{aligned}
$$

where Cauchy-Schwarz inequality is applied in the last inequality. Define $B(\xi) := |\widehat{b^p}(\xi+\pi)|^2 + |\widehat{b^n}(\xi)|^2$. Then the above inequality can be rewritten as

$$
f(B(\xi)) \geqslant 0 \quad \text{with} \quad f(x) := -x^2 + \big(2-|\widehat{a}(\xi)|^2-|\widehat{a}(\xi+\pi)|^2\big)x - |\widehat{a}(\xi)\widehat{a}(\xi+\pi)|^2. \tag{4.2.9}
$$

Since f is a quadratic polynomial, by calculation, f has two real roots:

$$
A(\xi) \quad \text{and} \quad 2-|\widehat{a}(\xi)|^2-|\widehat{a}(\xi+\pi)|^2-A(\xi),
$$

where $A(\xi)$ is defined in (4.2.2). Note that the function $C(\xi)$ can be rewritten as:

$$
C(\xi) = (2-|\widehat{a}(\xi)|^2-|\widehat{a}(\xi+\pi)|^2)^2 - 4|\widehat{a}(\xi)\widehat{a}(\xi+\pi)|^2 \leqslant (2-|\widehat{a}(\xi)|^2-|\widehat{a}(\xi+\pi)|^2)^2.
$$

From the expression of $A(\xi)$ and the above inequality, we see that $A(\xi) \geqslant 0$ and

$$
0 \leqslant A(\xi) \leqslant 2-|\widehat{a}(\xi)|^2-|\widehat{a}(\xi+\pi)|^2-A(\xi). \tag{4.2.10}
$$

In particular, $f(x) > 0$ if and only if $A(\xi) < x < 2-|\widehat{a}(\xi)|^2-|\widehat{a}(\xi+\pi)|^2-A(\xi)$. Therefore, since $f(x) < 0$ for all $x < A(\xi)$, by $f(B(\xi)) \geqslant 0$, $B(\xi) \geqslant A(\xi)$. Thus, we proved inequality (4.2.1).

We now show that the inequality in (4.2.1) is sharp by explicitly constructing a tight framelet filter bank $\{a; \mathring{b}^p, \mathring{b}^n\}$ satisfying $|\widehat{\mathring{b}^p}(\xi+\pi)|^2 + |\widehat{\mathring{b}^n}(\xi)|^2 = A(\xi)$ for all $\xi \in [0,\pi]$. In the following, we construct such 2π-periodic measurable functions $\widehat{\mathring{b}^p}$ and $\widehat{\mathring{b}^n}$ by defining $\widehat{\mathring{b}^p}(\xi), \widehat{\mathring{b}^p}(\xi+\pi), \widehat{\mathring{b}^n}(\xi),$ and $\widehat{\mathring{b}^n}(\xi+\pi)$ on the interval $\xi \in [0,\pi]$.

For $\xi \in [0,\pi]$, we define

$$\widehat{\mathring{b}^p}(\xi+\pi) = \begin{cases} \frac{1}{2}, & \text{if } C(\xi)=0, \\ \sqrt{\frac{1}{2}A(\xi)\left(1-\frac{|\widehat{a}(\xi)|^2-|\widehat{a}(\xi+\pi)|^2}{\sqrt{C(\xi)}}\right)}, & \text{otherwise,} \end{cases} \tag{4.2.11}$$

and

$$\widehat{\mathring{b}^n}(\xi) = \begin{cases} \frac{1}{2}, & \text{if } C(\xi)=0, \\ \sqrt{\frac{1}{2}A(\xi)\left(1+\frac{|\widehat{a}(\xi)|^2-|\widehat{a}(\xi+\pi)|^2}{\sqrt{C(\xi)}}\right)}, & \text{otherwise.} \end{cases} \tag{4.2.12}$$

We first show that both $\widehat{\mathring{b}^p}(\xi+\pi)$ and $\widehat{\mathring{b}^n}(\xi)$ are well defined nonnegative functions for $\xi \in [0,\pi]$. By the definition of $C(\xi)$ in (4.2.3), it is straightforward to see that $\sqrt{C(\xi)} \geqslant \left||\widehat{a}(\xi)|^2-|\widehat{a}(\xi+\pi)|^2\right|$ for $\xi \in [0,\pi]$. Consequently, we have

$$\left|\frac{|\widehat{a}(\xi)|^2-|\widehat{a}(\xi+\pi)|^2}{\sqrt{C(\xi)}}\right| \leqslant 1.$$

Since $A(\xi) \geqslant 0$, both $\widehat{\mathring{b}^p}(\xi+\pi)$ in (4.2.11) and $\widehat{\mathring{b}^n}(\xi)$ in (4.2.12) are well defined nonnegative functions for $\xi \in [0,\pi]$. Let $\beta(\xi)$ denote the phase of $\widehat{a}(\xi)\overline{\widehat{a}(\xi+\pi)}$, that is, $\beta(\xi)$ is a real-valued measurable function on $[0,\pi]$ such that

$$\widehat{a}(\xi)\overline{\widehat{a}(\xi+\pi)} = e^{i\beta(\xi)}|\widehat{a}(\xi)\overline{\widehat{a}(\xi+\pi)}|, \qquad \xi \in [0,\pi]. \tag{4.2.13}$$

If $\widehat{a}(\xi)\widehat{a}(\xi+\pi)=0$, define $\beta(\xi)=0$. For $\xi \in [0,\pi]$, define

$$\widehat{\mathring{b}^p}(\xi) = -e^{i\beta(\xi)}\sqrt{1-|\widehat{a}(\xi)|^2-|\widehat{\mathring{b}^n}(\xi)|^2} \tag{4.2.14}$$

and

$$\widehat{\mathring{b}^n}(\xi+\pi) = -e^{-i\beta(\xi)}\sqrt{1-|\widehat{a}(\xi+\pi)|^2-|\widehat{\mathring{b}^p}(\xi+\pi)|^2}. \tag{4.2.15}$$

We now prove both $\widehat{\mathring{b}^p}(\xi)$ and $\widehat{\mathring{b}^n}(\xi+\pi)$ are well defined functions by showing that for $\xi \in [0, \pi]$,

$$1 - |\widehat{a}(\xi)|^2 - |\widehat{\mathring{b}^n}(\xi)|^2 \geqslant 0 \quad \text{and} \quad 1 - |\widehat{a}(\xi+\pi)|^2 - |\widehat{\mathring{b}^p}(\xi+\pi)|^2 \geqslant 0 \tag{4.2.16}$$

and

$$|\widehat{a}(\xi)\widehat{a}(\xi+\pi)| = |\widehat{\mathring{b}^p}(\xi)\widehat{\mathring{b}^p}(\xi+\pi)| + |\widehat{\mathring{b}^n}(\xi)\widehat{\mathring{b}^n}(\xi+\pi)|. \tag{4.2.17}$$

We prove (4.2.16) and (4.2.17) by considering four cases.

Case 1: $C(\xi) = 0$. Since $C(\xi) = 0$, it follows from (4.2.11) and (4.2.12) that $\widehat{\mathring{b}^p}(\xi+\pi) = \widehat{\mathring{b}^n}(\xi) = \frac{1}{2}$. By $C(\xi) = 0$, it follows from the definition of $C(\xi)$ in (4.2.3) that $1 - |\widehat{a}(\xi)|^2 - |\widehat{a}(\xi+\pi)|^2 = 0$ and $|\widehat{a}(\xi)|^2 - |\widehat{a}(\xi+\pi)|^2 = 0$. Hence, $|\widehat{a}(\xi)|^2 = |\widehat{a}(\xi+\pi)|^2 = \frac{1}{2}$. Consequently, $1 - |\widehat{a}(\xi)|^2 - |\widehat{\mathring{b}^n}(\xi)|^2 = 1 - \frac{1}{2} - \frac{1}{4} = \frac{1}{4} \geqslant 0$ and $1 - |\widehat{a}(\xi+\pi)|^2 - |\widehat{\mathring{b}^p}(\xi+\pi)|^2 = 1 - \frac{1}{2} - \frac{1}{4} = \frac{1}{4} \geqslant 0$. Thus, (4.2.16) holds. Now by the definition of $\widehat{\mathring{b}^p}(\xi)$ in (4.2.14) and $\widehat{\mathring{b}^n}(\xi+\pi)$ in (4.2.15), we have $\widehat{\mathring{b}^p}(\xi) = -e^{i\beta(\xi)}/2$ and $\widehat{\mathring{b}^n}(\xi+\pi) = -e^{-i\beta(\xi)}/2$. Thus, it is straightforward to check that (4.2.17) holds.

Case 2: $C(\xi) \neq 0$ and $A(\xi) = 0$. By the definition of $\widehat{\mathring{b}^p}(\xi+\pi)$ in (4.2.11) and $\widehat{\mathring{b}^n}(\xi)$ in (4.2.12), we have $\widehat{\mathring{b}^p}(\xi+\pi) = \widehat{\mathring{b}^n}(\xi) = 0$. Clearly, (4.2.16) holds since $1 - |\widehat{a}(\xi)|^2 - |\widehat{a}(\xi+\pi)|^2 \geqslant 0$. It is also easy to see that $A(\xi) = 0$ implies $\widehat{a}(\xi)\widehat{a}(\xi+\pi) = 0$. Therefore, (4.2.17) is true.

Case 3: $C(\xi) \neq 0$, $A(\xi) \neq 0$, and $|\widehat{a}(\xi)|^2 - |\widehat{a}(\xi+\pi)|^2 = \sqrt{C(\xi)}$ or $-\sqrt{C(\xi)}$. Without loss of any generality, we only consider $|\widehat{a}(\xi)|^2 - |\widehat{a}(\xi+\pi)|^2 = \sqrt{C(\xi)}$, from which we deduce that

$$1 - |\widehat{a}(\xi)|^2 - |\widehat{a}(\xi+\pi)|^2 = 0, \quad \widehat{\mathring{b}^p}(\xi+\pi) = 0, \quad \text{and} \quad \widehat{\mathring{b}^n}(\xi) = \sqrt{A(\xi)}.$$

It follows from $1 - |\widehat{a}(\xi)|^2 - |\widehat{a}(\xi+\pi)|^2 = 0$ and the definition of $A(\xi)$ in (4.2.2) that $A(\xi) = \frac{1-|\widehat{a}(\xi)|^2+|\widehat{a}(\xi+\pi)|^2}{2} = |\widehat{a}(\xi+\pi)|^2$. Now we see that (4.2.16) is satisfied, since $1-|\widehat{a}(\xi+\pi)|^2-|\widehat{\mathring{b}^p}(\xi+\pi)|^2 = 1-|\widehat{a}(\xi+\pi)|^2 = |\widehat{a}(\xi)|^2 \geqslant 0$ and

$$1-|\widehat{a}(\xi)|^2-|\widehat{\mathring{b}^n}(\xi)|^2 = 1-|\widehat{a}(\xi)|^2 - A(\xi) = 1-|\widehat{a}(\xi)|^2-|\widehat{a}(\xi+\pi)|^2 = 0.$$

Consequently, we deduce from the above identity and the definition of $\widehat{\mathring{b}^p}(\xi)$ in (4.2.14) that $\widehat{\mathring{b}^p}(\xi)=0$. Since $\widehat{\mathring{b}^p}(\xi+\pi)=0$ and $A(\xi)=|\widehat{a}(\xi+\pi)|^2$, from the definition of $\widehat{\mathring{b}^n}(\xi+\pi)$ in (4.2.15) we deduce that

$$|\widehat{\mathring{b}^n}(\xi+\pi)|^2 = 1-|\widehat{a}(\xi+\pi)|^2-|\widehat{\mathring{b}^p}(\xi+\pi)|^2 = 1-|\widehat{a}(\xi+\pi)|^2 = |\widehat{a}(\xi)|^2.$$

Therefore, by $\widehat{\mathring{b}^p}(\xi)=\widehat{\mathring{b}^p}(\xi+\pi)=0$, $\widehat{\mathring{b}^n}(\xi)=\sqrt{A(\xi)}$, and $|\widehat{\mathring{b}^n}(\xi+\pi)|=|\widehat{a}(\xi)|$, we see that

$$|\widehat{\mathring{b}^p}(\xi)\widehat{\mathring{b}^p}(\xi+\pi)|+|\widehat{\mathring{b}^n}(\xi)\widehat{\mathring{b}^n}(\xi+\pi)| = |\widehat{\mathring{b}^n}(\xi)\widehat{\mathring{b}^n}(\xi+\pi)| = \sqrt{A(\xi)}|\widehat{a}(\xi)| = |\widehat{a}(\xi)\widehat{a}(\xi+\pi)|,$$

where we used the identity $A(\xi)=|\widehat{a}(\xi+\pi)|^2$ in the last identity. Hence, (4.2.17) holds.

Case 4: $C(\xi)\neq 0$, $A(\xi)\neq 0$, and $|\widehat{a}(\xi)|^2-|\widehat{a}(\xi+\pi)|^2\neq \pm\sqrt{C(\xi)}$. Note that the last two conditions imply that $\widehat{\mathring{b}^p}(\xi+\pi)\neq 0$ and $\widehat{\mathring{b}^n}(\xi)\neq 0$. From the definition of $\widehat{\mathring{b}^p}(\xi+\pi)$ in (4.2.11) and $\widehat{\mathring{b}^n}(\xi)$ in (4.2.12), we see that

$$\frac{|\widehat{\mathring{b}^p}(\xi+\pi)|^2}{|\widehat{\mathring{b}^n}(\xi)|^2} = \frac{\sqrt{C(\xi)}-(|\widehat{a}(\xi)|^2-|\widehat{a}(\xi+\pi)|^2)}{\sqrt{C(\xi)}+(|\widehat{a}(\xi)|^2-|\widehat{a}(\xi+\pi)|^2)} = \frac{1-|\widehat{a}(\xi)|^2-A(\xi)}{1-|\widehat{a}(\xi+\pi)|^2-A(\xi)}, \tag{4.2.18}$$

where the relation $\sqrt{C(\xi)}=2-|\widehat{a}(\xi)|^2-|\widehat{a}(\xi+\pi)|^2-2A(\xi)$ (derived from the definition of $A(\xi)$ in (4.2.2)) is applied in the last identity. Since $C(\xi)\neq 0$, we deduce from the definition of $\widehat{\mathring{b}^p}(\xi+\pi)$ in (4.2.11) and $\widehat{\mathring{b}^n}(\xi)$ in (4.2.12) that $|\widehat{\mathring{b}^p}(\xi+\pi)|^2+|\widehat{\mathring{b}^n}(\xi)|^2=A(\xi)$. Now it follows directly from (4.2.18) that

$$\frac{|\widehat{\mathring{b}^p}(\xi+\pi)|^2}{|\widehat{\mathring{b}^n}(\xi)|^2} = \frac{1-|\widehat{a}(\xi)|^2-A(\xi)}{1-|\widehat{a}(\xi+\pi)|^2-A(\xi)} = \frac{1-|\widehat{a}(\xi)|^2-A(\xi)+|\widehat{\mathring{b}^p}(\xi+\pi)|^2}{1-|\widehat{a}(\xi+\pi)|^2-A(\xi)+|\widehat{\mathring{b}^n}(\xi)|^2}$$

$$= \frac{1 - |\widehat{a}(\xi)|^2 - |\widehat{\mathring{b}^n}(\xi)|^2}{1 - |\widehat{a}(\xi+\pi)|^2 - |\widehat{\mathring{b}^p}(\xi+\pi)|^2}.$$

That is, we proved

$$\frac{|\widehat{\mathring{b}^p}(\xi+\pi)|^2}{|\widehat{\mathring{b}^n}(\xi)|^2} = \frac{1 - |\widehat{a}(\xi)|^2 - |\widehat{\mathring{b}^n}(\xi)|^2}{1 - |\widehat{a}(\xi+\pi)|^2 - |\widehat{\mathring{b}^p}(\xi+\pi)|^2}. \tag{4.2.19}$$

From the identity in (4.2.19), we further deduce that

$$\begin{aligned}
\frac{|\widehat{\mathring{b}^p}(\xi+\pi)|^2}{A(\xi)} &= \frac{|\widehat{\mathring{b}^p}(\xi+\pi)|^2}{|\widehat{\mathring{b}^p}(\xi+\pi)|^2 + |\widehat{\mathring{b}^n}(\xi)|^2} \\
&= \frac{1 - |\widehat{a}(\xi)|^2 - |\widehat{\mathring{b}^n}(\xi)|^2}{(1 - |\widehat{a}(\xi)|^2 - |\widehat{\mathring{b}^n}(\xi)|^2) + (1 - |\widehat{a}(\xi+\pi)|^2 - |\widehat{\mathring{b}^p}(\xi+\pi)|^2)} \\
&= \frac{1 - |\widehat{a}(\xi)|^2 - |\widehat{\mathring{b}^n}(\xi)|^2}{2 - |\widehat{a}(\xi)|^2 - |\widehat{a}(\xi+\pi)|^2 - A(\xi)}.
\end{aligned}$$

In other words, we proved

$$\frac{|\widehat{\mathring{b}^p}(\xi+\pi)|^2}{A(\xi)} = \frac{1 - |\widehat{a}(\xi)|^2 - |\widehat{\mathring{b}^n}(\xi)|^2}{2 - |\widehat{a}(\xi)|^2 - |\widehat{a}(\xi+\pi)|^2 - A(\xi)}. \tag{4.2.20}$$

Similarly, we can prove that

$$\frac{|\widehat{\mathring{b}^n}(\xi)|^2}{A(\xi)} = \frac{1 - |\widehat{a}(\xi+\pi)|^2 - |\widehat{\mathring{b}^p}(\xi+\pi)|^2}{2 - |\widehat{a}(\xi)|^2 - |\widehat{a}(\xi+\pi)|^2 - A(\xi)}. \tag{4.2.21}$$

By our assumption $A(\xi) > 0$, we see from (4.2.10) that $2 - |\widehat{a}(\xi)|^2 - |\widehat{a}(\xi+\pi)|^2 - A(\xi) \geqslant A(\xi) > 0$. Since $\widehat{\mathring{b}^p}(\xi+\pi) \neq 0$ and $\widehat{\mathring{b}^n}(\xi) \neq 0$, we deduce from (4.2.20) that $1 - |\widehat{a}(\xi)|^2 - |\widehat{\mathring{b}^n}(\xi)|^2 > 0$. By the same argument, we deduce from‘(4.2.21) that $1 - |\widehat{a}(\xi+\pi)|^2 - |\widehat{\mathring{b}^p}(\xi+\pi)|^2 > 0$. Hence, we proved (4.2.16). Therefore, $\widehat{\mathring{b}^p}(\xi)$ and $\widehat{\mathring{b}^n}(\xi+\pi)$ are well defined. It now follows from (4.2.19) that

$$\frac{|\widehat{\mathring{b}^p}(\xi+\pi)|^2}{|\widehat{\mathring{b}^n}(\xi)|^2} = \frac{1 - |\widehat{a}(\xi)|^2 - |\widehat{\mathring{b}^n}(\xi)|^2}{1 - |\widehat{a}(\xi+\pi)|^2 - |\widehat{\mathring{b}^p}(\xi+\pi)|^2} = \frac{|\widehat{\mathring{b}^p}(\xi)|^2}{|\widehat{\mathring{b}^n}(\xi+\pi)|^2}$$

from which we see that the vector $(|\widehat{\mathring{b}^p}(\xi+\pi)|, |\widehat{\mathring{b}^n}(\xi)|)$ is parallel to the vector $(|\widehat{\mathring{b}^p}(\xi)|, |\widehat{\mathring{b}^n}(\xi+\pi)|)$. Consequently, we must have

$$|\widehat{\mathring{b}^p}(\xi)\widehat{\mathring{b}^p}(\xi+\pi)|+|\widehat{\mathring{b}^n}(\xi)\widehat{\mathring{b}^n}(\xi+\pi)| = \sqrt{|\widehat{\mathring{b}^p}(\xi+\pi)|^2+|\widehat{\mathring{b}^n}(\xi)|^2}\sqrt{|\widehat{\mathring{b}^p}(\xi)|^2+|\widehat{\mathring{b}^n}(\xi+\pi)|^2}.$$

By the definition of $\widehat{\mathring{b}^p}(\xi+\pi)$ in (4.2.11), $\widehat{\mathring{b}^n}(\xi)$ in (4.2.12), $\widehat{\mathring{b}^p}(\xi)$ in (4.2.14), and $\widehat{\mathring{b}^n}(\xi+\pi)$ in (4.2.15), we conclude that

$$\begin{aligned}
&|\widehat{\mathring{b}^p}(\xi)\widehat{\mathring{b}^p}(\xi+\pi)|+|\widehat{\mathring{b}^n}(\xi)\widehat{\mathring{b}^n}(\xi+\pi)|\\
=&\sqrt{|\widehat{\mathring{b}^p}(\xi+\pi)|^2+|\widehat{\mathring{b}^n}(\xi)|^2}\sqrt{|\widehat{\mathring{b}^p}(\xi)|^2+|\widehat{\mathring{b}^n}(\xi+\pi)|^2}\\
=&\sqrt{A(\xi)(2-|\widehat{a}(\xi)|^2-|\widehat{a}(\xi+\pi)|^2-A(\xi))} = |\widehat{a}(\xi)\widehat{a}(\xi+\pi)|,
\end{aligned}$$

where in the last identity we used the fact that $A(\xi)$ and $2-|\widehat{a}(\xi)|^2-|\widehat{a}(\xi+\pi)|^2-A(\xi)$ are the two roots of f in (4.2.9) and $f(0) = -|\widehat{a}(\xi)\widehat{a}(\xi+\pi)|^2$. Thus, we proved (4.2.17).

By our construction, $|\widehat{\mathring{b}^p}(\xi+\pi)|^2+|\widehat{\mathring{b}^n}(\xi)|^2 = A(\xi)$ for all $\xi\in[0,\pi]$ such that $C(\xi)\neq 0$. If $C(\xi)=0$, as discussed in Case 1, then we have $A(\xi)=\frac{1}{2}$ and $|\widehat{\mathring{b}^p}(\xi+\pi)|^2+|\widehat{\mathring{b}^n}(\xi)|^2 = \frac{1}{4}+\frac{1}{4}=\frac{1}{2}=A(\xi)$. To complete the proof, we now show that $\{a;\mathring{b}^p,\mathring{b}^n\}$ is a tight framelet filter bank. By our construction of $\widehat{\mathring{b}^p}$ and $\widehat{\mathring{b}^n}$, (4.2.5) and (4.2.6) are satisfied with b^p and b^n being replaced by $\mathring{b}^p$ and $\mathring{b}^n$, respectively. To check (4.2.7), we have

$$\begin{aligned}
&\widehat{a}(\xi)\overline{\widehat{a}(\xi+\pi)}+\widehat{\mathring{b}^p}(\xi)\overline{\widehat{\mathring{b}^p}(\xi+\pi)}+\widehat{\mathring{b}^n}(\xi)\overline{\widehat{\mathring{b}^n}(\xi+\pi)}\\
=&e^{i\beta(\xi)}|\widehat{a}(\xi)\widehat{a}(\xi+\pi)|-e^{i\beta(\xi)}(|\widehat{\mathring{b}^p}(\xi)\widehat{\mathring{b}^p}(\xi+\pi)|+|\widehat{\mathring{b}^n}(\xi)\widehat{\mathring{b}^n}(\xi+\pi)|)=0,
\end{aligned}$$

where (4.2.17) is applied in the last identity. Therefore, $\{a;\mathring{b}^p,\mathring{b}^n\}$ is indeed a tight framelet filter bank.

If the filter a is real, $\widehat{a}(\xi) = \overline{\widehat{a}(-\xi)}$ a.e. $\xi \in \mathbb{R}$. Consequently,

$$|\widehat{a}(-\xi)| = |\widehat{a}(\xi)| \quad \text{and} \quad C(-\xi) = C(\xi) = C(\pi - \xi), \quad A(-\xi) = A(\xi) = A(\pi - \xi). \tag{4.2.22}$$

We now prove that $\overline{\widehat{\mathring{b}}^p(-\xi)} = \widehat{\mathring{b}}^n(\xi)$ a.e. $\xi \in \mathbb{R}$, which is equivalent to verify that

$$\overline{\widehat{\mathring{b}}^p(-\xi)} = \widehat{\mathring{b}}^n(\xi) \quad \text{and} \quad \overline{\widehat{\mathring{b}}^p(\pi - \xi)} = \widehat{\mathring{b}}^n(\xi - \pi), \qquad a.e.\ \xi \in [0, \pi]. \tag{4.2.23}$$

By (4.2.22) and the definition of $\widehat{\mathring{b}}^p(\xi + \pi)$ in (4.2.11) and $\widehat{\mathring{b}}^n(\xi)$ in (4.2.12),

$$\overline{\widehat{\mathring{b}}^p(-\xi)} = \overline{\widehat{\mathring{b}}^p((\pi - \xi) + \pi)} = \widehat{\mathring{b}}^p((\pi - \xi) + \pi) = \widehat{\mathring{b}}^n(\xi), \qquad \xi \in [0, \pi],$$

which is the first identity in (4.2.23). Similarly, we have

$$\begin{aligned}\overline{\widehat{\mathring{b}}^p(\pi - \xi)} &= -e^{-i\beta(\pi-\xi)}\sqrt{1 - |\widehat{a}(\pi - \xi)|^2 - |\widehat{\mathring{b}}^n(\pi - \xi)|^2} \\ &= -e^{-i\beta(\pi-\xi)}\sqrt{1 - |\widehat{a}(\xi + \pi)|^2 - |\widehat{\mathring{b}}^p(\xi + \pi)|^2} = e^{i(\beta(\xi)-\beta(\pi-\xi))}\widehat{\mathring{b}}^n(\xi + \pi),\end{aligned}$$

where (4.2.15) and the first identity in (4.2.23) are used. If we can prove that

$$e^{i(\beta(\xi)-\beta(\pi-\xi))} = 1, \qquad \xi \in [0, \pi], \tag{4.2.24}$$

then the second identity in (4.2.23) holds and therefore, we proved $\overline{\widehat{\mathring{b}}^p(-\xi)} = \widehat{\mathring{b}}^n(\xi)$ a.e. $\xi \in \mathbb{R}$.

We now prove (4.2.24). Replacing ξ by $\pi - \xi$ in the definition of $\beta(\xi)$ in (4.2.13) and using (4.2.22),

$$\widehat{a}(\pi - \xi)\overline{\widehat{a}(2\pi - \xi)} = e^{i\beta(\xi-\pi)}|\widehat{a}(\pi - \xi)\widehat{a}(2\pi - \xi)| = e^{i\beta(\xi-\pi)}|\widehat{a}(\xi)\widehat{a}(\xi + \pi)|.$$

Since $\widehat{a}(\xi) = \overline{\widehat{a}(-\xi)}$, we have

$$\widehat{a}(\pi - \xi)\overline{\widehat{a}(2\pi - \xi)} = \overline{\widehat{a}(\xi - \pi)}\ \overline{\widehat{a}(-\xi)} = \overline{\widehat{a}(\xi + \pi)}\widehat{a}(\xi) = \widehat{a}(\xi)\overline{\widehat{a}(\xi + \pi)}.$$

Consequently, comparing with (4.2.13), we conclude that for $\xi \in [0, \pi]$ such that $\widehat{a}(\xi)\widehat{a}(\xi+\pi) \neq 0$, we must have $e^{i\beta(\pi-\xi)} = e^{i\beta(\xi)}$, which is simply (4.2.24). For the case that $\widehat{a}(\xi)\widehat{a}(\xi+\pi) = 0$, (4.2.24) is true since $\beta(\xi) = \beta(\pi-\xi) = 0$. This completes the proof of Theorem 6. □

Let a be a finitely supported low-pass filter such that $\widehat{a}(0) = 1$ and $\widehat{a}(\pi) = 0$. By (4.2.2) and (4.2.3), we have $C(0) = C(\pi) = 1$ and $A(0) = A(\pi) = 0$. Now by the definition of $\widehat{\mathring{b}^p}(\xi)$ and $\widehat{\mathring{b}^n}(\xi)$, we see that $\lim_{\xi\to\pi^+} \left|\widehat{\mathring{b}^p}(\xi)\right| = 0$ and $\lim_{\xi\to\pi^-} \left|\widehat{\mathring{b}^n}(\xi)\right| = 0$. Now it follows directly from (4.2.14) that

$$\lim_{\xi\to\pi^-} \left|\widehat{\mathring{b}^p}(\xi)\right| = \lim_{\xi\to\pi^-} \sqrt{1 - |\widehat{a}(\xi)|^2 - \left|\widehat{\mathring{b}^n}(\xi)\right|^2} = 1.$$

However $\lim_{\xi\to\pi^+} \left|\widehat{\mathring{b}^p}(\xi)\right| = 0$, therefore $\widehat{\mathring{b}^p}(\xi)$ must be discontinuous at $\xi = \pi$. Similarly, $\widehat{\mathring{b}^n}(\xi)$ must be discontinuous at $\xi = \pi$. Hence, though the two high-pass filters $\mathring{b}^p$ and $\mathring{b}^n$ achieve the optimal theoretical lower bound $A(\xi)$, they cannot be finitely supported in the time domain and have slow decay filter coefficients.

Interestingly, as demonstrated by the following result, the frequency separation function $A(\xi)$ in (4.2.2) is often very small for most known low-pass filters in the literature.

Theorem 7. *Let $A(\xi)$ be the frequency separation function defined in (4.2.2) associated with a filter $a \in l_2(\mathbb{Z})$ satisfying $|\widehat{a}(\xi)|^2 + |\widehat{a}(\xi+\pi)|^2 \leqslant 1, \quad a.e. \xi \in \mathbb{R}$. Then*

$$0 \leqslant A(\xi) \leqslant \min(|\widehat{a}(\xi)|^2, |\widehat{a}(\xi+\pi)|^2), \quad a.e.\ \xi \in \mathbb{R}. \qquad (4.2.25)$$

In particular,

(1) $A(\xi) = 0,\ a.e. \xi \in [0, \pi]$ *if and only if* $\widehat{a}(\xi)\widehat{a}(\xi+\pi) = 0,\ a.e. \xi \in \mathbb{R}$.

(2) $A(\xi) = \min(|\widehat{a}(\xi)|^2, |\widehat{a}(\xi+\pi)|^2),\ a.e. \xi \in [0, \pi]$ *if and only if* $|\widehat{a}(\xi)|^2 +$

$|\widehat{a}(\xi+\pi)|^2 = 1,\ a.e.\xi \in \mathbb{R}$ *with* $\min(|\widehat{a}(\xi)|^2, |\widehat{a}(\xi+\pi)|^2) \neq 0$. *In particular, if* $|\widehat{a}(\xi)|^2 + |\widehat{a}(\xi+\pi)|^2 = 1,\ a.e.\xi \in \mathbb{R}$ *(that is, a is an orthogonal filter), then* $A(\xi) = \min(|\widehat{a}(\xi)|^2, |\widehat{a}(\xi+\pi)|^2),\ a.e.\xi \in [0, \pi]$.

(3) *If a is the B-spline filter a_m^B of order m given by $\widehat{a_m^B}(\xi) := \cos^{2m}(\xi/2)$ with $m \in \mathbb{N}$, then*

$$4^{-m}\sin^m(\xi) \leqslant A(\xi) \leqslant 4^{1-m}\sin^m(\xi), \quad \xi \in [0, \pi]. \tag{4.2.26}$$

Proof. Define $x := |\widehat{a}(\xi)|^2$ and $y := |\widehat{a}(\xi+\pi)|^2$. Then $0 \leqslant x, y \leqslant 1$ and $0 \leqslant x + y \leqslant 1$. In terms of x and y, the function $A(\xi)$ in (4.2.2) can be rewritten as

$$A(\xi) = \tfrac{1}{2}\mathsf{A}(x,y) \quad \text{with} \quad \mathsf{A}(x,y) := 2 - x - y - \sqrt{4(1-x-y) + (x-y)^2}.$$

By direct calculation,

$$\tfrac{1}{2}\mathsf{A}(x,y) = x - \frac{4x(1-x-y)}{g(x,y)} \leqslant x, \tag{4.2.27}$$

where $g(x,y) := 2-3x-y+\sqrt{4(1-x-y)+(x-y)^2} \geqslant 2-3x-y+(x-y) = 2(1-x-y) \geqslant 0$.

If $g(x,y) > 0$, by the symmetry of x and y in $\mathsf{A}(x,y)$, it follows from (4.2.27) that $A(\xi) = \frac{1}{2}\mathsf{A}(x,y) \leqslant \min(x,y) = \min(|\widehat{a}(\xi)|^2, |\widehat{a}(\xi+\pi)|^2)$. Note that $g(x,y) = 0$ if and only if $x + y = 1$ and $x \geqslant y$.

If $g(x,y) = 0$, $A(\xi) = \frac{1}{2}\mathsf{A}(x,y) = y = \min(x,y) = \min(|\widehat{a}(\xi)|^2, |\widehat{a}(\xi+\pi)|^2)$. Therefore, we proved the inequality (4.2.25).

Item (1) follows directly from the definition of $A(\xi)$ and the relation in (4.2.3). Item (2) follows directly from (4.2.27). For item (3), by the definition of the function A with $a = a_m^B$, we have $A(\xi) = \frac{1}{2}\mathsf{A}(x,y)$ and

$$\sin^{2m}(\xi) = 2^{2m}\sin^{2m}(\xi/2)\cos^{2m}(\xi/2) = 4^m xy.$$

Note that

$$\mathsf{A}(x,y) = (2-x-y) - \sqrt{(2-x-y)^2 - 4xy} = \frac{4xy}{(2-x-y) + \sqrt{(2-x-y)^2 - 4xy}}.$$

Since $0 \leqslant x, y \leqslant 1$, $0 \leqslant \sqrt{(2-x-y)^2 - 4xy} \leqslant 2 - x - y$. We conclude that $\frac{2xy}{2-x-y} \leqslant \mathsf{A}(x,y) \leqslant \frac{4xy}{2-x-y}$. Consequently, by $0 \leqslant x, y \leqslant 1$ and $x + y \leqslant 1$,

$$xy \leqslant \frac{2xy}{2-x-y} \leqslant \mathsf{A}(x,y) \leqslant \frac{4xy}{2-x-y} \leqslant 4xy.$$

This completes the proof of (4.2.26). □

For each low-pass filter $a \in l_2(\mathbb{Z})$, Theorem 6 provides a sharp lower bound for the frequency separation of the associated high-pass filter b^p and b^n. Theorem 6 guarantees the existence of a tight framelet filter bank $\{a; \mathring{b}^p, \mathring{b}^n\}$ achieving this optimal lower bound. However, the 2π-periodic functions $\widehat{\mathring{b}^p}(\xi)$ and $\widehat{\mathring{b}^n}(\xi)$ must be discontinuous. As a consequence, the high-pass filters $\mathring{b}^p$ and $\mathring{b}^n$ cannot be finitely supported with slowly decay filter coefficients. The theoretical optimal lower bound $A(\xi)$ can only be approximated at the cost of long filter supports for both b^p and b^n. The main purpose of this chapter is to obtain finitely supported tight framelet filter banks $\{a; b^p, b^n\}$ with short support and good frequency separation. We often slightly sacrifice the optimal frequency separation given in Theorem 4.2.1 to have finitely supported complex tight framelet with short support and good directions.

The following result shows that for a tight framelet filter bank $\{a; b^p, b^n\}$, if the high-pass filters b^p and b^n are real (but a can be a complex filter), then the frequency separation of b^p and b^n cannot be good. Moreover, the best possible frequency separation between two real high-pass filters b^p and b^n in a tight framelet filter bank $\{a; b^p, b^n\}$ is achieved when a is an orthogonal filter. However, Theorem 7 tells us that the frequency separation between two complex high-pass filters b^p and b^n in a complex tight framelet filter bank $\{a; b^p, b^n\}$ is the worst when a is an orthogonal filter.

Theorem 8. *Let $a, b^p, b^n \in l_2(\mathbb{Z})$ such that $\{a; b^p, b^n\}$ is a tight framelet filter bank and the two high-pass filters b^p and b^n are real (but a may be complex). Then*

$$\int_0^\pi \left[|\widehat{b^p}(\xi+\pi)|^2+|\widehat{b^n}(\xi)|^2\right]d\xi = \frac{1}{2}\int_0^\pi \left[2-|\widehat{a}(\xi)|^2-|\widehat{a}(\xi+\pi)|^2\right]d\xi \geqslant \frac{\pi}{2}, \quad (4.2.28)$$

where the equal sign holds if and only if a is an orthogonal filter (that is, $|\widehat{a}(\xi)|^2 + |\widehat{a}(\xi+\pi)|^2 = 1,\ a.e.\xi \in \mathbb{R}$).

Proof. Define $B(\xi) := |\widehat{b^p}(\xi+\pi)|^2 + |\widehat{b^n}(\xi)|^2$. Note that a filter u has real coefficients if and only if $\overline{\widehat{u}(\xi)} = \widehat{u}(-\xi)$. Then $\widehat{b^p}(\xi+\pi) = \widehat{b^p}(\xi-\pi) = \overline{\widehat{b^p}(\pi-\xi)}$ and $B(\xi) = |\widehat{b^p}(\pi-\xi)|^2 + |\widehat{b^n}(\xi)|^2$.

By $|\widehat{a}(\xi)|^2+|\widehat{b^p}(\xi)|^2+|\widehat{b^n}(\xi)|^2 = 1$, we have $|\widehat{a}(\pi-\xi)|^2+|\widehat{b^p}(\pi-\xi)|^2+|\widehat{b^n}(\pi-\xi)|^2 = 1$. Therefore,

$$\begin{aligned} B(\xi) + B(\pi-\xi) &= |\widehat{b^p}(\pi-\xi)|^2 + |\widehat{b^n}(\xi)|^2 + |\widehat{b^p}(\xi)|^2 + |\widehat{b^n}(\pi-\xi)|^2 \\ &= 2 - |\widehat{a}(\xi)|^2 - |\widehat{a}(\pi-\xi)|^2. \end{aligned} \quad (4.2.29)$$

Note that

$$\begin{aligned} 1 = |\widehat{a}(-\xi)|^2 + |\widehat{b^p}(-\xi)|^2 + |\widehat{b^n}(-\xi)|^2 &= |\widehat{a}(-\xi)|^2 + |\widehat{b^p}(\xi)|^2 + |\widehat{b^n}(\xi)|^2 \\ &= 1 + |\widehat{a}(-\xi)|^2 - |\widehat{a}(\xi)|^2, \end{aligned}$$

we must have $|\widehat{a}(-\xi)| = |\widehat{a}(\xi)|$. Therefore, it follows from (4.2.29) that $B(\xi) + B(\pi-\xi) = 2 - |\widehat{a}(\xi)|^2 - |\widehat{a}(\xi+\pi)|^2$, from which

$$\int_0^\pi \left[2 - |\widehat{a}(\xi)|^2 - |\widehat{a}(\xi+\pi)|^2\right]d\xi = \int_0^\pi \left[B(\xi) + B(\pi-\xi)\right]d\xi = 2\int_0^\pi B(\xi)d\xi.$$

Since $|\widehat{a}(\xi)|^2 + |\widehat{a}(\xi+\pi)|^2 \leqslant 1,\ a.e.\xi \in \mathbb{R}$, we conclude from the above identity that (4.2.28) holds. ☐

4.3 Structure of finitely supported complex tight framelet filter banks

In order to design directional finitely supported complex tight framelet filter banks $\{a; b^p, b^n\}$, this section investigates the structure of all possible finitely supported complex high-pass filters b^p and b^n from the tight framelet filter bank $\{a; b^p, b^n\}$. We are interested in finding all possible finitely supported complex tight framelet filter banks $\{a; b^p, b^n\}$ from a given finite supported low-pass filter a. For prescribed support lengths of b^p and b^n, such result enables us to find the complex tight framelet filter bank $\{a; b^p, b^n\}$ with the best possible frequency separation by optimization techniques.

To construct finitely supported tight framelet filter banks, it is convenient to use Laurent polynomials instead of 2π-periodic trigonometric polynomials. Recall that $l_0(\mathbb{Z})$ denotes the linear space of all finitely supported sequences on $\mathbb{Z}$. For a sequence $u = \{u(k)\}_{k\in\mathbb{Z}} \in l_0(\mathbb{Z})$, its *z-transform* is a Laurent polynomial defined by

$$\mathsf{u}(z) := \sum_{k\in\mathbb{Z}} u(k)z^k, \qquad z \in \mathbb{C}\backslash\{0\}.$$

Let $u : \mathbb{Z} \to \mathbb{C}^{r\times s}$ be a sequence of $r \times s$ matrices. We define $u^\star$ to be its *associated adjoint sequence* by $u^\star(k) := \overline{u(-k)}^{\mathsf{T}}$, $k \in \mathbb{Z}$. In terms of Fourier series, we have $\widehat{u^\star}(\xi) = \overline{\widehat{u}(\xi)}^{\mathsf{T}}$ and $\widehat{u}(\xi) = \mathsf{u}(e^{-i\xi})$. Using Laurent polynomials, we have

$$\mathsf{u}^\star(z) := [\mathsf{u}(z)]^\star := \sum_{k\in\mathbb{Z}} \overline{u(k)}^{\mathsf{T}} z^{-k}, \qquad z \in \mathbb{C}\backslash\{0\}.$$

In terms of Laurent polynomials, for $a, b_1, b_2 \in l_0(\mathbb{Z})$, $\{a; b_1, b_2\}$ is a tight framelet filter bank if

$$\begin{bmatrix} \mathsf{a}(z) & \mathsf{b}_1(z) & \mathsf{b}_2(z) \\ \mathsf{a}(-z) & \mathsf{b}_1(-z) & \mathsf{b}_2(-z) \end{bmatrix} \begin{bmatrix} \mathsf{a}(z) & \mathsf{b}_1(z) & \mathsf{b}_2(z) \\ \mathsf{a}(-z) & \mathsf{b}_1(-z) & \mathsf{b}_2(-z) \end{bmatrix}^{\star} = \mathsf{I}_2 \qquad (4.3.1)$$

for all $z \in \mathbb{C}\backslash\{0\}$, where I_2 is the 2×2 identity matrix. It is easy to see that (4.3.1) is equivalent to

$$\begin{bmatrix} \mathsf{b}_1(z) & \mathsf{b}_2(z) \\ \mathsf{b}_1(-z) & \mathsf{b}_2(-z) \end{bmatrix} \begin{bmatrix} \mathsf{b}_1(z) & \mathsf{b}_2(z) \\ \mathsf{b}_1(-z) & \mathsf{b}_2(-z) \end{bmatrix}^{\star} = \mathcal{M}_a(z) \qquad (4.3.2)$$

with

$$\mathcal{M}_a(z) := \begin{bmatrix} 1 - \mathsf{a}(z)\mathsf{a}^{\star}(z) & -\mathsf{a}(z)\mathsf{a}^{\star}(-z) \\ -\mathsf{a}(-z)\mathsf{a}^{\star}(z) & 1 - \mathsf{a}(-z)\mathsf{a}^{\star}(-z) \end{bmatrix}.$$

For a 2×2 matrix U of Laurent polynomials, we say that U is *paraunitary* if $\mathsf{U}(z)\mathsf{U}^{\star}(z) = I_2$ for all $z \in \mathbb{T} := \{\zeta \in \mathbb{C} : |\zeta| = 1\}$, or equivalently, $\mathsf{U}(e^{-i\xi})\overline{\mathsf{U}(e^{-i\xi})}^{\mathsf{T}} = I_2$ for all $\xi \in \mathbb{R}$.

For a Laurent polynomial u, the notation $\mathsf{u} \equiv 0$ denotes u is identically zero, while the notation $\mathsf{u} \not\equiv 0$ denotes u is not identically zero. We say that u is an *orthogonal filter* if $\mathsf{u}(z)\mathsf{u}^{\star}(z) + \mathsf{u}(-z)\mathsf{u}^{\star}(-z) = 1$ for all $z \in \mathbb{C}\backslash\{0\}$.

The main result in this chapter is as follows:

Theorem 9. *Let $a, b_1, b_2, b^p, b^n \in l_0(\mathbb{Z})$ such that $\{a; b_1, b_2\}$ is a tight framelet filter bank and a is not identically zero. Suppose that*

$$|\mathsf{a}(z)|^2 + |\mathsf{a}(-z)|^2 \leqslant 1, \qquad z \in \mathbb{T}.$$

Then the following are equivalent:

(1) $\{a; b^p, b^n\}$ is a finitely supported tight framelet filter bank and

$$\mathsf{b}^p(z)\mathsf{b}^n(-z) - \mathsf{b}^p(-z)\mathsf{b}^n(z) = \lambda z^{2k}[\mathsf{b}_1(z)\mathsf{b}_2(-z) - \mathsf{b}_1(-z)\mathsf{b}_2(z)] \quad (4.3.3)$$

for some $k \in \mathbb{Z}$ *and* $\lambda \in \mathbb{T}$. *Remove condition* (4.3.3) *if* a *is an orthogonal filter.*

(2) There exists a 2×2 *paraunitary matrix* U *of Laurent polynomials such that*

$$\begin{bmatrix} \mathsf{b}^p(z) & \mathsf{b}^n(z) \end{bmatrix} = \begin{bmatrix} \mathsf{b}_1(z) & \mathsf{b}_2(z) \end{bmatrix} \mathsf{U}(z^2), \quad z \in \mathbb{C}\backslash\{0\}. \tag{4.3.4}$$

To prove Theorem 9, we need several auxiliary results. Let us first introduce some definitions. We say that u is a trivial factor if it is a nonzero monomial, that is, $\mathsf{u}(z) = \lambda z^k$ for some $\lambda \in \mathbb{C}\backslash\{0\}$ and $k \in \mathbb{Z}$. For two Laurent polynomials u and v, by $\gcd(\mathsf{u}, \mathsf{v})$ we denote the greatest common factor of u and v. In particular, we use the notation $\gcd(\mathsf{u}, \mathsf{v}) = 1$ to mean that u and v do not have a nontrivial common factor.

Lemma 1. *Let* $\mathsf{p}_1, \mathsf{p}_2, \mathsf{p}_3, \mathsf{p}_4$ *be Laurent polynomials. Define*

$$\mathsf{P}(z) := \begin{bmatrix} \mathsf{p}_1(z) & \mathsf{p}_3(z) \\ \mathsf{p}_2(z) & \mathsf{p}_4(z) \end{bmatrix}. \tag{4.3.5}$$

Then the following are equivalent:

(1) $\det(\mathsf{P}(z)) = 0$ *for all* $z \in \mathbb{C}\backslash\{0\}$.

(2) $\mathsf{p}_1(z)\mathsf{p}_4(z) - \mathsf{p}_2(z)\mathsf{p}_3(z) = 0$ *for all* $z \in \mathbb{C}\backslash\{0\}$.

(3) There exist Laurent polynomials $\mathsf{q}_1, \mathsf{q}_2, \mathsf{q}_3, \mathsf{q}_4$ *such that*

$$\begin{aligned} \mathsf{p}_1(z) = \mathsf{q}_1(z)\mathsf{q}_3(z), \ \ \mathsf{p}_2(z) = \mathsf{q}_2(z)\mathsf{q}_3(z), \\ \mathsf{p}_3(z) = \mathsf{q}_1(z)\mathsf{q}_4(z), \ \ \mathsf{p}_4(z) = \mathsf{q}_2(z)\mathsf{q}_4(z). \end{aligned} \tag{4.3.6}$$

(4) There exist Laurent polynomials $\mathsf{q}_1, \mathsf{q}_2, \mathsf{q}_3, \mathsf{q}_4$ *such that*

$$\mathsf{P}(z) = \begin{bmatrix} \mathsf{q}_1(z) \\ \mathsf{q}_2(z) \end{bmatrix} \begin{bmatrix} \mathsf{q}_3(z) & \mathsf{q}_4(z) \end{bmatrix}.$$

Proof. If P is identically zero, then all claims hold obviously. Hence, we assume that at least one of $\mathsf{p}_1, \mathsf{p}_2, \mathsf{p}_3, \mathsf{p}_4$ is not identically zero. Since (1)$\Longrightarrow$(2) and (3)$\Longrightarrow$(4)$\Longrightarrow$(1) are obvious, it suffices to prove (2)$\Longrightarrow$(3) to complete the proof.

If both p_1 and p_2 are identically zero, then the claim in item (3) obviously holds by taking $\mathsf{q}_1 = \mathsf{p}_3, \mathsf{q}_2 = \mathsf{p}_4, \mathsf{q}_3 = 0$ and $\mathsf{q}_4 = 1$. Now we assume that either $\mathsf{p}_1 \not\equiv 0$ or $\mathsf{p}_2 \not\equiv 0$, that is, at least one of p_1 and p_2 is not identically zero. Define

$$\mathsf{q}_3 := \gcd(\mathsf{p}_1, \mathsf{p}_2) \quad \text{and} \quad \mathsf{q}_1 := \mathsf{p}_1/\mathsf{q}_3, \quad \mathsf{q}_2 := \mathsf{p}_2/\mathsf{q}_3. \tag{4.3.7}$$

Since q_3 is not identically zero, all $\mathsf{q}_1, \mathsf{q}_2, \mathsf{q}_3$ are well-defined Laurent polynomials and at least one of q_1 and q_2 are not identically zero. Moreover, $\mathsf{p}_1 = \mathsf{q}_1\mathsf{q}_3$, $\mathsf{p}_2 = \mathsf{q}_2\mathsf{q}_3$, and $\gcd(\mathsf{q}_1, \mathsf{q}_2) = 1$, which means that q_1 and q_2 have no nontrivial common factor. By item (2), we have $0 = \mathsf{p}_1\mathsf{p}_4 - \mathsf{p}_2\mathsf{p}_3 = \mathsf{q}_3(\mathsf{q}_1\mathsf{p}_4 - \mathsf{q}_2\mathsf{p}_3)$. Since q_3 is not identically zero, from the above identity we must have $\mathsf{q}_1\mathsf{p}_4 = \mathsf{q}_2\mathsf{p}_3$. Because at least one of q_1 and q_2 is not identically zero, without loss of generality, we may assume that q_1 is not identically zero. By $\gcd(\mathsf{q}_1, \mathsf{q}_2) = 1$ and $\mathsf{q}_1\mathsf{p}_4 = \mathsf{q}_2\mathsf{p}_3$, we must have $\mathsf{q}_1 \mid \mathsf{p}_3$. Then we define $\mathsf{q}_4 = \mathsf{p}_3/\mathsf{q}_1$, which is a well-defined Laurent polynomial. By $\mathsf{q}_1\mathsf{p}_4 = \mathsf{q}_2\mathsf{p}_3$, we see that $\mathsf{p}_4 = \mathsf{q}_2\mathsf{q}_4$. Using (4.3.7), now one can directly check that (4.3.6) holds. Therefore, we complete the proof of (2)$\Longrightarrow$(3). ◻

Proposition 4.1. *Let Q and V be 2×2 matrices of Laurent polynomials. If*

$$\mathsf{V}(z)\mathsf{Q}(z) = \begin{bmatrix} \mathsf{c}(z) & 0 \\ 0 & \mathsf{d}(z) \end{bmatrix}, \tag{4.3.8}$$

then there exist Laurent polynomials $\mathsf{u}_1, \mathsf{u}_2, \mathsf{u}_3, \mathsf{u}_4, \mathsf{v}_1, \mathsf{v}_2, \mathsf{v}_3, \mathsf{v}_4$ such that

$$\begin{aligned} \mathsf{c}(z) &= \mathsf{v}_1(z)\mathsf{v}_3(z)\big(\mathsf{u}_1(z)\mathsf{u}_4(z) + \mathsf{u}_2(z)\mathsf{u}_3(z)\big), \\ \mathsf{d}(z) &= \mathsf{v}_2(z)\mathsf{v}_4(z)\big(\mathsf{u}_1(z)\mathsf{u}_4(z) + \mathsf{u}_2(z)\mathsf{u}_3(z)\big), \end{aligned} \tag{4.3.9}$$

and

$$\mathsf{V}(z) = \begin{bmatrix} \mathsf{v}_1(z) & 0 \\ 0 & \mathsf{v}_2(z) \end{bmatrix} \begin{bmatrix} \mathsf{u}_1(z) & -\mathsf{u}_3(z) \\ \mathsf{u}_2(z) & \mathsf{u}_4(z) \end{bmatrix}, \quad \mathsf{Q}(z) = \begin{bmatrix} \mathsf{u}_4(z) & \mathsf{u}_3(z) \\ -\mathsf{u}_2(z) & \mathsf{u}_1(z) \end{bmatrix} \begin{bmatrix} \mathsf{v}_3(z) & 0 \\ 0 & \mathsf{v}_4(z) \end{bmatrix}. \tag{4.3.10}$$

If $\mathsf{c} = 1$*, then we can particularly take* $\mathsf{v}_1 = \mathsf{v}_3 = 1$ *so that* $\mathsf{u}_1(z)\mathsf{u}_4(z)+\mathsf{u}_2(z)\mathsf{u}_3(z) = 1$ *and* $\mathsf{d}(z) = \mathsf{v}_2(z)\mathsf{v}_4(z)$.

Proof. By our assumption in (4.3.8), we have $[\mathsf{V}(z)\mathsf{Q}(z)]_{1,2}(z) = \mathsf{V}_{1,1}(z)\mathsf{Q}_{1,2}(z) + \mathsf{V}_{1,2}(z)\mathsf{Q}_{2,2}(z) = 0$ for all $z \in \mathbb{C}\backslash\{0\}$. By Lemma 1, there exist Laurent polynomials $\mathsf{u}_1, \mathsf{u}_3, \mathsf{v}_1, \mathsf{v}_4$ such that

$$\begin{bmatrix} \mathsf{V}_{1,1}(z) & \mathsf{V}_{1,2}(z) \\ -\mathsf{Q}_{2,2}(z) & \mathsf{Q}_{1,2}(z) \end{bmatrix} = \begin{bmatrix} \mathsf{v}_1(z) \\ -\mathsf{v}_4(z) \end{bmatrix} \begin{bmatrix} \mathsf{u}_1(z) & -\mathsf{u}_3(z) \end{bmatrix}.$$

Similarly, we have $[\mathsf{V}(z)\mathsf{Q}(z)]_{2,1}(z) = \mathsf{V}_{2,1}(z)\mathsf{Q}_{1,1}(z) + \mathsf{V}_{2,2}(z)\mathsf{Q}_{2,1}(z) = 0$ for all $z \in \mathbb{C}\backslash\{0\}$. By Lemma 1, there exist Laurent polynomials $\mathsf{u}_2, \mathsf{u}_4, \mathsf{v}_2, \mathsf{v}_3$ such that

$$\begin{bmatrix} \mathsf{V}_{2,1}(z) & \mathsf{V}_{2,2}(z) \\ -\mathsf{Q}_{2,1}(z) & \mathsf{Q}_{1,1}(z) \end{bmatrix} = \begin{bmatrix} \mathsf{v}_2(z) \\ \mathsf{v}_3(z) \end{bmatrix} \begin{bmatrix} \mathsf{u}_2(z) & \mathsf{u}_4(z) \end{bmatrix}.$$

Now we can directly check that both (4.3.10) and (4.3.9) are satisfied.

If $\mathsf{c} = 1$, then it follows from (4.3.9) that all $\mathsf{v}_1, \mathsf{v}_3$ and $\mathsf{u}_1\mathsf{u}_4 + \mathsf{u}_2\mathsf{u}_3$ must be monomials. Now it follows directly from (4.3.10) that

$$\mathsf{V}(z) = \begin{bmatrix} 1 & 0 \\ 0 & \frac{\mathsf{v}_2(z)}{\mathsf{v}_3(z)} \end{bmatrix} \begin{bmatrix} \mathsf{u}_1(z)\mathsf{v}_1(z) & -\mathsf{u}_3(z)\mathsf{v}_1(z) \\ \mathsf{u}_2(z)\mathsf{v}_3(z) & \mathsf{u}_4(z)\mathsf{v}_3(z) \end{bmatrix}$$

and

$$\mathsf{Q}(z) = \begin{bmatrix} \mathsf{u}_4(z)\mathsf{v}_3(z) & \mathsf{u}_3(z)\mathsf{v}_1(z) \\ -\mathsf{u}_2(z)\mathsf{v}_3(z) & \mathsf{u}_1(z)\mathsf{v}_1(z) \end{bmatrix} \begin{bmatrix} 1 & 0 \\ 0 & \frac{\mathsf{v}_4(z)}{\mathsf{v}_1(z)} \end{bmatrix}.$$

Redefine $\mathsf{u}_1, \mathsf{u}_2, \mathsf{u}_3, \mathsf{u}_4, \mathsf{v}_2, \mathsf{v}_4$ as $\mathsf{u}_1\mathsf{v}_1, \mathsf{u}_2\mathsf{v}_3, \mathsf{u}_3\mathsf{v}_1, \mathsf{u}_4\mathsf{v}_3, \mathsf{v}_2/\mathsf{v}_3, \mathsf{v}_4/\mathsf{v}_1$, respectively. We now see that the claim holds for the particular case of $\mathsf{c} = 1$. $\square$

The following two corollaries are direct consequences of Proposition 4.1.

Corollary 1. *Let* P *be a* 2×2 *matrix of Laurent polynomials defined in* (4.3.5). *Then* P *is paraunitary, that is,* $\mathsf{P}(z)\mathsf{P}^\star(z) = I_2$ *for all* $z \in \mathbb{C}\backslash\{0\}$, *if and only if*

$$\mathsf{p}_3(z) = -\lambda z^k \mathsf{p}_2^\star(z),\ \mathsf{p}_4(z) = \lambda z^k \mathsf{p}_1^\star(z),\ \mathsf{p}_1(z)\mathsf{p}_1^\star(z) + \mathsf{p}_2(z)\mathsf{p}_2^\star(z) = 1, \quad \lambda \in \mathbb{T},\ k \in \mathbb{Z}. \tag{4.3.11}$$

Proof. Let Q and V be the 2×2 matrix of Laurent polynomials defined by

$$\mathsf{V}(z) := \mathsf{P}(z) \quad \text{and} \quad \mathsf{Q}(z) := \mathsf{P}^\star(z) = \begin{bmatrix} \mathsf{p}_1^\star(z) & \mathsf{p}_2^\star(z) \\ \mathsf{p}_3^\star(z) & \mathsf{p}_4^\star(z) \end{bmatrix}.$$

If P is paraunitary, then $\mathsf{V}(z)\mathsf{Q}(z) = I_2$. By Proposition 4.1 with $\mathsf{c} = 1$, we see that (4.3.11) must hold.

Conversely, if (4.3.11) is satisfied, then we can directly check that P is a paraunitary matrix. $\square$

Corollary 2. *Let* $\mathsf{Q}, \mathsf{V}, \mathring{\mathsf{Q}}, \mathring{\mathsf{V}}$ *be* 2×2 *matrices of Laurent polynomials. If*

$$\mathsf{V}(z)\mathsf{Q}(z) = \begin{bmatrix} 1 & 0 \\ 0 & \mathsf{d}(z) \end{bmatrix} = \mathring{\mathsf{V}}(z)\mathring{\mathsf{Q}}(z)$$

and $\det(\mathring{\mathsf{V}}(z)) = \lambda z^k \det(\mathsf{V}(z))$, *for some* $\lambda \in \mathbb{C}\backslash\{0\},\ k \in \mathbb{Z}$, *then there exists a* 2×2 *matrix* U *of Laurent polynomials such that* $\det(\mathsf{U}(z)) = \lambda z^k$ *and*

$$\mathring{\mathsf{V}}(z) = \mathsf{V}(z)\mathsf{U}(z). \tag{4.3.12}$$

Proof. By Proposition 4.1 with $\mathsf{c} = 1$, we see that

$$\mathsf{V}(z) = \begin{bmatrix} 1 & 0 \\ 0 & \det(\mathsf{V}(z)) \end{bmatrix} \mathsf{U}_1(z), \quad \mathring{\mathsf{V}}(z) = \begin{bmatrix} 1 & 0 \\ 0 & \det(\mathring{\mathsf{V}}(z)) \end{bmatrix} \mathsf{U}_2(z),$$

where $\mathsf{U}_1, \mathsf{U}_2$ are 2×2 matrices of Laurent polynomials such that $\det(\mathsf{U}_1(z)) = \det(\mathsf{U}_2(z)) = 1$. Therefore, $[\mathsf{U}_1(z)]^{-1}$ is also a matrix of Laurent polynomials. Define

$$\mathsf{U}(z) := [\mathsf{U}_1(z)]^{-1} \begin{bmatrix} 1 & 0 \\ 0 & \lambda z^k \end{bmatrix} \mathsf{U}_2(z).$$

Now it is trivial to check that (4.3.12) holds and $\det(\mathsf{U}(z)) = \lambda z^k$ is a nontrivial monomial. □

Now we have the following result about the essential uniqueness of factorization of a positive semidefinite 2×2 matrix of Laurent polynomials.

Theorem 10. *Let* P *be a* 2×2 *matrix of Laurent polynomials given in* (4.3.5) *such that* $\gcd(\mathsf{p}_1, \mathsf{p}_2, \mathsf{p}_3, \mathsf{p}_4) = 1$. *If* V *and* $\mathring{\mathsf{V}}$ *are* 2×2 *matrices of Laurent polynomials satisfying*

$$\mathsf{V}(z)\mathsf{V}^\star(z) = \mathsf{P}(z) = \mathring{\mathsf{V}}(z)\mathring{\mathsf{V}}^\star(z) \tag{4.3.13}$$

and $\det(\mathring{\mathsf{V}}(z)) = \lambda z^k \det(\mathsf{V}(z))$ *for some* $\lambda \in \mathbb{T}$, $k \in \mathbb{Z}$, *then there exists a* 2×2 *paraunitary matrix* U *of Laurent polynomials such that* $\mathring{\mathsf{V}}(z) = \mathsf{V}(z)\mathsf{U}(z)$, $\det(\mathsf{U}(z)) = \lambda z^k$, *and* $\mathsf{U}(z)\mathsf{U}^\star(z) = I_2$ *for all* $z \in \mathbb{C}\backslash\{0\}$.

Proof. It is a basic result in linear algebra that there exist two 2×2 matrices A and B of Laurent polynomials satisfying $\det(\mathsf{A}(z)) = \det(\mathsf{B}(z)) = 1$ and

$$\mathsf{A}(z)\mathsf{P}(z)\mathsf{B}(z) = \begin{bmatrix} \mathsf{c}(z) & 0 \\ 0 & \mathsf{d}(z) \end{bmatrix} \tag{4.3.14}$$

with c, d being Laurent polynomials satisfying $\mathsf{c} \mid \mathsf{d}$. The above result can be proved using elementary matrix forms and Euclidean division of Laurent polynomials. The diagonal matrix $\operatorname{diag}(\mathsf{c}, \mathsf{d})$ is called the Smith normal form of P and such Laurent polynomials c, d are essentially unique. See [49] for a detailed proof of the above result. Moreover, one can directly verify that

$$\mathsf{c} = \gcd(\mathsf{p}_1, \mathsf{p}_2, \mathsf{p}_3, \mathsf{p}_4) = 1 \quad \text{and} \quad \mathsf{d} = \det(\mathsf{P})/\mathsf{c}. \tag{4.3.15}$$

Consequently, by (4.3.13), we have

$$(\mathsf{A}(z)\mathsf{V}(z))(\mathsf{V}^\star(z)\mathsf{B}(z)) = \begin{bmatrix} 1 & 0 \\ 0 & \mathsf{d}(z) \end{bmatrix} = (\mathsf{A}(z)\mathring{\mathsf{V}}(z))(\mathring{\mathsf{V}}^\star(z)\mathsf{B}(z)). \tag{4.3.16}$$

We now consider two cases: $\det(\mathsf{P}(z)) \not\equiv 0$ or $\det(\mathsf{P}(z)) \equiv 0$.

We first consider the case $\det(\mathsf{P}(z)) \not\equiv 0$, that is, the determinant of P is not identically zero. Note that $\det(\mathsf{A}(z)\mathring{\mathsf{V}}(z)) = \det(\mathsf{A}(z))\det(\mathring{\mathsf{V}}(z)) = \det(\mathring{\mathsf{V}}(z)) = \lambda z^k \det(\mathsf{V}(z)) = \lambda z^k \det(\mathsf{A}(z)\mathsf{V}(z))$. Consequently, it follows from Corollary 2 that there exists a 2×2 matrix U of Laurent polynomials such that $\det(\mathsf{U}(z)) = \lambda z^k$ and $\mathsf{A}(z)\mathring{\mathsf{V}}(z) = \mathsf{A}(z)\mathsf{V}(z)\mathsf{U}(z)$, from which we have $\mathring{\mathsf{V}}(z) = \mathsf{V}(z)\mathsf{U}(z)$ since $\det(\mathsf{A}(z)) = 1$. Therefore, it follows from (4.3.13) that $\mathsf{V}(z)\mathsf{V}^\star(z) = \mathring{\mathsf{V}}(z)\mathring{\mathsf{V}}^\star(z)$ which leads to

$$\mathsf{V}(z)\big(\mathsf{U}(z)\mathsf{U}^\star(z) - I_2\big)\mathsf{V}^\star(z) = 0.$$

By (4.3.13), we have $\det(\mathsf{V}(z))\det(\mathsf{V}^\star(z)) = \det(\mathsf{P}(z)) \not\equiv 0$, hence, $\det(\mathsf{V}(z)) \not\equiv 0$. Therefore, $\mathsf{V}(z)$ is invertible for all z satisfying $\det(\mathsf{V}(z)) \neq 0$. Now we deduce from the above identity that we must have $\mathsf{U}(z)\mathsf{U}^\star(z) = I_2$ for all $z \in \mathbb{C}\backslash\{0\}$. This proves the claim for the case $\det(\mathsf{P}(z)) \not\equiv 0$.

We now study the case $\det(\mathsf{P}(z)) \equiv 0$. Then (4.3.15) implies $\mathsf{d} \equiv 0$ and (4.3.13) implies $\det(\mathsf{V}(z)) \equiv 0$. Applying Proposition 4.1 to the first identity in (4.3.16) and noting that $\mathsf{d} = \det(\mathsf{V}) = 0$, we must have

$$\mathsf{A}(z)\mathsf{V}(z) = \begin{bmatrix} 1 & 0 \\ 0 & 0 \end{bmatrix} \begin{bmatrix} \mathsf{u}_1(z) & -\mathsf{u}_3(z) \\ \mathsf{u}_2(z) & \mathsf{u}_4(z) \end{bmatrix} \quad \text{and} \quad \mathsf{u}_1(z)\mathsf{u}_4(z) + \mathsf{u}_2(z)\mathsf{u}_3(z) = 1$$

for some Laurent polynomials $\mathsf{u}_1, \mathsf{u}_2, \mathsf{u}_3$ and u_4. By (4.3.13) and $\mathsf{V}(z)\mathsf{V}^\star(z) = \mathsf{P}(z)$, it follows from the above identity that

$$\mathsf{A}(z)\mathsf{P}(z)\mathsf{A}^\star(z) = \begin{bmatrix} 1 & 0 \\ 0 & 0 \end{bmatrix} \begin{bmatrix} \mathsf{u}_1(z) & -\mathsf{u}_3(z) \\ \mathsf{u}_2(z) & \mathsf{u}_4(z) \end{bmatrix} \begin{bmatrix} \mathsf{u}_1^\star(z) & \mathsf{u}_2^\star(z) \\ -\mathsf{u}_3^\star(z) & \mathsf{u}_4^\star(z) \end{bmatrix} \begin{bmatrix} 1 & 0 \\ 0 & 0 \end{bmatrix} = \begin{bmatrix} \mathsf{q}(z) & 0 \\ 0 & 0 \end{bmatrix}, \tag{4.3.17}$$

where $\mathsf{q}(z) := \mathsf{u}_1(z)\mathsf{u}_1^\star(z) + \mathsf{u}_3(z)\mathsf{u}_3^\star(z)$. Since $\det(\mathsf{A}(z)) = 1$, by our assumption $\gcd(\mathsf{p}_1, \mathsf{p}_2, \mathsf{p}_3, \mathsf{p}_4) = 1$, the Laurent polynomial q must be a nonzero monomial. Since $\mathsf{q}^\star = \mathsf{q}$, q must be a positive real number. Redefining A, B through scaling by $\text{diag}(\mathsf{q}^{-1/2}, \mathsf{q}^{1/2})\mathsf{A}$ and $\mathsf{B}\text{diag}(\mathsf{q}^{1/2}, \mathsf{q}^{-1/2})$, respectively, we conclude that all (4.3.14), (4.3.16), and (4.3.17) with $\mathsf{q} = 1$ are still satisfied and

$$\mathsf{A}(z)\mathsf{V}(z) = \begin{bmatrix} 1 & 0 \\ 0 & 0 \end{bmatrix} \mathsf{U}_1(z), \ \mathsf{U}_1(z)\mathsf{U}_1^\star(z) = I_2 \text{ with } \mathsf{U}_1(z) := \mathsf{q}^{-1/2} \begin{bmatrix} \mathsf{u}_1(z) & -\mathsf{u}_3(z) \\ \mathsf{u}_3^\star(z) & \mathsf{u}_1^\star(z) \end{bmatrix}.$$

Similarly, by $\mathsf{d} = \det(\mathring{\mathsf{V}}) = 0$ and (4.3.17) with $\mathsf{q} = 1$, we can apply Proposition 4.1 to the second identity in (4.3.16) and conclude that there exists a 2×2 paraunitary matrix U_2 of Laurent polynomials such that

$$\mathsf{A}(z)\mathring{\mathsf{V}}(z) = \begin{bmatrix} 1 & 0 \\ 0 & 0 \end{bmatrix} \mathsf{U}_2(z) \quad \text{and} \quad \mathsf{U}_2(z)\mathsf{U}_2^\star(z) = I_2.$$

Note that there is no further rescaling on the matrices A and B due to the identity in (4.3.17) with $\mathsf{q} = 1$. Define $\mathsf{U}(z) := \mathsf{U}_1^\star(z)\mathsf{U}_2(z)$. Then $\mathring{\mathsf{V}}(z) = \mathsf{V}(z)\mathsf{U}(z)$ holds. Moreover, U is a paraunitary matrix and $\det(\mathsf{U}(z)) = 1$. It is also obvious that $\det(\mathsf{V}) = \det(\mathring{\mathsf{V}}) = 0$. This proves the claim for the case $\det(\mathsf{P}(z)) \equiv 0$. □

We are now ready to prove Theorem 9.

Proof of Theorem 9. (2)$\Longrightarrow$(1) is straightforward. Note that (4.3.4) is equivalent to

$$\begin{bmatrix} \mathsf{b}^p(z) & \mathsf{b}^n(z) \\ \mathsf{b}^p(-z) & \mathsf{b}^n(-z) \end{bmatrix} = \begin{bmatrix} \mathsf{b}_1(z) & \mathsf{b}_2(z) \\ \mathsf{b}_1(-z) & \mathsf{b}_2(-z) \end{bmatrix} \mathsf{U}(z^2), \qquad z \in \mathbb{C}\backslash\{0\}. \tag{4.3.18}$$

Since $\{a; b_1, b_2\}$ is a tight framelet filter bank and U is paraunitary, it follows directly from (4.3.2) and (4.3.18) that $\{a; b^p, b^n\}$ is a finitely supported tight framelet filter bank. Moreover, it follows directly from (4.3.18) that (4.3.3) holds with $\lambda z^k := \det(\mathsf{U}(z))$.

We now prove (1)$\Longrightarrow$(2). For a sequence $u : \mathbb{Z} \to \mathbb{C}$ and $\gamma \in \mathbb{Z}$, its coset sequence $u^{[\gamma]}$ is defined to be $u^{[\gamma]}(k) := u(\gamma+2k)$, $k \in \mathbb{Z}$. Since both $\{a; b_1, b_2\}$ and $\{a; b^p, b^n\}$ are finitely supported tight framelet filter banks, using coset sequences, we see from (4.3.2) that

$$\begin{bmatrix} \mathsf{b}^{p,[0]}(z) & \mathsf{b}^{n,[0]}(z) \\ \mathsf{b}^{p,[1]}(z) & \mathsf{b}^{n,[1]}(z) \end{bmatrix} \begin{bmatrix} \mathsf{b}^{p,[0]}(z) & \mathsf{b}^{n,[0]}(z) \\ \mathsf{b}^{p,[1]}(z) & \mathsf{b}^{n,[1]}(z) \end{bmatrix}^\star = \mathcal{N}_a(z) = \begin{bmatrix} \mathsf{b}_1^{[0]}(z) & \mathsf{b}_2^{[0]}(z) \\ \mathsf{b}_1^{[1]}(z) & \mathsf{b}_2^{[1]}(z) \end{bmatrix} \begin{bmatrix} \mathsf{b}_1^{[0]}(z) & \mathsf{b}_2^{[0]}(z) \\ \mathsf{b}_1^{[1]}(z) & \mathsf{b}_2^{[1]}(z) \end{bmatrix}^\star,$$

where

$$\mathcal{N}_a(z) := \begin{bmatrix} \frac{1}{2} - \mathsf{a}^{[0]}(z)(\mathsf{a}^{[0]}(z))^\star & -\mathsf{a}^{[0]}(z)(\mathsf{a}^{[1]}(z))^\star \\ -(\mathsf{a}^{[0]}(z))^\star \mathsf{a}^{[1]}(z) & \frac{1}{2} - \mathsf{a}^{[1]}(z)(\mathsf{a}^{[1]}(z))^\star \end{bmatrix}.$$

Define $\mathsf{c}(z) := \gcd([\mathcal{N}_a(z)]_{1,1}, [\mathcal{N}_a(z)]_{1,2}, [\mathcal{N}_a(z)]_{2,1}, [\mathcal{N}_a(z)]_{2,2})$. Then we have $2\det(\mathcal{N}_a(z)) = \frac{1}{2} - \mathsf{a}^{[0]}(z)(\mathsf{a}^{[0]}(z))^\star - \mathsf{a}^{[1]}(z)(\mathsf{a}^{[1]}(z))^\star$ and $\operatorname{trace}(\mathcal{N}_a(z)) = 1 - \mathsf{a}^{[0]}(z)(\mathsf{a}^{[0]}(z))^\star - \mathsf{a}^{[1]}(z)(\mathsf{a}^{[1]}(z))^\star$. Therefore, c must be a factor of $\operatorname{trace}(\mathcal{N}_a(z)) - 2\det(\mathcal{N}_a(z)) = 1/2$. Consequently, we conclude that $\mathsf{c} = 1$. By Theorem 10, there must exist a 2×2 paraunitary matrix U of Laurent polynomials such that

$$\begin{bmatrix} \mathsf{b}^{p,[0]}(z) & \mathsf{b}^{n,[0]}(z) \\ \mathsf{b}^{p,[1]}(z) & \mathsf{b}^{n,[1]}(z) \end{bmatrix} = \begin{bmatrix} \mathsf{b}_1^{[0]}(z) & \mathsf{b}_2^{[0]}(z) \\ \mathsf{b}_1^{[1]}(z) & \mathsf{b}_2^{[1]}(z) \end{bmatrix} \mathsf{U}(z) \tag{4.3.19}$$

for all $z \in \mathbb{C}\backslash\{0\}$. Since $\mathsf{u}(z) = \mathsf{u}^{[0]}(z^2) + z\mathsf{u}^{[1]}(z^2)$ holds for any $u \in l_0(\mathbb{Z})$, it is straightforward to deduce from (4.3.19) that (4.3.4) holds. Hence item (ii) is proved.

$\square$

4.4 Algorithms of directional compactly supported complex tight framelet filter banks

This section proposes an algorithm to construct finitely supported complex tight framelet filter banks $\{a; b^p, b^n\}$ with good frequency separation from any eligible finitely supported low-pass filter a. Several examples is provided to illustrate our algorithm.

We first explain how to construct all tight framelet filter banks using Theorem 9. For $b_1,\ b_2 \in l_0(\mathbb{Z})$, define a Laurent polynomial d_{b_1,b_2} by

$$\mathsf{d}_{b_1,b_2}(z^2) := z[\mathsf{b}_1(z)\mathsf{b}_2(-z) - \mathsf{b}_1(-z)\mathsf{b}_2(z)].$$

Then d_{b_1,b_2} is a well-defined Laurent polynomial. It follows from (4.3.2) that

$$|\mathsf{d}_{b_1,b_2}(z^2)|^2 = \det(\mathcal{M}_a(z)) = 1 - |\mathsf{a}(z)|^2 - |\mathsf{a}(-z)|^2, \qquad z \in \mathbb{T}. \tag{4.4.1}$$

If a is an orthogonal filter, $\mathsf{d}_{b_1,b_2} \equiv 0$. Define

$$\mathsf{b}_1(z) := z\mathsf{a}^\star(-z), \quad \mathsf{b}_2(z) \equiv 0. \tag{4.4.2}$$

For $\mathsf{d}_{b_1,b_2} \not\equiv 0$, by Fejér-Riesz lemma, we see that up to a monomial factor there are essentially only finitely many Laurent polynomials d_{b_1,b_2} satisfying (4.4.1). All finitely supported complex tight framelet filter banks $\{a; b_1, b_2\}$ having the shortest possible filter supports can be derived from the low-pass filter a by solving a linear equation system. Consequently, Theorem 9 allows us to obtain all finitely supported complex tight framelet filter banks $\{a; b_1, b_2\}$ with the given low-pass filter a.

For a finitely supported sequence $u = \{u(k)\}_{k\in\mathbb{Z}}$ such that $u(k) = 0$ for all $k \in \mathbb{Z}\backslash[m, n]$ and $u(m)u(n) \neq 0$, define $\operatorname{fsupp}(u) := \operatorname{fsupp}(\mathsf{u}) := [m, n]$ to be the filter support of u and $\operatorname{len}(u) := \operatorname{len}(\mathsf{u}) := n - m$ to be the length of the filter u. We now recall an algorithm, which is a special case of [20, Algorithm 4], to construct an initial finitely supported tight framelet filter bank $\{a; b_1, b_2\}$. In fact, this algorithm can construct all possible complex tight framelet filter banks $\{a; b_1, b_2\}$ with the shortest support length.

Algorithm 1. *Let $a \in l_0(\mathbb{Z})$ be a finitely supported filter on $\mathbb{Z}$ such that $|\mathsf{a}(z)|^2 + |\mathsf{a}(-z)|^2 \leqslant 1$ for all $z \in \mathbb{T}$ and a is not an orthogonal filter.*

(S1) Define $\mathsf{A}(z) := 1 - \mathsf{a}(z)\mathsf{a}^\star(z)$, $\mathsf{B}(z) := -\mathsf{a}(z)\mathsf{a}^\star(-z)$, and $\mathsf{D}(z^2) := 1 - \mathsf{a}(z)\mathsf{a}^\star(z) - \mathsf{a}(-z)\mathsf{a}^\star(-z)$.

(S2) Select $\epsilon, s_1, s_2 \in \{0, 1\}$ and a polynomial d satisfying $\mathsf{d}(z)\mathsf{d}^\star(z) = \mathsf{D}(z)$ with $\lceil \frac{s_1+s_2-1}{2} \rceil \leqslant m_{\mathsf{d}} \leqslant n_{\mathsf{d}} \leqslant \lfloor \frac{s_1+s_2-1}{2} \rfloor + n_0 + \epsilon$, where $[-n_0, n_0] := \operatorname{fsupp}(\mathsf{A})$ and $[m_{\mathsf{d}}, n_{\mathsf{d}}] := \operatorname{fsupp}(\mathsf{d})$.

(S3) Parameterize a filter b_1 by $\mathsf{b}_1(z) = z^{s_1}\sum_{j=0}^{n_0+\epsilon} t_j z^j$. Find the unknown coefficients $\{t_0, \ldots, t_{n_0+\epsilon}\}$ by solving a system X of linear equations induced by $\mathcal{R}(z) \equiv 0$ and coeff$(\mathsf{b}_2^\star, z, j) = 0$ with $j = s_1 - n_0 - 2m_{\mathsf{d}} - 1, \ldots, -s_2 - n_0 - \epsilon - 1$ and $j = 1 - s_2, \ldots, s_1 + 2n_0 - 2n_{\mathsf{d}} + \epsilon - 1$, where $\mathcal{R}$ and $\mathsf{b}_1^\star$ are uniquely determined by $\operatorname{fsupp}(\mathcal{R}) \subseteq [2m_{\mathsf{d}}, 2n_{\mathsf{d}} - 1]$ and

$$\mathsf{B}(-z)\mathsf{b}_1(z) - \mathsf{A}(z)\mathsf{b}_1(-z) = \mathsf{d}(z^2)z\mathsf{b}_2^\star(z) + \mathcal{R}(z).$$

(S4) For any nontrivial solution to the system X in (S3), there must exist $\lambda > 0$ such that

$$\lambda \mathsf{d}(z^2) = z^{-1}[\mathsf{b}_1(z)\mathsf{b}_2(-z) - \mathsf{b}_1(-z)\mathsf{b}_2(z)]$$

holds. Replace $\mathsf{b}_1, \mathsf{b}_2$ by $\lambda^{-1/2}\mathsf{b}_1, \lambda^{-1/2}\mathsf{b}_2$, respectively.

Then $\{a; b_1, b_2\}$ is a finitely supported tight framelet filter bank satisfying

$$\max(\mathrm{len}(b_1), \mathrm{len}(b_2)) \leqslant \mathrm{len}(a) + \epsilon,$$

with $\mathrm{fsupp}(\mathsf{b}_1) \subseteq [s_1, s_1 + n_0 + \epsilon]$ and $\mathrm{fsupp}(\mathsf{b}_2) \subseteq [s_2, s_2 + n_0 + \epsilon]$.

We are now ready to present an algorithm to construct finitely supported complex tight framelet filter banks with frequency separation.

Algorithm 2. *Let $a \in l_0(\mathbb{Z})$ be a finitely supported filter on $\mathbb{Z}$ such that $|\mathsf{a}(z)|^2 + |\mathsf{a}(-z)|^2 \leqslant 1$ for all $z \in \mathbb{T}$.*

(S1) If a is not an orthogonal filter, construct a finitely supported tight framelet filter bank $\{a; b_1, b_2\}$ by Algorithm 1; if a is an orthogonal filter, construct $\{a; b_1, b_2\}$ by (4.4.2).

(S2) Choose a suitable filter length $N \in \mathbb{N} \cup \{0\}$ and parameterize filters u_1 and u_2 by

$$\mathsf{u}_1(z) := c_0 + c_1 z + \cdots + c_N z^N, \qquad \mathsf{u}_2(z) := d_0 + d_1 z + \cdots + d_N z^N,$$

where $c_0, \ldots, c_N, d_0, \ldots, d_N$ are complex numbers to be determined later. We can further assume $c_0 \in \mathbb{R}$ by normalizing the first filter u_1.

(S3) Define new high-pass filters b^p and b^n by

$$\mathsf{b}^p(z) := \mathsf{b}_1(z)\mathsf{u}_1(z^2) + \mathsf{b}_2(z)\mathsf{u}_2(z^2), \quad \mathsf{b}^n(z) := z^{2m}[\mathsf{b}_2(z)\mathsf{u}_1^\star(z^2) - \mathsf{b}_1(z)\mathsf{u}_2^\star(z^2)],$$

where m is an integer such that the centers of $\operatorname{fsupp}(\mathsf{b}^p)$ *and* $\operatorname{fsupp}(\mathsf{b}^n)$ *are close to each other.*

(S4) *If in addition the given filter a is real, then we further require that the initial filters b_1, b_2 should be real and $c_0, \dots, c_N, d_0, \dots, d_N \in \mathbb{R}$. Further replace the filters b^p and b^n in (S3) by $[\mathsf{b}^p(z) + i\mathsf{b}^n(z)]/\sqrt{2}$ and $[\mathsf{b}^p(z) - i\mathsf{b}^n(z)]/\sqrt{2}$, respectively.*

(S5) *Find a solution $\{c_0, \dots, c_N, d_0, \dots, d_N\}$ of the following constrained optimization problem:*

$$\min_{u_1,u_2} \int_0^{\pi} [|\mathsf{b}^p(-e^{-i\xi})|^2 + |\mathsf{b}^n(e^{-i\xi})|^2] d\xi$$

under the constraint $|\mathsf{u}_1(e^{-i\xi})|^2 + |\mathsf{u}_2(e^{-i\xi})|^2 = 1$ for all $\xi \in \mathbb{R}$ (such constraint on u_1, u_2 can be rewritten as equations using $c_0, \dots, c_N, d_0, \dots, d_N$).

Then $\{a; b^p, b^n\}$ is a tight framelet filter bank. For a real filter a, we additionally have $b^n = \overline{b^p}$.

4.5 Exmaples

Here several examples are presented to illustrate Algorithms 1 and 2. In order to see the improvement of directionality of a tight framelet filter bank $\{a; b^p, b^n\}$, we use the following quantities:

$$\begin{aligned} &d_{\mathbb{R}} := \tfrac{1}{2}\int_0^{\pi} [2 - |\widehat{a}(\xi)|^2 - |\widehat{a}(\xi+\pi)|^2] d\xi, \quad d_A := \int_0^{\pi} A(\xi) d\xi, \\ &d_B := \int_0^{\pi} [|\widehat{b^p}(\xi+\pi)|^2 + |\widehat{b^n}(\xi)|^2] d\xi, \end{aligned} \tag{4.5.1}$$

where the sharp theoretical lower bound frequency separation function A is defined in (4.2.2) and the subscript $\mathbb{R}$ in $d_{\mathbb{R}}$ refers to the case of real high-pass filters. By

Theorem 6, we always have $d_A \leqslant d_B$. If both b^p and b^n are real filters, by Theorem 8 we always have $d_{\mathbb{R}} = d_B$.

Example 5. Let $\mathsf{a}(z) = (z^{-1}+2+z)/4 = \{\frac{1}{4}, \frac{1}{2}, \frac{1}{4}\}_{[-1,1]}$ be the B-spline filter of order 2. Using Algorithm 1, we obtain a tight framelet filter bank $\{a; b_1, b_2\}$ with $\mathsf{b}_1(z) = \frac{\sqrt{6}}{6}(1-z^{-1})$ and $\mathsf{b}_2(z) = \frac{\sqrt{3}}{12}(1-z^{-1})(1+3z)$. Applying Algorithm 2 with $N = 0$, we have a finitely supported complex tight framelet filter bank $\{a; b^p, b^n\}$ with $b^n = \overline{b^p}$ and

$$\mathsf{b}^p(z) := \tfrac{1}{8}(1-z^{-1})[(-\sqrt{2}+2i)z + (\sqrt{2}+2i)].$$

By calculation we have $d_{\mathbb{R}} = \frac{5}{8}\pi \approx 1.96349$, $d_A \approx 0.05339$, and $d_B \approx 0.549282$. If we take $N = 2$, then

$$\begin{aligned}\mathsf{b}^p(z) =&(-0.029642235761 + 0.024549845327i)z^{-3} + (0.065991543776\\ &- 0.054654520855i)z^{-2} - (0.134097034666 - 0.310569363503i)z^{-1}\\ &- (0.199259492567 + 0.279133899131i) + (0.256396707847\\ &- 0.0503651650857i)z + (0.00392785810329 + 0.00474261627248i)z^2\\ &+ (0.0366826532672 + 0.0442917599689i)z^3.\end{aligned}$$

By calculation, we have $d_B \approx 0.329559$. See Figure 4.1 for the graphs of the eight tight framelet generators in the associated two-dimensional real tight framelet for $L_2(\mathbb{R}^2)$ in (2.2.9).

Example 6. Let $\mathsf{a}(z) = z^{-2}(1+z)^4/16 = \{\frac{1}{16}, \frac{1}{4}, \frac{3}{8}, \frac{1}{4}, \frac{1}{16}\}_{[-2,2]}$ be the B-spline filter of order 4. Using Algorithm 1, we obtain a tight framelet filter bank $\{a; b_1, b_2\}$ with $\mathsf{b}_1(z) = \frac{1}{80}(z-1)(3z^3+15z^2+41z+5)$ and $\mathsf{b}_2(z) = \frac{1}{80}(4+\sqrt{14})(z-1)(z+5)(z^2+15-4\sqrt{14})$. Applying Algorithm 2 with $N = 0$, we have a finitely

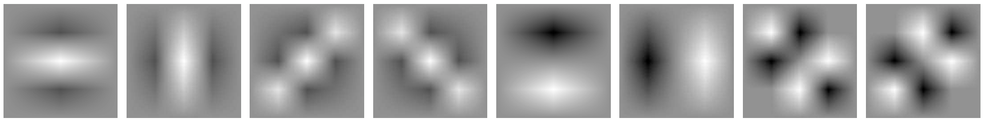

Figure 4.1: The eight two-dimensional generators of compactly supported $\mathrm{TP}\text{-}\mathbb{C}\mathrm{TF}_3$ in Example 5 with $N = 0$: the first four for real part and the last four for imaginary part.

supported complex tight framelet filter bank $\{a; b^p, b^n\}$ with $b^n = \overline{b^p}$ and

$$\begin{aligned}\mathsf{b}^p(z) =& (-0.00557089416719 + 0.0731736018309i)z^{-2} + (-0.0222835766688\\ &+ 0.292694407324i)z^{-1} - (0.318357701145 + 0.258767723882i)\\ &+ (0.307215912811 - 0.0833775092464i)z + (0.0389962591703\\ &- 0.0237227760259i)z^2.\end{aligned}$$

By calculation we have $d_{\mathbb{R}} = \frac{93}{128}\pi \approx 2.28256$, $d_A \approx 0.00187$, and $d_B \approx 0.762678$. If we take $N = 2$, then

$$\begin{aligned}\mathsf{b}^p(z) =& (0.0136422120987 - 0.00936825359825i)z^{-4} + (0.0545688483947\\ &- 0.0374730143930i)z^{-3} - (0.117755602061 - 0.0384179743194i)z^{-2}\\ &+ (0.176657429397 - 0.291096804867i)z^{-1} + (0.215352648865\\ &+ 0.333764545470i) - (0.226650219509 - 0.0670651937025i)z\\ &- (0.0454200982851 - 0.00120108848925i)z^2 - (0.0601885257055\\ &+ 0.0876475668564i)z^3 - (0.0102066931945 + 0.0148631622666i)z^4.\end{aligned}$$

By calculation, we have $d_B \approx 0.283860$. See Figure 4.2 for the graphs of the eight tight framelet generators in the associated two-dimensional real tight framelet for $L_2(\mathbb{R}^2)$ in (2.2.9).

Example 7. Let $\mathsf{a}(z) = -\frac{1}{32}z^{-3} + \frac{9}{32}z^{-1} + \frac{1}{2} + \frac{9}{32}z - \frac{1}{32}z^3 = \{-\frac{1}{32}, 0, \frac{9}{32}, \frac{1}{2}, \frac{9}{32}, 0, -\frac{1}{32}\}_{[-3,3]}$

be an interpolatory filter. Using Algorithm 1, we obtain a tight framelet filter bank $\{a; b_1, b_2\}$ with $\mathsf{b}_1(z) = \frac{\sqrt{33}}{1056} z^{-3}(z-1)^2(z+3)(z-5)(z^2+4z+1)$ and $\mathsf{b}_2(z) = -\frac{\sqrt{22}}{1056} z^{-3}(z-1)^2(2\sqrt{3}+3)(z+2-\sqrt{3})(z-2+\sqrt{3})(z^2+2z+9)$. Applying Algorithm 2 with $N = 0$, we have a finitely supported complex tight framelet filter bank $\{a; b^p, b^n\}$ with $b^n = \overline{b^p}$ and

$$\begin{aligned}\mathsf{b}^p(z) =&(0.000765760176767 + 0.00404161855344i)z^{-3} - (0.0403653729403\\&+ 0.0880450827059i)z^{-1} - (0.0122521628283 + 0.0646658968550i)\\&+ (0.267462323475 + 0.228631206606i)z - (0.341301227765\\&- 0.0646658968550i)z^2 + (0.125690679882 - 0.144627742454i)z^3.\end{aligned}$$

By calculation we have $d_{\mathbb{R}} = \frac{151}{256}\pi \approx 1.85305$, $d_A \approx 0.03719$, and $d_B \approx 0.690756$. If we take $N = 2$, then

$$\begin{aligned}\mathsf{b}^p(z) =&(0.000127813163114 + 0.000468578346241i)z^{-5} - (0.00306783185075\\&+ 0.0157028980677i)z^{-3} - (0.00204501060982 + 0.00749725353985i)z^{-2}\\&+ (-0.0374047192910 + 0.0481138677951i)z^{-1} - (0.0665960959763\\&+ 0.172855502749i) + (0.350214784764 + 0.131605792365i)z\\&- (0.245342403089 - 0.169559360297i)z^2 - (0.0151368278988\\&+ 0.148441081755i)z^3 - (0.0395698809181 - 0.0107933959918i)z^4\end{aligned}$$

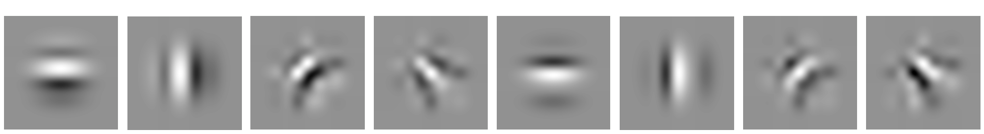

Figure 4.2: The eight two-dimensional generators of compactly supported $\mathrm{TP}\text{-}\mathbb{C}\mathrm{TF}_3$ in Example 6 with $N = 2$: the first four for real part and the last four for imaginary part.

$$+ (0.0588201717073 - 0.0160442586840i)z^5.$$

By calculation, we have $d_B \approx 0.307271$. See Figure 4.3 for the graphs of the eight tight framelet generators in the associated two-dimensional real tight framelet for $L_2(\mathbb{R}^2)$ in (2.2.9).

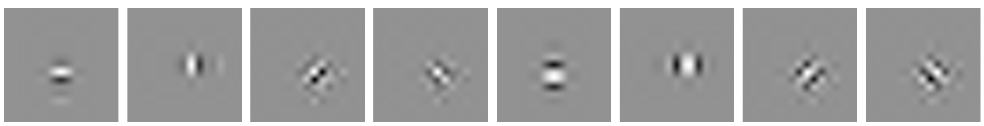

Figure 4.3: The eight two-dimensional generators of compactly supported $\mathrm{TP}\text{-}\mathbb{C}\mathrm{TF}_3$ in Example 7 with $N = 2$: the first four for real part and the last four for imaginary part.

Example 8. Let $\mathsf{a}(z) = -\frac{3}{64}z^{-2} + \frac{5}{64}z^{-1} + \frac{15}{32} + \frac{15}{32}z + \frac{5}{64}z^2 - \frac{3}{64}z^3 = \{-\frac{3}{64}, \frac{5}{64}, \frac{15}{32}, \frac{15}{32}, \frac{5}{64}, -\frac{3}{64}\}_{[-2,3]}$. Using Algorithm 1, we obtain a tight framelet filter bank $\{a; b_1, b_2\}$ with

$$\mathsf{b}_1(z) = \frac{\sqrt{297879}}{6354752}z^{-2}(z-1)^2(3203z^3 + 1921z^2 - 31z - 93),$$
$$\mathsf{b}_2(z) = -\frac{\sqrt{496465}}{794344}z^{-2}(z-1)^2(248z^2 + z + 3).$$

Applying Algorithm 2 with $N = 0$, we have a finitely supported complex tight framelet filter bank $\{a; b^p, b^n\}$ with $b^n = \overline{b^p}$ and

$$\begin{aligned}\mathsf{b}^p(z) =& (-0.00427685553137 + 0.00414104756178i)z^{-2} + (0.00712809255228 \\ & - 0.00690174593631i)z^{-1} - (0.0855371106274 + 0.173923997595i) \\ & + (0.256611331882 + 0.179445394344i)z - (0.263739424434 \\ & - 0.169782950033i)z^2 + (0.0898139661588 - 0.172543648408i)z^3.\end{aligned}$$

By calculation we have $d_{\mathbb{R}} = \frac{557}{1024}\pi \approx 1.70885$, $d_A \approx 0.12595$, and $d_B \approx 0.444929$.

If we take $N = 2$, then

$$
\begin{aligned}
\mathsf{b}^p(z) =&(0.000174962462941 + 0.000667428960698i)z^{-4} - (0.000291604104902 \\
&+ 0.00111238160116i)z^{-3} + (0.00604271655936 + 0.00470763073231i)z^{-2} \\
&- (0.0147368599440 + 0.0256441568391i)z^{-1} + (0.119900001836 \\
&+ 0.197463905829i) - (0.282016222613 + 0.153449185519i)z \\
&(0.207557346014 - 0.197627972771i)z^2 + (-0.0335526030334 \\
&+ 0.174187921033i)z^3 + (0.0198783637212 - 0.00521099275084i)z^4 \\
&+ (-0.0229561008975 + 0.00601780292595i)z^5.
\end{aligned}
$$

By calculation, we have $d_B \approx 0.387149$. See Figure 4.4 for the graphs of the eight tight framelet generators in the associated two-dimensional real tight framelet for $L_2(\mathbb{R}^2)$ in (2.2.9).

Figure 4.4: The eight two-dimensional generators of compactly supported $\mathrm{TP}\text{-}\mathbb{C}\mathrm{TF}_3$ in Example 8 with $N = 2$: the first four for real part and the last four for imaginary part.

Chapter 5

Compactly Supported Tensor Product Complex Tight Framelets $\mathrm{TP}\text{-}\mathbb{C}\mathrm{TF}_4$ and $\mathrm{TP}\text{-}\mathbb{C}\mathrm{TF}_6$

Compactly supported wavelets and framelets are important due to good space-frequency localization and efficient computational algorithms. Based on the exemplary role of compactly supported $\mathrm{TP}\text{-}\mathbb{C}\mathrm{TF}_3$, this chapter studies and constructs compactly supported $\mathrm{TP}\text{-}\mathbb{C}\mathrm{TF}_4$ and $\mathrm{TP}\text{-}\mathbb{C}\mathrm{TF}_6$ by optimization techniques such that they perform comparably well as their band-limited counterpart in image processing. We completely answer the question on what type of low-pass filters are suitable for the construction of compactly supported $\mathrm{TP}\text{-}\mathbb{C}\mathrm{TF}_4$ and $\mathrm{TP}\text{-}\mathbb{C}\mathrm{TF}_6$. Step-by-step algorithms are provided for constructing finitely supported $\mathrm{TP}\text{-}\mathbb{C}\mathrm{TF}_4$ and $\mathrm{TP}\text{-}\mathbb{C}\mathrm{TF}_6$ having small frequency separation with prescribed filter supports. Several concrete numerical examples are presented to illustrate the results and algorithms. The results in this chapter have been summarized in [22].

5.1 Splitting low-pass filters with frequency separation property

As discussed in [23, 24], the directionality of tensor product filters is closely related to the frequency separation. For a filter $b = \{b(k)\}_{k\in\mathbb{Z}}$ which is not identically zero, we define the following quantities to measure the frequency separation of filter b:

$$\mathrm{fsp}(b) := \frac{\min\left\{2\int_{-\pi}^{0}|\widehat{b}(\xi)|^2 d\xi, 2\int_{0}^{\pi}|\widehat{b}(\xi)|^2 d\xi\right\}}{\int_{-\pi}^{\pi}|\widehat{b}(\xi)|^2 d\xi}. \tag{5.1.1}$$

It is straightforward to observe that $0 \leqslant \mathrm{fsp}(b) \leqslant 1$. The smaller the quantity $\mathrm{fsp}(b)$ is, the better the frequency separation of the filter b will have. If b is a real filter, since $\widehat{b}(\xi) = \overline{\widehat{b}(-\xi)}$, it is trivial to see that $\mathrm{fsp}(b) = 1$. However, things can be quite different for complex filters.

For any complex tight framelet filter bank $\{a; b^p, b^n\}$ with $\widehat{b^n}(\xi) = \overline{\widehat{b^p}(-\xi)}$, Theorem 6 implies that

$$\mathrm{fsp}(b^p) = \mathrm{fsp}(b^n) \geqslant \frac{2\int_0^{\pi} A(\xi)d\xi}{\int_{-\pi}^{\pi} 1 - |\widehat{a}(\xi)|^2 d\xi} =: \mathrm{fsp}(a|\mathbf{hp}),$$

where hp in $\mathrm{fsp}(a|\mathbf{hp})$ stands for high-pass. As shown in [23, Theorem 2], the quantity $\mathrm{fsp}(a|\mathbf{hp})$ is often very small for most known low-pass filters in the literature.

Note that the main difference between $\mathbb{C}\mathrm{TF}_{2s+1}$ and $\mathbb{C}\mathrm{TF}_{2s+2}$ lies in that the low-pass filter a in $\mathbb{C}\mathrm{TF}_{2s+1}$ has to be split into two one-sided auxiliary filters a^p and a^n. This section discusses how to split a given real low-pass filter a into two one-sided auxiliary filters a^p and a^n such that $a^n = \overline{a^p}$.

5.1.1 Analysis and algorithm for splitting a low-pass filter into two auxiliary filters

Similarly to Theorem 6, a^p and a^n still have a sharp lower bound as demonstrated by the following result.

Theorem 11. *Let $a \in l_2(\mathbb{Z})$ be a complex filter on $\mathbb{Z}$. For any complex filters $a^p, a^n \in l_2(\mathbb{Z})$ satisfying*

$$|\widehat{a^p}(\xi)|^2 + |\widehat{a^n}(\xi)|^2 = |\widehat{a}(\xi)|^2, \quad \widehat{a^p}(\xi)\overline{\widehat{a^p}(\xi+\pi)} + \widehat{a^n}(\xi)\overline{\widehat{a^n}(\xi+\pi)} = \widehat{a}(\xi)\overline{\widehat{a}(\xi+\pi)}, \tag{5.1.2}$$

for $a.e.\, \xi \in \mathbb{R}$, then

$$|\widehat{a^p}(\xi+\pi)|^2 + |\widehat{a^n}(\xi)|^2 \geqslant \min(|\widehat{a}(\xi)|^2, |\widehat{a}(\xi+\pi)|^2), \quad a.e.\, \xi \in [0, \pi]. \tag{5.1.3}$$

Moreover, the inequality in (5.1.3) is sharp in the sense that there exist filters $a^p, a^n \in l_2(\mathbb{Z})$ satisfying (5.1.2) and

$$|\widehat{a^p}(\xi+\pi)|^2 + |\widehat{a^n}(\xi)|^2 = \min(|\widehat{a}(\xi)|^2, |\widehat{a}(\xi+\pi)|^2), \qquad a.e.\, \xi \in [0, \pi]. \tag{5.1.4}$$

If in addition a is real (or more generally, $|\widehat{a}(-\xi)| = |\widehat{a}(\xi)|$), then the relation $a^n = \overline{a^p}$ is also satisfied by the particular filters a^p, a^n defined in (5.1.9) and (5.1.10).

Proof. Since $\widehat{a}$ is a 2π-periodic function, the conditions in (5.1.2) are equivalent to

$$|\widehat{a^p}(\xi)|^2 + |\widehat{a^n}(\xi)|^2 = |\widehat{a}(\xi)|^2, \tag{5.1.5}$$

$$|\widehat{a^p}(\xi+\pi)|^2 + |\widehat{a^n}(\xi+\pi)|^2 = |\widehat{a}(\xi+\pi)|^2, \tag{5.1.6}$$

$$\widehat{a^p}(\xi)\overline{\widehat{a^p}(\xi+\pi)} + \widehat{a^n}(\xi)\overline{\widehat{a^n}(\xi+\pi)} = \widehat{a}(\xi)\overline{\widehat{a}(\xi+\pi)}, \tag{5.1.7}$$

for almost every $\xi \in [0, \pi]$. Consequently, by (5.1.5) – (5.1.7) and Cauchy-Schwarz inequality, we have

$$
\begin{aligned}
|\widehat{a}(\xi)\widehat{a}(\xi+\pi)|^2 &\leqslant \left(|\widehat{a^p}(\xi+\pi)\widehat{a^p}(\xi)| + |\widehat{a^n}(\xi)\widehat{a^n}(\xi+\pi)|\right)^2 \\
&\leqslant \left(|\widehat{a^p}(\xi+\pi)|^2 + |\widehat{a^n}(\xi)|^2\right)\left(|\widehat{a^p}(\xi)|^2 + |\widehat{a^n}(\xi+\pi)|^2\right) \\
&= \left(|\widehat{a^p}(\xi+\pi)|^2 + |\widehat{a^n}(\xi)|^2\right)\left(|\widehat{a}(\xi)|^2 - |\widehat{a^n}(\xi)|^2 + |\widehat{a}(\xi+\pi)|^2 - |\widehat{a^p}(\xi+\pi)|^2\right),
\end{aligned}
$$

for $\xi \in [0,\pi]$. Let $F(\xi) := |\widehat{a^p}(\xi+\pi)|^2 + |\widehat{a^n}(\xi)|^2$. Then the above inequality can be rewritten as

$$
|\widehat{a}(\xi)\widehat{a}(\xi+\pi)|^2 \leqslant F(\xi)\left(|\widehat{a}(\xi)|^2 + |\widehat{a}(\xi+\pi)|^2 - F(\xi)\right). \tag{5.1.8}
$$

Solving (5.1.8) for $F(\xi)$, we conclude that

$$
\begin{aligned}
F(\xi) \geqslant& \frac{|\widehat{a}(\xi)|^2 + |\widehat{a}(\xi+\pi)|^2 - \sqrt{(|\widehat{a}(\xi)|^2 + |\widehat{a}(\xi+\pi)|^2)^2 - 4|\widehat{a}(\xi)\widehat{a}(\xi+\pi)|^2}}{2} \\
=& \frac{|\widehat{a}(\xi)|^2 + |\widehat{a}(\xi+\pi)|^2 - \left||\widehat{a}(\xi)|^2 - |\widehat{a}(\xi+\pi)|^2\right|}{2} = \min(|\widehat{a}(\xi)|^2, |\widehat{a}(\xi+\pi)|^2).
\end{aligned}
$$

This proves (5.1.3).

We now concretely construct filters $a^p, a^n \in l_2(\mathbb{Z})$ satisfying (5.1.3), (5.1.5) and (5.1.6).

For $\xi \in [0,\pi]$, we define

$$
\widehat{a^p}(\xi+\pi) := \begin{cases} |\widehat{a}(\xi)|/\sqrt{2} & \text{if } |\widehat{a}(\xi)| = |\widehat{a}(\xi+\pi)|, \\ |\widehat{a}(\xi+\pi)| & \text{if } |\widehat{a}(\xi)| > |\widehat{a}(\xi+\pi)|, \\ 0 & \text{if } |\widehat{a}(\xi)| < |\widehat{a}(\xi+\pi)|, \end{cases} \tag{5.1.9}
$$

$$
\widehat{a^n}(\xi) := \begin{cases} |\widehat{a}(\xi)|/\sqrt{2} & \text{if } |\widehat{a}(\xi)| = |\widehat{a}(\xi+\pi)|, \\ 0 & \text{if } |\widehat{a}(\xi)| > |\widehat{a}(\xi+\pi)|, \\ |\widehat{a}(\xi)| & \text{if } |\widehat{a}(\xi)| < |\widehat{a}(\xi+\pi)|, \end{cases} \tag{5.1.10}
$$

and

$$\begin{aligned}\widehat{a^p}(\xi) &:= -e^{i\beta(\xi)}\sqrt{|\widehat{a}(\xi)|^2 - |\widehat{a^n}(\xi)|^2}\\ \widehat{a^n}(\xi+\pi) &:= -e^{-i\beta(\xi)}\sqrt{|\widehat{a}(\xi+\pi)|^2 - |\widehat{a^p}(\xi+\pi)|^2},\end{aligned} \tag{5.1.11}$$

where $\beta(\xi)$ is defined in (4.2.13) denoting the phase of $\widehat{a}(\xi)\overline{\widehat{a}(\xi+\pi)}$.

We show that $\widehat{a^p}(\xi)$ and $\widehat{a^n}(\xi+\pi)$ in (5.1.11) are well defined and all the conditions in (5.1.4) and (5.1.5) – (5.1.7) are satisfied. Let $\xi \in [0,\pi]$ be arbitrarily fixed. We now consider three cases.

Case 1: $|\widehat{a}(\xi)| = |\widehat{a}(\xi+\pi)|$. By (5.1.9) and (5.1.10), we have

$$\widehat{a^p}(\xi+\pi) = |\widehat{a}(\xi)|/\sqrt{2} = |\widehat{a}(\xi+\pi)|/\sqrt{2}, \quad \widehat{a^n}(\xi) = |\widehat{a}(\xi)|/\sqrt{2}.$$

The above identities imply that $\widehat{a^p}(\xi)$ and $\widehat{a^n}(\xi+\pi)$ in (5.1.11) are well defined. More explicitly,

$$\begin{aligned}\widehat{a^p}(\xi) &:= -e^{i\beta(\xi)}\sqrt{|\widehat{a}(\xi)|^2 - |\widehat{a^n}(\xi)|^2} = -e^{i\beta(\xi)}|\widehat{a}(\xi)|/\sqrt{2},\\ \widehat{a^n}(\xi+\pi) &:= -e^{-i\beta(\xi)}\sqrt{|\widehat{a}(\xi+\pi)|^2 - |\widehat{a^p}(\xi+\pi)|^2} = -e^{-i\beta(\xi)}|\widehat{a}(\xi+\pi)|/\sqrt{2}.\end{aligned}$$

By the definition of $\beta(\xi)$, all (5.1.4) and (5.1.5) – (5.1.7) are satisfied.

Case 2: $|\widehat{a}(\xi)| > |\widehat{a}(\xi+\pi)|$. By (5.1.9) and (5.1.10), we have

$$\widehat{a^p}(\xi+\pi) = |\widehat{a}(\xi+\pi)|, \quad \widehat{a^n}(\xi) = 0.$$

The above identities imply that $\widehat{a^p}(\xi)$ and $\widehat{a^n}(\xi+\pi)$ in (5.1.11) are well defined. More explicitly,

$$\begin{aligned}\widehat{a^p}(\xi) &:= -e^{i\beta(\xi)}\sqrt{|\widehat{a}(\xi)|^2 - |\widehat{a^n}(\xi)|^2} = -e^{i\beta(\xi)}|\widehat{a}(\xi)|,\\ \widehat{a^n}(\xi+\pi) &:= -e^{-i\beta(\xi)}\sqrt{|\widehat{a}(\xi+\pi)|^2 - |\widehat{a^p}(\xi+\pi)|^2} = 0.\end{aligned}$$

By the definition of $\beta(\xi)$, (5.1.4) and (5.1.5)– (5.1.7) are satisfied.

Case 3: $|\widehat{a}(\xi)| < |\widehat{a}(\xi+\pi)|$. This case is similar to Case 2. By (5.1.9) and

(5.1.10), we have

$$\widehat{a^p}(\xi+\pi)=0, \quad \widehat{a^n}(\xi)=|\widehat{a}(\xi)|.$$

The above identities imply that

$$\widehat{a^p}(\xi) := -e^{i\beta(\xi)}\sqrt{|\widehat{a}(\xi)|^2-|\widehat{a^n}(\xi)|^2}=0,$$
$$\widehat{a^n}(\xi+\pi) := -e^{-i\beta(\xi)}\sqrt{|\widehat{a}(\xi+\pi)|^2-|\widehat{a^p}(\xi+\pi)|^2}=-e^{-i\beta(\xi)}|\widehat{a}(\xi+\pi)|^2.$$

By the definition of $\beta(\xi)$, all (5.1.4) and (5.1.5) – (5.1.7) are satisfied. □

For a real filter a, according to Theorem 11, we must have

$$\mathrm{fsp}(a^p)=\mathrm{fsp}(a^n)\geqslant \frac{2\int_0^\pi \min(|\widehat{a}(\xi)|^2,|\widehat{a}(\xi+\pi)|^2)d\xi}{\int_{-\pi}^\pi |\widehat{a}(\xi)|^2 d\xi} =: \mathrm{fsp}(a|\mathbf{lp}),$$

where lp in $\mathrm{fsp}(a|\mathrm{lp})$ stands for low-pass.

We now study how to split filter a into two finitely supported filters a^p and a^n.

Theorem 12. *Let $a, a^p, a^n \in l_0(\mathbb{Z})$ be filters on $\mathbb{Z}$ such that the two Laurent polynomials $\sum_{k\in\mathbb{Z}} a(k)z^k$ and $\sum_{k\in\mathbb{Z}} a(k)(-z)^k$ do not have common zeros on $\mathbb{C}\backslash\{0\}$. Then (5.1.2) holds if and only if there exist $u_1, u_2 \in l_0(\mathbb{Z})$ such that*

$$\widehat{a^p}(\xi)=\widehat{a}(\xi)\widehat{u_1}(2\xi), \quad \widehat{a^n}(\xi)=\widehat{a}(\xi)\widehat{u_2}(2\xi), \quad |\widehat{u_1}(\xi)|^2+|\widehat{u_2}(\xi)|^2=1. \quad (5.1.12)$$

If in addition a is real, then both $a^n=\overline{a^p}$ and (5.1.2) are satisfied if and only if (5.1.12) holds for some $u_1, u_2 \in l_0(\mathbb{Z})$ satisfying $u_2=\overline{u_1}$.

Proof. Necessity is a direct calculation. We only need to prove the sufficient part.

Suppose (5.1.2) holds. In terms of matrices, (5.1.2) is

$$\begin{bmatrix} \widehat{a^p}(\xi) & \widehat{a^n}(\xi) \\ \widehat{a^p}(\xi+\pi) & \widehat{a^n}(\xi+\pi) \end{bmatrix} \begin{bmatrix} \overline{\widehat{a^p}(\xi)} & \overline{\widehat{a^p}(\xi+\pi)} \\ \overline{\widehat{a^n}(\xi)} & \overline{\widehat{a^n}(\xi+\pi)} \end{bmatrix} = \begin{bmatrix} |\widehat{a}(\xi)|^2 & \widehat{a}(\xi)\overline{\widehat{a}(\xi+\pi)} \\ \overline{\widehat{a}(\xi)}\widehat{a}(\xi+\pi) & |\widehat{a}(\xi+\pi)|^2 \end{bmatrix}. \quad (5.1.13)$$

For a sequence $u : \mathbb{Z} \to \mathbb{C}$ and $\gamma \in \mathbb{Z}$, the coset sequence $u^{[\gamma]}$ is defined to be $u^{[\gamma]}(k) := u(\gamma + 2k), k \in \mathbb{Z}$. Since a^p, a^n, and a are all finitely supported filters, we see that (5.1.13) in terms of coset sequences is

$$\begin{bmatrix} \widehat{a^{p[0]}}(\xi) & \widehat{a^{n[0]}}(\xi) \\ \widehat{a^{p[1]}}(\xi) & \widehat{a^{n[1]}}(\xi) \end{bmatrix} \begin{bmatrix} \overline{\widehat{a^{p[0]}}(\xi)} & \overline{\widehat{a^{p[1]}}(\xi)} \\ \overline{\widehat{a^{n[0]}}(\xi)} & \overline{\widehat{a^{n[1]}}(\xi)} \end{bmatrix} = \begin{bmatrix} \widehat{a^{[0]}}(\xi)\overline{\widehat{a^{[0]}}(\xi)} & \widehat{a^{[0]}}(\xi)\overline{\widehat{a^{[1]}}(\xi)} \\ \widehat{a^{[1]}}(\xi)\overline{\widehat{a^{[0]}}(\xi)} & \widehat{a^{[1]}}(\xi)\overline{\widehat{a^{[1]}}(\xi)} \end{bmatrix}$$
$$= \begin{bmatrix} \widehat{a^{[0]}}(\xi) & 0 \\ \widehat{a^{[1]}}(\xi) & 0 \end{bmatrix} \begin{bmatrix} \overline{\widehat{a^{[0]}}(\xi)} & \overline{\widehat{a^{[1]}}(\xi)} \\ 0 & 0 \end{bmatrix}.$$

Since $\sum_{k\in\mathbb{Z}} a(k)z^k$ and $\sum_{k\in\mathbb{Z}} a(k)(-z)^k$ do not have common zeros on $\mathbb{C}\backslash\{0\}$, $\widehat{a^{[0]}}(\xi)\overline{\widehat{a^{[0]}}(\xi)}$, $\widehat{a^{[0]}}(\xi)\overline{\widehat{a^{[1]}}(\xi)}$, $\widehat{a^{[1]}}(\xi)\overline{\widehat{a^{[0]}}(\xi)}$, and $\widehat{a^{[1]}}(\xi)\overline{\widehat{a^{[1]}}(\xi)}$ have no common zeros for $\xi \in \mathbb{T}$. Also, since $\widehat{a^p}(\xi)$ and $\widehat{a^n}(\xi)$ are 2π periodic functions, by direct calculation, we have $\det(\left[\begin{smallmatrix} \widehat{a^{p[0]}}(\xi) & \widehat{a^{n[0]}}(\xi) \\ \widehat{a^{p[1]}}(\xi) & \widehat{a^{n[1]}}(\xi) \end{smallmatrix}\right]) = \det(\left[\begin{smallmatrix} \widehat{a^{[0]}}(\xi) & 0 \\ \widehat{a^{[1]}}(\xi) & 0 \end{smallmatrix}\right]) = 0$. Then by Theorem 10, there exists a 2×2 paraunitary matrix U of Laurent polynomials such that

$$\begin{bmatrix} \widehat{a^{p[0]}}(\xi) & \widehat{a^{n[0]}}(\xi) \\ \widehat{a^{p[1]}}(\xi) & \widehat{a^{n[1]}}(\xi) \end{bmatrix} = \begin{bmatrix} \widehat{a^{[0]}}(\xi) & 0 \\ \widehat{a^{[1]}}(\xi) & 0 \end{bmatrix} \mathsf{U}(\xi), \quad \xi \in \mathbb{T}.$$

Since $\widehat{u(\xi)} = \widehat{u^{[0]}}(2\xi) + e^{-i\cdot\xi}\widehat{u^{[1]}}(2\xi)$ holds for any $u \in l_0(\mathbb{Z})$ and U is a paraunitary matrix, it is straightforward to check that (5.1.12) holds. This completes the proof of Theorem 12. $\square$

Now an algorithm is presented to apply Theorem 12 to split a low-pass filter a into two one-sided auxiliary filters a^p and a^n by optimization techniques.

Algorithm 3. *Let $a \in l_0(\mathbb{Z})$ be a finitely supported complex filter on $\mathbb{Z}$.*

(S1) Choose $N \in \mathbb{N}$ and define

$$\mathsf{U}(\xi) := \begin{bmatrix} \cos(t_0) & -\sin(t_0) \\ \sin(t_0) & \cos(t_0) \end{bmatrix} \prod_{j=1}^{N} \begin{bmatrix} \cos(t_j) & -\sin(t_j) \\ e^{-i\xi}\sin(t_j) & e^{-i\xi}\cos(t_j) \end{bmatrix}, \quad (5.1.14)$$

where $t_0, \dots, t_N \in [-\pi, \pi]$ are real numbers to be determined later.

(S2) Define $a^p := [a^r + ia^i]/\sqrt{2}$ and $a^n := [a^r - ia^i]/\sqrt{2}$, where the filters a^r and a^i are defined to be

$$\widehat{a^r}(\xi) := \widehat{a}(\xi)\mathsf{U}_{1,1}(2\xi), \qquad \widehat{a^i}(\xi) := \widehat{a}(\xi)\mathsf{U}_{1,2}(2\xi),$$

where $\mathsf{U}_{j,k}$ is the (j,k)-entry of the 2×2 matrix U.

(S3) Find a solution $\{t_0, \dots, t_N\}$ of the following constrained optimization problem:

$$\min_{t_0,\dots,t_N} \int_0^{\pi} |\widehat{a^p}(\xi + \pi)|^2 + |\widehat{a^n}(\xi)|^2 d\xi.$$

Then a^p and a^n satisfy the conditions in (5.1.2) with frequency separation quantities $\mathrm{fsp}(a^p)$ and $\mathrm{fsp}(a^n)$ small. Moreover, if the low-pass filter a is real, then $a^n = \overline{a^p}$, $\mathrm{fsp}(a^n) = \mathrm{fsp}(a^p)$ and the optimization problem in item (S3) is equivalent to $\min_{t_0,\dots,t_N} \mathrm{fsp}(a^p)$.

5.1.2 Design and choice of low-pass filters for $\mathrm{TP}\text{-}\mathbb{C}\mathrm{TF}_n$

As discussed in [17], a few statistics-related quantities are of interested in applications. For a sequence $a = \{a(k)\}_{k\in\mathbb{Z}} \in l_0(\mathbb{Z})$, we define its expectation/mean $\mathrm{E}(a)$ and variance $\mathrm{Var}(a)$ by

$$\mathrm{E}(a) := \frac{\sum_{k\in\mathbb{Z}} |a(k)|^2 k}{\|a\|^2_{l_2(\mathbb{Z})}} \quad \text{and} \quad \mathrm{Var}(a) := \frac{\sum_{k\in\mathbb{Z}} |a(k)|^2 (k - \mathrm{E}(a))^2}{\|a\|^2_{l_2(\mathbb{Z})}}.$$

Note that $\mathrm{Var}(a) = \min_{c\in\mathbb{R}} \sum_{k\in\mathbb{Z}} |a(k)|^2 (k-c)^2/\|a\|^2_{l_2(\mathbb{Z})}$, with the minimum value achieved at $c = \mathrm{E}(a)$.

For an orthogonal low-pass filter, by Theorem 7, we have $A(\xi) = \min(|\widehat{a}(\xi)|^2, |\widehat{a}(\xi+\pi)|^2)$. Therefore, $\mathrm{fsp}(a|\mathrm{hp}) = \mathrm{fsp}(a|\mathrm{lp})$ and $\|a\|^2_{l_2(\mathbb{Z})} = 1/2$.

In Table 5.1, we list the frequency separation quantities $\operatorname{fsp}(a|\text{lp})$ and $\operatorname{fsp}(a|\text{hp})$ as well as their l_2-norms for three families of well-known low-pass filters: the B-spline filters a_m^B, the interpolatory filters a_{2m}^I, and the Daubechies orthogonal filters a_m^D for $m \in \mathbb{N}$. The B-spline filter a_m^B of order m is given by $\widehat{a_m^B}(\xi) = 2^{-m}(1 + e^{-i\xi})^m$. The interpolatory filter a_{2m}^I is given by $\widehat{a_{2m}^I}(\xi) := \cos^{2m}(\xi/2)\mathsf{P}_m(\sin^2(\xi/2))$, where

$$\mathsf{P}_m(x) := \sum_{j=0}^{m-1} \binom{m+j-1}{j} x^j. \tag{5.1.15}$$

A Daubechies orthogonal low-pass filter a_m^D of order m is supported inside $[0, 2m-1]$ and satisfies $|\widehat{a_m^D}(\xi)|^2 = \widehat{a_{2m}^I}(\xi) = \cos^{2m}(\xi/2)\mathsf{P}_m(\sin^2(\xi/2))$.

m	1	2	3	4	5	6
$\|a_m^B\|_{l_2(\mathbb{Z})}^2$	0.5	0.375	0.3125	0.273438	0.246094	0.273438
$\operatorname{Var}(a_m^B)$	0.25	0.333333	0.45	0.571429	0.694444	0.818182
$\operatorname{fsp}(a_m^B\|\text{hp})$	0.363380	0.027195	0.004327	0.000822	0.000170	0.000037
$\operatorname{fsp}(a_m^B\|\text{lp})$	0.363380	0.151173	0.066291	0.029913	0.013745	0.006395
$\|a_{2m}^I\|_{l_2(\mathbb{Z})}^2$	0.375	0.410156	0.426498	0.436333	0.443063	0.448035
$\operatorname{Var}(a_{2m}^I)$	0.333333	0.428571	0.507137	0.574308	0.633798	0.687718
$\operatorname{fsp}(a_{2m}^I\|\text{hp})$	0.027195	0.020072	0.016720	0.014666	0.013237	0.012168
$\operatorname{fsp}(a_{2m}^I\|\text{lp})$	0.151173	0.094585	0.073303	0.061623	0.054049	0.048651
$\operatorname{Var}(a_m^D)$	0.25	0.328124	0.453684	0.425360	0.559572	0.531640
$\operatorname{fsp}(a_m^D\|\text{hp})$	0.363380	0.257277	0.209530	0.181110	0.161768	0.147526

Table 5.1: The frequency separation quantities $\operatorname{fsp}(a|\text{hp})$ and $\operatorname{fsp}(a|\text{lp})$ for three families of low-pass filters including Daubechies orthogonal filters a_m^D, B-spline filters a_m^B, and interpolatory filters a_m^I for $m = 1, \dots, 6$. Note that for Daubechies orthogonal filters, $\operatorname{fsp}(a_m^D|\text{lp}) = \operatorname{fsp}(a_m^D|\text{hp})$ and $\|a_m^D\|_{l_2(\mathbb{Z})}^2 = 1/2$ for all $m \in \mathbb{N}$. The listed $\operatorname{Var}(a_m^D)$ is the smallest among all possible choices of a_m^D satisfying $|\widehat{a_m^D}(\xi)|^2 = \widehat{a_{2m}^I}(\xi)$.

We now discuss how to choose the low-pass filter a so that the directional tensor product tight framelet filter banks can be built with the following desirable properties:

(1) short support for computational efficiency;

(2) small $\mathrm{Var}(a)$ for good spatial localizations;

(3) small frequency separation quantities $\mathrm{fsp}(a^p), \mathrm{fsp}(a^n), \mathrm{fsp}(b_1), \ldots, \mathrm{fsp}(b_s)$;

(4) all $\|a^p\|^2_{l_2(\mathbb{Z})}, \|a^n\|^2_{l_2(\mathbb{Z})}, \|b_1\|^2_{l_2(\mathbb{Z})}, \ldots, \|b_s\|^2_{l_2(\mathbb{Z})}$ are approximately around $1/(s+2)$;

(5) $\widehat{a}(\xi)$ should be almost 1 in a neighborhood of the origin. This necessarily implies that $|\widehat{a}(\xi)|^2 = 1 + \mathcal{O}(|\xi|^n)$ as $\xi \to 0$ with a largest possible integer $n \in \mathbb{N}$ and is closely related to the vanishing moments of $b_1, \ldots, b_s$.

By Theorem 6 and (5.1.3), to achieve (3), it is necessary that the frequency separation quantities $\mathrm{fsp}(a^p|\mathrm{hp})$ and $\mathrm{fsp}(a^p|\mathrm{lp})$ must be very small. Since $\|a\|^2_{l_2(\mathbb{Z})} = \frac{1}{2\pi}\int_{-\pi}^{\pi} |\widehat{a}(\xi)|^2 d\xi$, the l_2-norm of a roughly reflects the percentage of frequency occupation covered by the filter a in the frequency domain. Since there are $s+2$ number of filters in $\{a^p, a^n; b_1, \ldots, b_s\}$, it is necessary to require (4) so that all filters work more or less equally effective. (5) deals with the frequency separation between low-pass filters and high-pass filters. For an input signal v, most large coefficients of the discrete Fourier transform $\widehat{v}$ of v are concentrated around the origin. If $1 - |\widehat{a}(\xi)|^2$ is not very small in a neighborhood of the origin, then low frequency information of v will significantly leak into the high frequencies and result in a not-so-good frequency separation between the low-pass filter and high-pass filters.

As demonstrated in Table 5.1, though the B-spline filters have very short support and very small frequency separation quantities $\mathrm{fsp}(a^B_m|\mathrm{hp})$ and $\mathrm{fsp}(a^B_m|\mathrm{lp})$, their variances are generally large. More importantly, a^B_m satisfy item (5) only with $n = 1$ (the interval that $|\widehat{a^B_m}(\xi)|^2 \approx 1$ is too small) and the quantity $\|a^B_m\|^2_{l_2(\mathbb{Z})}$ is often small as well. Hence, a significant percentage of low frequency information is shifted to the high-pass filters. This requires the high-pass filters to be extremely efficient for reasonably good performance in applications.

While the Daubechies orthogonal filters have the ideal norm $\|a_m^D\|_{l_2(\mathbb{Z})}^2 = 1/2$ and reasonably small variance $\mathrm{Var}(a_m^D)$, the frequency separation quantities $\mathrm{fsp}(a_m^D|\mathrm{hp})$ is not that small and decreases slowly at the expenses of longer filter supports. In particular, for low-pass filters a_m^D,

$$A(\xi) = \min(|\widehat{a_m^D}(\xi)|^2, |\widehat{a_m^D}(\xi+\pi)|^2).$$

Due to the relation $|\widehat{a_m^D}(\xi)|^2 + |\widehat{a_m^D}(\xi+\pi)|^2 = 1$, we have

$$A(\pi/2) = |\widehat{a_m^D}(\pi/2)|^2 = 1/2,$$

which is independent of the choice of m. This creates a fixed peak point for the function $A(\xi)$ and forces the frequency separation of all its derived high-pass filters cannot be that good.

Table 5.1 indicates that the family of interpolatory filters a_{2m}^I is a good choice as the low-pass filters for our purposes. Experimental results show that directional tensor product complex tight framelets built from a_{2m}^I perform quite well in applications. Though a_{2m}^I filters have symmetry, the filter support of a_{2m}^I is twice as long as that of a_m^D. Therefore, the high-pass filters derived from a_{2m}^I tend to have long support.

We propose a method of constructing low-pass filters with the advantages of both interpolatory and orthogonal filters. To do so, the following lemma is needed to guarantee the existence.

Lemma 2. *Let $n, m \in \mathbb{N}$ with $n \leqslant m$ and $\frac{1}{2} < c \leqslant 1$. Define*

$$\mathsf{P}(x) := \sum_{j=0}^{n-1} \binom{m+j-1}{j} x^j + x^n \left(c_0 - (c_1 + 2c_0)x\right) \tag{5.1.16}$$

with

$$c_0 = \frac{c\mathsf{P}'_m(c) - (m+1)\mathsf{P}_m(c)}{c^m}, \quad c_1 = \frac{(1-2c)\mathsf{P}'_m(c) + (2+2m-m/c)\mathsf{P}_m(c)}{c^m}, \tag{5.1.17}$$

where P_m *is defined in* (5.1.15). *Then* $c_1 \geqslant 0,\ \mathsf{P}(x) \geqslant 0$*, and*

$$(1-x)^m\mathsf{P}(x) + x^m\mathsf{P}(1-x) \leqslant 1, \quad 0 \leqslant x \leqslant 1.$$

Proof. Define $\mathsf{P}_{m,n}(x) := \sum_{j=0}^{n-1}\binom{m+j-1}{j}x^j$. Since the binomial coefficients $\binom{m+j-1}{j}$ are all positive for $j = n, n+1, \cdots, m-1$, it is suffice to show that these conclusions hold when $n = m$. Then $\mathsf{P}_{m,n}$ becomes P_m defined in (5.1.15).

We first show $c_1 \geqslant 0$ by induction.

When $m = 1$,

$$c_1 = \frac{1}{c}((1-2c)\mathsf{P}'_1(c) + (2+2-\frac{1}{c})\mathsf{P}_1(c)) = \frac{1}{c}(4-\frac{1}{c}) \geqslant 0, \quad c \in (\frac{1}{2}, 1].$$

When $m = k$, assume $(1-2c)\mathsf{P}'_k(c) + (2+2k-\frac{k}{c})\mathsf{P}_k(c) \geqslant 0$.

Then, when $m = k+1$ we have

$$\begin{aligned}
&(1-2c)\mathsf{P}'_{k+1}(c) + \left(2+2(k+1)-\frac{k+1}{c}\right)\mathsf{P}_{k+1}(c)\\
\geqslant\ &(1-2c)\mathsf{P}'_{k+1}(c) + \left(2+2k-\frac{k}{c}\right)\mathsf{P}_{k+1}(c)\\
\geqslant\ &(1-2c)\mathsf{P}'_{k}(c) + \left(2+2k-\frac{k}{c}\right)\mathsf{P}_{k}(c), \quad c \in (\frac{1}{2}, 1],
\end{aligned}$$

because

$$\mathsf{P}_{k+1}(x) - \mathsf{P}_k(x) = \sum_{j=0}^{k}\left(\binom{k+j}{j} - \binom{k+j-1}{j}\right)x^j = \sum_{j=1}^{k}\binom{k+j-1}{j-1}x^j \geqslant 0,$$

and

$$\begin{aligned}\mathsf{P}'_{k+1}(x) - \mathsf{P}'_k(x) &= \sum_{j=1}^{k} \left(\binom{k+j}{j} - \binom{k+j-1}{j} \right) jx^{j-1} \\ &= \sum_{j=1}^{k} \binom{k+j-1}{j-1} jx^{j-1} \geqslant 0, \qquad\qquad x \in [0,1].\end{aligned}$$

Therefore, by induction,

$$c_1 = \frac{1}{c^m} \Big((1-2c)\mathsf{P}'_m(c) + \Big(2 + 2m - \frac{m}{c}\Big) \mathsf{P}_m(c) \Big) \geqslant 0, \quad m \in \mathbb{N}.$$

Next we prove $\mathsf{P}(x) \geqslant 0$. Note that c_0, c_1 are obtained through the equations $\mathsf{P}(c) = 0$ and $\mathsf{P}'(c) = 0$, then we have

$$\mathsf{P}(x) = (1 - \frac{x}{c})^2 Q(x),$$

where $Q(x)$ is a polynomial of degree $m-1$. Since it is well known that $(1-x)^m \mathsf{P}_m(x) + x^m \mathsf{P}_m(1-x) = 1$, consider

$$\begin{aligned}(1-x)^m \mathsf{P}(x) =&(1-m)^m (\mathsf{P}_m(x) + c_0 x^m - (c_1 + 2c_0)x^{m+1}) \\ =&1 + x^m((1-x)^m(c_0 - (c_1+2c_0)x) - \mathsf{P}_m(1-x)).\end{aligned}$$

Also, $(1-x)^m \mathsf{P}(x) = (1-x)^m (1-\frac{x}{c})^2 Q(x)$, thus we have

$$Q(x) = \frac{1}{(1-x)^m(1-\frac{x}{c})^2} + x^m \frac{(1-x)^m(c_0 + (c_1+2c_0)x) - \mathsf{P}_m(1-x)}{(1-x)^m(1-\frac{x}{c})^2},$$

that is,

$$Q(x) = \frac{1}{(1-x)^m(1-\frac{x}{c})^2} + \mathcal{O}(|x|^m), \quad x \to 0.$$

Since $Q(x)$ is a polynomial of degree $m-1$, by the uniqueness of Taylor expansion, $Q(x)$ is exact the truncated Taylor expansion for $\frac{1}{(1-x)^m(1-\frac{x}{c})^2}$ to degree $m-1$. Because the coefficients of Taylor expansion for $\frac{1}{(1-x)^m(1-\frac{x}{c})^2}$ are all positive, we have $Q(x) \geqslant 0$ for $x \in [0,1]$. Therefore,

$$\mathsf{P}(x) = (1 - \frac{x}{c})^2 Q(x) \geqslant 0, \quad x \in [0,1].$$

By $(1-x)^m \mathsf{P}_m(x) + x^m \mathsf{P}_m(1-x) = 1$, we see that $\int_0^1 (1-x)^m \mathsf{P}_m(x) dx = 1/2$ and

$$\int_0^1 (1-x)^m \mathsf{P}(x) dx = \frac{1}{2} - \frac{m!}{2^{m+1}(2m+1)!!} c_1.$$

Consequently, by $\mathsf{P}(x) = \mathsf{P}_m(x) + x^m(c_0 - (c_1 + 2c_0)x)$ and $c_1 \geqslant 0$ we deduce that

$$1 - (1-x)^m \mathsf{P}(x) - x^m \mathsf{P}(1-x) = c_1 x^m (1-x)^m \geqslant 0, \quad x \in [0,1].$$

□

Based on Lemma 2, we provide an algorithm to design the desired low-pass filter a for the construction of TP-$\mathbb{C}$TF$_4$ and TP-$\mathbb{C}$TF$_6$.

Algorithm 4. *Let* $m,\ n \in \mathbb{N}$ *and* $\frac{1}{2} < c \leqslant 1$.

(S1) Choose $n = m$ *or* $n = m - 1$ *and define a polynomial* P *as in* (5.1.16) *with* c_0, c_1 *being given in* (5.1.17)*. Then by lemma 2, we have*

$$\cos^{2m}(\xi/2)\mathsf{P}(\sin^2(\xi/2)) \geqslant 0, \quad \xi \in \mathbb{R}.$$

(S2) Using Fejér-Riesz lemma, we can always get the factorization $|\widehat{a}(\xi)|^2 = \cos^{2m}(\xi/2)\mathsf{P}(\sin^2(\xi/2))$*, satisfying the following properties:*

$$\widehat{a}(0) = 1, \quad (1 + e^{-i\xi})^m \mid \widehat{a}(\xi), \quad |\widehat{a}(\xi)|^2 + |\widehat{a}(\xi + \pi)|^2 \leqslant 1, \quad \xi \in \mathbb{R}.$$

Then the obtained real $a \in l_0(\mathbb{Z})$ *is the desired low-pass filter.*

If we choose $c_0 = c_1 = 0$ in (5.1.16), the low-pass filter a constructed in Algorithm 4 is simply the Daubechies orthogonal low-pass filter. The two free parameters c_0 and c_1 are used to add a double root to the polynomial P at the point c so that the frequency response $\widehat{a}$ is dumped near the point $0 < 2\arcsin\sqrt{c} \leqslant \pi$, with the frequency separation quantities $\operatorname{fsp}(a|\text{hp})$ and $\operatorname{fsp}(a|\text{lp})$ small. In application, we often choose $c = 1$.

5.2 Construction of compactly supported $\text{TP-}\mathbb{C}\text{TF}_4$ and $\text{TP-}\mathbb{C}\text{TF}_6$

This section provides algorithms for constructing directional compactly supported $\text{TP-}\mathbb{C}\text{TF}_4$ and $\text{TP-}\mathbb{C}\text{TF}_6$.

Let us first discuss how to construct the one-dimensional finitely supported $\mathbb{C}\text{TF}_4$ by splitting the low-pass filter a into a^p and a^n in the filter bank $\{a; b^p, b^n\}$. By modifying Algorithm 2, the algorithm for constructing $\mathbb{C}\text{TF}_4 = \{a^p, a^n; b^p, b^n\}$ is given by

Algorithm 5. *Let $a \in l_0(\mathbb{Z})$ be a finitely supported real filter on $\mathbb{Z}$ satisfying $|\widehat{a}(\xi)|^2 + |\widehat{a}(\xi + \pi)|^2 \leqslant 1$ for all $\xi \in \mathbb{R}$.*

(S1) Construct two auxiliary filters a^p and a^n by Algorithm 3 so that $\operatorname{fsp}(a^p)$ is reasonably small.

(S2) Construct a finitely supported real tight framelet filter bank $\{a; b_1, b_2\}$ by Algorithm 1.

(S3) Choose a suitable filter length $N \in \mathbb{N}$ and define a 2×2 matrix $\mathsf{U}(\xi)$ as in (5.1.14), where $t_0, \ldots, t_N \in [-\pi, \pi]$ are real numbers to be determined later.

(S4) *Define* $b^p := [b^r + ib^i]/\sqrt{2}$ *and* $b^n := [b^r - ib^i]/\sqrt{2}$, *where the real filters* b^r *and* b^i *are defined to be*

$$\widehat{b^r}(\xi) := \widehat{b_1}(\xi)\mathsf{U}_{1,1}(2\xi)+\widehat{b_2}(\xi)\mathsf{U}_{2,1}(2\xi),\ \ \widehat{b^i}(\xi) := \widehat{b_1}(\xi)\mathsf{U}_{1,2}(2\xi)+\widehat{b_2}(\xi)\mathsf{U}_{2,2}(2\xi),$$

where $\mathsf{U}_{j,k}$ *is the* (j,k)*-entry of the* 2×2 *matrix* U.

(S5) *Find a solution* $\{t_0,\dots,t_N\}$ *to the following constrained optimization problem:*

$$\min_{t_0,\dots,t_N}\int_0^{\pi}|\widehat{b^p}(\xi+\pi)|^2 d\xi,$$

which is equivalent to the optimization problem: $\min_{t_0,\dots,t_N}\operatorname{fsp}(b^p)$.

Then $\mathbb{C}\mathrm{TF}_4 := \{a^p, a^n; b^p, b^n\}$ *is a compactly supported tight framelet filter bank with frequency separation quantities* $\operatorname{fsp}(a^p)$, $\operatorname{fsp}(a^n)$, $\operatorname{fsp}(b^p)$, *and* $\operatorname{fsp}(b^n)$ *small.*

Now we present how to construct finitely supported one-dimensional $\mathbb{C}\mathrm{TF}_6$. We first split the low-pass a into a^p and a^n by Algorithm 3, then directly apply optimization techniques to find the optimal frequency separation quantities of $b^{1,p}$, $b^{2,p}$, $b^{1,n}$, and $b^{2,n}$ instead of studying the structure of all finitely supported $\mathbb{C}\mathrm{TF}_6$ filter banks.

Algorithm 6. *Let* $a \in l_0(\mathbb{Z})$ *be a finitely supported real filter on* $\mathbb{Z}$ *satisfying* $|\widehat{a}(\xi)|^2 + |\widehat{a}(\xi+\pi)|^2 \leqslant 1$ *for all* $\xi \in \mathbb{R}$.

(S1) *Construct two auxiliary filters* a^p *and* a^n *by Algorithm 3 so that* $\operatorname{fsp}(a^p)$ *and* $\operatorname{fsp}(a^n)$ *are reasonably small.*

(S2) *Choose a suitable filter length* $N \in \mathbb{N}$ *and parameterize filters* b_1, b_2, b_3, *and*

b_4 by

$$\widehat{b_j}(\xi) := c_{j,0} + c_{j,1}e^{-i\cdot\xi} + \cdots + c_{j,N}e^{-iN\cdot\xi}, \quad j = 1, \cdots, 4,$$

where $c_{j,k}$ are real numbers to be determined later with $j = 1, \ldots, 4$ and $k = 0, \ldots, N$.

(S3) Define new high-pass filters $b^{1,p}$, $b^{2,p}$, $b^{1,n}$, and $b^{2,n}$ by

$$\widehat{b^{1,p}}(\xi) := \widehat{b_1}(\xi) + i\widehat{b_2}(\xi), \quad \widehat{b^{1,n}}(\xi) := \widehat{b_1}(\xi) - i\widehat{b_2}(\xi),$$
$$\widehat{b^{2,p}}(\xi) := \widehat{b_3}(\xi) + i\widehat{b_4}(\xi), \quad \widehat{b^{2,n}}(\xi) := \widehat{b_3}(\xi) - i\widehat{b_4}(\xi).$$

(S4) Find a solution $c_{j,k}$ with $j = 1, \cdots, 4,\ k = 0, \cdots, N$ to the following constrained optimization problem:

$$\min_{c_{j,k}} \left\{ \lambda_1 \int_{\frac{\pi}{4}}^{\frac{\pi}{4}+\frac{\pi}{3}} |\widehat{b^{1,p}}(\xi)|^2 d\xi + \lambda_2 \int_{\frac{\pi}{2}}^{\frac{\pi}{2}+\frac{\pi}{3}} |\widehat{b^{2,n}}(\xi)|^2 d\xi - \lambda_3 \int_{-\frac{\pi}{2}}^{-\frac{\pi}{2}+\frac{\pi}{3}} |\widehat{b^{1,p}}(\xi)|^2 d\xi \right.$$
$$\left. -\lambda_4 \int_{-\frac{3\pi}{4}}^{-\frac{3\pi}{4}+\frac{\pi}{3}} |\widehat{b^{1,n}}(\xi)|^2 d\xi \right\},$$

under the constraints:

$$|\widehat{a}(\xi)|^2 + |\widehat{b^{1,p}}(\xi)|^2 + |\widehat{b^{2,p}}(\xi)|^2 + |\widehat{b^{1,n}}(\xi)|^2 + |\widehat{b^{2,n}}(\xi)|^2 = 1,$$
$$\widehat{a}(\xi)\overline{\widehat{a}(\xi+\pi)} + \sum_{\ell=1}^{2} \widehat{b^{\ell,p}}(\xi)\overline{\widehat{b^{\ell,p}}(\xi+\pi)} + \sum_{m=1}^{2} \widehat{b^{m,n}}(\xi)\overline{\widehat{b^{m,n}}(\xi+\pi)} = 0,$$

for all $\xi \in \mathbb{R}$ (such constraints on $b^{1,p}$, $b^{2,p}$, $b^{1,n}$, and $b^{2,n}$ can be rewritten as equations using $c_{j,k}$ with $j = 1, \cdots, 4$ and $k = 0, \cdots, N$), where $\lambda_1, \cdots, \lambda_4$ are real multipliers.

Then $\mathbb{C}\mathrm{TF}_6 := \{a^p, a^n; b^{1,p}, b^{2,p}, b^{1,n}, b^{2,n}\}$ is a compactly supported tight framelet filter bank with frequency separation quantities $\mathrm{fsp}(a^p)$, $\mathrm{fsp}(a^n)$, $\mathrm{fsp}(b^{1,p})$, $\mathrm{fsp}(b^{2,p})$, $\mathrm{fsp}(b^{1,n})$, and $\mathrm{fsp}(b^{2,n})$ small.

5.3 Examples

Many examples of compactly supported complex tight framelet filter banks with good frequency separation can be constructed by using Algorithm 5 and 6. Several concrete examples are presented to illustrate Algorithms 3, 4, 5, and 6. Again, Laurent polynomial is used to represent filters for our convenience.

Example 9. Let $m = 1$, $n = 1$, and $c = 1$. By Algorithm 4, we obtain the low-pass filter

$$\mathsf{a}(z) = \tfrac{1}{8}\, z^2 + \tfrac{3}{8}\, z + \tfrac{3}{8} + \tfrac{1}{8}\, z^{-1}.$$

Applying Algorithm 3 with $N = 2$, we obtain two finitely supported complex tight framelet filters a^p and a^n with $a^n = \overline{a^p}$, and

$$\begin{aligned}\mathsf{a}^p(z) = {}& -0.00794848752\, iz^6 - 0.02384546256\, iz^5 - (0.00748434124 + 0.0839743577\, i)\, z^4 \\ & - (0.02245302373 + 0.1883351730\, i)\, z^3 + (0.04140480387 - 0.1803866855\, i)\, z^2 \\ & + (0.1840891416 - 0.06012889515\, i)\, z + 0.1915734828 + 0.06385782760\, z^{-1}.\end{aligned}$$

Example 10. Let $m = 2$, $n = 2$, and $c = 1$. By Algorithm 4, we obtain the low-pass filter

$$\mathsf{a}(z) = \tfrac{\sqrt{5}+1}{32} z^3 + \tfrac{3\sqrt{5}+5}{32} z^2 + \tfrac{\sqrt{5}+5}{16} z + \tfrac{5-\sqrt{5}}{16} + \tfrac{5-3\sqrt{5}}{32} z^{-1} + \tfrac{1-\sqrt{5}}{32} z^{-2}.$$

Applying Algorithm 3 with $N = 2$, we obtain two finitely supported complex tight framelet filters a^p and a^n with $a^n = \overline{a^p}$, and

$$\begin{aligned}\mathsf{a}^p(z) = {}& - 0.004349695057\, iz^7 - 0.01573734456\, iz^6 - (0.004227143772 + 0.06910881945\, i)\, z^5 \\ & - (0.01529394984 + 0.1870886796\, i)\, z^4 + (0.03219164397 - 0.2197740875\, i)\, z^3 \\ & + (0.1776462614 - 0.08316180815\, i)\, z^2 + (0.2307396411 + 0.02621182382\, i)\, z \\ & + 0.08889702305 + 0.01896705390\, i - 0.02697174423\, z^{-1} - 0.01951693746\, z^{-2}.\end{aligned}$$

Example 11. Let $m = 3$, $n = 3$, and $c = 1$. By Algorithm 4, we obtain the low-pass filter

$$\mathsf{a}(z) = \left(\frac{\sqrt{7+2\sqrt{21}}}{128} + \frac{\sqrt{21}+1}{128}\right) z^4 + \left(\frac{5\sqrt{7+2\sqrt{21}}}{128} + \frac{7+3\sqrt{21}}{128}\right) z^3 + \left(\frac{21+\sqrt{21}}{128} + \frac{9\sqrt{7+2\sqrt{21}}}{128}\right) z^2$$
$$+ \left(\frac{35-5\sqrt{21}}{128} + \frac{5\sqrt{7+2\sqrt{21}}}{128}\right) z - \frac{5\sqrt{7+2\sqrt{21}}}{128} + \frac{35-5\sqrt{21}}{128} + \left(-\frac{9\sqrt{7+2\sqrt{21}}}{128} + \frac{21+\sqrt{21}}{128}\right) z^{-1}$$
$$+ \left(-\frac{5\sqrt{7+2\sqrt{21}}}{128} + \frac{3\sqrt{21}+7}{128}\right) z^{-2} + \left(-\frac{\sqrt{7+2\sqrt{21}}}{128} + \frac{1+\sqrt{21}}{128}\right) z^{-3}.$$

Applying Algorithm 3 with $N = 2$, we obtain two finitely supported complex tight framelet filters a^p and a^n with $a^n = \overline{a^p}$, and

$$\mathsf{a}^p(z) = -0.002431485651\, iz^8 - 0.01034323888\, iz^7 - (0.002391775334 + 0.052764700\, i)\, z^6$$
$$- (0.01017431612 + 0.1660768426\, i)\, z^5 + (0.02235770774 - 0.2367616231\, i)\, z^4$$
$$+ (0.1525311712 - 0.1217604482\, i)\, z^3 + (0.2447522517 + 0.03082550567\, i)\, z^2$$
$$+ (0.1291518972 + 0.04059411758\, i)\, z - 0.03166384949 - 0.002492654040\, i$$
$$- (0.04205918078 + 0.006038545210\, i)\, z^{-1} + 0.002534039267\, z^{-2} + 0.006138802345\, z^{-3}.$$

Example 12. Let $m = 4$, $n = 3$, and $c = 1$. By Algorithm 4, we obtain the low-pass filter

$$\mathsf{a}(z) = \left(\frac{1+\sqrt{28}}{256} + \frac{\sqrt{8+2\sqrt{28}}}{256}\right) z^4 + \left(\frac{1+\sqrt{7}}{32} + \frac{3\sqrt{8+2\sqrt{28}}}{128}\right) z^3 + \left(\frac{7+\sqrt{28}}{64} + \frac{7\sqrt{8+2\sqrt{28}}}{128}\right) z^2$$
$$+ \left(\frac{7-\sqrt{7}}{32} + \frac{7\sqrt{8+2\sqrt{28}}}{128}\right) z + \frac{35-5\sqrt{28}}{128} + \left(\frac{7-\sqrt{7}}{32} - \frac{7\sqrt{8+2\sqrt{28}}}{128}\right) z^{-1}$$
$$+ \left(\frac{7+\sqrt{28}}{64} - \frac{7\sqrt{8+2\sqrt{28}}}{128}\right) z^{-2} + \left(\frac{1+\sqrt{7}}{32} - \frac{3\sqrt{8+2\sqrt{28}}}{128}\right) z^{-3} + \left(\frac{1+\sqrt{28}}{256} - \frac{\sqrt{8+2\sqrt{28}}}{256}\right) z^{-4}.$$

Applying Algorithm 3 with $N = 2$, we obtain two finitely supported complex tight framelet filters a^p and a^n with $a^n = \overline{a^p}$, and

$$\mathsf{a}^p(z) = -0.001610384272\, iz^8 - 0.008358632665\, iz^7 - (0.001572980556 + 0.03703693068\, i)\, z^6$$
$$- (0.008164490235 + 0.1203552630\, i)\, z^5 + (0.004639289884 - 0.2133425722\, i)\, z^4$$
$$+ (0.09429382335 - 0.1792921519\, i)\, z^3 + (0.2132241120 - 0.03117824642\, i)\, z^2$$

$+ (0.1913092832 + 0.04860219956\, i)\, z + 0.03531841033 + 0.02122319973\, i$

$- (0.05076102270 + 0.006352614540\, i)\, z^{-1} - (0.02232972752 + 0.003811528158\, i)\, z^{-2}$

$+ 0.006503672580\, z^{-3} + 0.003902162030\, z^{-4}$

See Figure 5.1 for the graphs of the corresponding wavelet frame functions and frequency separations of a^p with $m = 1, 2, 3, 4$.

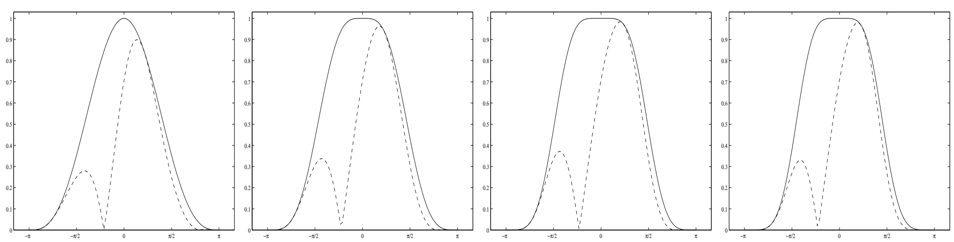

Figure 5.1: The magnitudes of $\widehat{a}$ and $\widehat{a^p}$: the solid line is for $\widehat{a}$ and the dashed line is for $\widehat{a^p}$. The first column is for Example 9, the second column is for Example 10, the third column is for Example 11, and the last column is for Example 12.

Example 13. Let $m = 3$, $n = 3$, and $c = 1$. Applying Algorithm 5 with $N = 3$, we have finitely supported complex tight framelet filters b^p and b^n with $b^n = \overline{b^p}$ and

$$\begin{aligned}
\mathsf{b}^p(z) &= (0.0007476670045 - 0.0007002035305\, i)\, z^{10} + (0.003180482860 - 0.002978579118\, i)\, z^9 \\
&- (0.007223295040 - 0.006554742760\, i)\, z^8 + (0.01423548086 - 0.01422510646\, i)\, z^7 \\
&+ (0.1024049440 - 0.06284697495\, i)\, z^6 - (0.1746180510 - 0.2915247702\, i)\, z^5 \\
&- (0.1091807890 + 0.3181734521\, i)\, z^4 + (0.2068595684 + 0.05519129755\, i)\, z^3 \\
&+ (0.004606785266 + 0.03038696555\, i)\, z^2 - (0.02118423369 - 0.03696722410\, i)\, z \\
&- 0.008199923925 - 0.008910041145\, i - (0.01327749368 + 0.01455126886\, i)\, z^{-1} \\
&+ (0.0004817649521 + 0.0005144215105\, i)\, z^{-2} + (0.001167093146 + 0.001246204852\, i)\, z^{-3}.
\end{aligned}$$

Applying Algorithm 6 with $N = 3$, we have finitely supported complex tight framelet filters $b^{1,p}$, $b^{2,p}$, $b^{1,n}$ and $b^{2,n}$ with $b^{1,n} = \overline{b^{1,p}}$ and $b^{2,n} = \overline{b^{2,p}}$, where $b^{1,p}$ and

$b^{2,p}$ are given by:

$$\begin{aligned}\mathsf{b}^{1,p}(z) &= (-0.0006928637152 + 0.00002962954706\,i)\,z^8 - (0.002947356452 - 0.0001260404244\,i)\,z^7 \\ &\quad - (0.004923137834 - 0.0004482249293\,i)\,z^6 - (0.00430741995 - 0.001195316105\,i)\,z^5 \\ &\quad + (0.002494118451 - 0.007748024540\,i)\,z^4 + (0.02011745310 - 0.03907249541\,i)\,z^3 \\ &\quad + (0.06911031776 - 0.01452451456\,i)\,z^2 - (0.03722884294 - 0.1731281984\,i)\,z \\ &\quad + (0.02200254375 - 0.1599836419\,i)\,z^{-1} + (0.1101609272 + 0.01398707627\,i)\,z^{-2} \\ &\quad - (0.02446606216 - 0.05990110653\,i)\,z^{-3} - (0.03633367460 + 0.02040494922\,i)\,z^{-4} \\ &\quad + (0.01409575615 + 0.007916160189\,i)\,z^{-5} - 0.1270817587 - 0.01499812678\,i,\end{aligned}$$

$$\begin{aligned}\mathsf{b}^{2,p}(z) &= -0.1120785661 - 0.1786963212\,i + (0.0006291132418 - 0.0002444780665\,i)\,z^8 \\ &\quad + (0.002676169832 - 0.001039979423\,i)\,z^7 + (0.001011376705 + 0.001036252694\,i)\,z^6 \\ &\quad - (0.01080213930 - 0.01027777649\,i)\,z^5 - (0.01092476539 - 0.006815808054\,i)\,z^4 \\ &\quad + (0.02793651200 - 0.03423800993\,i)\,z^3 + (0.005883393031 - 0.01417034898\,i)\,z^2 \\ &\quad - (0.00890280119 - 0.1154111572\,i)\,z + (0.2496167834 + 0.1007144269\,i)\,z^{-1} \\ &\quad - (0.2078663904 - 0.03651159370\,i)\,z^{-2} + (0.07251662177 - 0.07893887976\,i)\,z^{-3} \\ &\quad - (0.01584078814 - 0.05973560735\,i)\,z^{-4} + (0.006145480446 - 0.02317460493\,i)\,z^{-5}.\end{aligned}$$

See Figure 5.2 for the graphs of the frequency separations of b^p, $b^{1,p}$, and $b^{2,p}$ with $m = 3$ and $n = 3$.

Example 14. Let $m = 4$, $n = 3$, and $c = 1$. Applying Algorithm 5, we have finitely supported complex tight framelet filters b^p and b^n with $b^n = \overline{b^p}$ and

$$\begin{aligned}\mathsf{b}^{p}(z) &= 0.02250135114 + 0.05506310548\,i - (0.0003443801525 - 0.0002527203580\,i)\,z^6 \\ &\quad - (0.001787490874 - 0.001311734519\,i)\,z^5 - (0.004300699297 - 0.001960737896\,i)\,z^4\end{aligned}$$

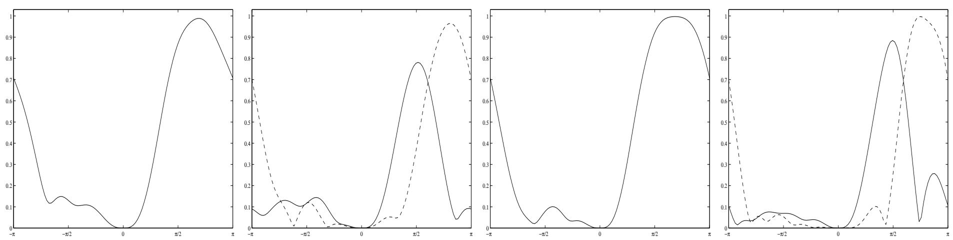

Figure 5.2: The first and second are for $m = 3$ and $n = 3$ in Example 13. The first is for the magnitude of $\widehat{b^p}$ in $\mathbb{C}\mathrm{TF}_4$. The second is for the magnitudes of $\widehat{b^{1,p}}$ and $\widehat{b^{2,p}}$ in $\mathbb{C}\mathrm{TF}_6$: the solid line is for $\widehat{b^{1,p}}$ and the dashed line is for $\widehat{b^{2,p}}$. The third and fourth are for $m = 4$ and $n = 3$ in Example 14: the third is for the magnitude of $\widehat{b^p}$ in $\mathbb{C}\mathrm{TF}_4$. The fourth is for the magnitudes of $\widehat{b^{1,p}}$ and $\widehat{b^{2,p}}$ in $\mathbb{C}\mathrm{TF}_6$.

$$
\begin{aligned}
&- (0.006950362108 + 0.001103654279\, i)\, z^3 - (0.003342185452 - 0.0001403005844\, i)\, z^2 \\
&+ (0.01954528967 + 0.02700956160\, i)\, z + (0.1637178323 - 0.1836739625\, i)\, z^{-1} \\
&- (0.3703940856 + 0.06711333459\, i)\, z^{-2} + (0.1508313466 + 0.2608716562\, i)\, z^{-3} \\
&+ (0.04308758525 - 0.07759772125\, i)\, z^{-4} + (0.008585532825 + 0.01169944173\, i)\, z^{-5} \\
&- (0.02114973436 + 0.02882058572\, i)\, z^{-6}.
\end{aligned}
$$

Applying Algorithm 6 with $N = 4$, we have finitely supported complex tight framelet filters $b^{1,p}$, $b^{2,p}$, $b^{1,n}$ and $b^{2,n}$ with $b^{1,n} = \overline{b^{1,p}}$ and $b^{2,n} = \overline{b^{2,p}}$, where $b^{1,p}$ and $b^{2,p}$ are given by:

$$
\begin{aligned}
\mathsf{b}^{1,p}(z) = &-0.07017678857 + 0.1204610765\, i - (0.001132750766 - 0.0005481354075\, i)\, z^8 \\
&- (0.005879495790 - 0.002845074060\, i)\, z^7 - (0.006767265847 - 0.003340854930\, i)\, z^6 \\
&+ (0.01543785096 - 0.007126777580\, i)\, z^5 - (0.005993067370 - 0.03986936013\, i)\, z^4 \\
&- (0.05597939029 + 0.07211098886\, i)\, z^3 + (0.1049841862 - 0.08187164366\, i)\, z^2 \\
&+ (0.06844160670 + 0.1123035699\, i)\, z - (0.1287264047 + 0.06066939528\, i)\, z^{-1} \\
&+ (0.03833231590 - 0.1241611254\, i)\, z^{-2} + (0.06490831962 + 0.05687919330\, i)\, z^{-3} \\
&+ (0.01744911612 - 0.009692666600\, i)\, z^{-4},
\end{aligned}
$$

$$
\begin{aligned}
\mathsf{b}^{2,p}(z) &= 0.1889939478 - 0.1172709272\,i + (0.0007818352229 - 0.0004202485500\,i)\,z^{8} \\
&\quad + (0.004058083243 - 0.002181282639\,i)\,z^{7} + (0.002079721417 + 0.001630026732\,i)\,z^{6} \\
&\quad - (0.02410439374 - 0.02721939390\,i)\,z^{5} + (0.007321862450 - 0.04871391588\,i)\,z^{4} \\
&\quad + (0.008513641570 - 0.007801830049\,i)\,z^{3} + (0.06403680485 + 0.06340749535\,i)\,z^{2} \\
&\quad - (0.1622776543 + 0.008414146780\,i)\,z - (0.1049455509 - 0.2155499924\,i)\,z^{-1} \\
&\quad - (0.04132617871 + 0.1877097344\,i)\,z^{-2} + (0.09263166169 + 0.07156537920\,i)\,z^{-3} \\
&\quad - (0.03576378056 + 0.006860201970\,i)\,z^{-4}.
\end{aligned}
$$

See Figure 5.2 for the graphs of the frequency separations of b^p, $b^{1,p}$, and $b^{2,p}$ with $m = 4$ and $n = 3$.

Chapter 6

Applications of Tensor Product Complex Tight Framelets

This chapter concentrates on the application of proposed directional tensor product complex tight framelets in image and video processing. In image denoising problems, bivariate shrinkage [45, 46] and Gaussian Scale Mixture (GSM) model [41, 51] are applied to test the performance. Strong statistical model can improve the estimation of framelet coefficients in such image restoration applications. For video denoising in three dimensions, we compare the performance of directional tensor product complex tight framelet with low redundancy rate with many other multi-directional representation systems. In all this chapter, we assume that the images or videos are contaminated with independent identically distributed (i.i.d.) white Gaussian noise with standard deviation σ known in advance.

6.1 Image denoising

This section comprehensively tests the performance of directional tensor product complex tight framelet in image denoising. Many signals and images contain noise due to the imperfect acquisition procedure. As the simplest image inverse problem, noise removing is essential to many other applications. In the past five decades, numerous researches were devoted to this problem from many different perspectives. There are four denoising principles can be concluded from all these approaches [31]:

- Bayesian patch-based methods;
- transform thresholding;
- sparse coding;
- pixel averaging and block averaging.

The denoising methods in this chapter belong to the transform thresholding. The basic philosophy for this principle is that wavelets or framelets can not approximate the noise well and so the noise stays in small coefficients while the true signal will reside in the large coefficients. By thresholding small coefficients, a majority of the noise will be removed. However, the wavelet coefficient of true signal will be suppressed as well. Thus, statistical model of wavelet or framelet coefficients is needed to distinguish the noise from the signal.

The general model for denoising can be expressed as

$$y = x + n, \tag{6.1.1}$$

with observed value y, original data x, and additional noise n. We want to recover x from the observed y.

As usual, the image restoration performance is measured by the peak signal-to-noise ratio (PSNR) which is defined to be

$$\text{PSNR}(x, \mathring{x}) = 10 \log_{10} \frac{\max(x)}{\text{MSE}(x - \mathring{x})},$$

where x is the original data, $\mathring{x}$ is the reconstructed data, $\max(x)$ is the maximum possible value of the original data x which is 255 in our experiment, and $\text{MSE}(\cdot)$ is the mean squared error defined by

$$\mathrm{MSE}(x - \mathring{x}) = \frac{1}{N} \sum_{i=1}^{N} (x_i - \mathring{x}_i),$$

where N is the total number of pixels.

It is well known that wavelet coefficients are statistically dependent: if a wavelet coefficient is large or small, the adjacent ones are likely to be large or small; in addition, large or small coefficients tend to propagate across the scales. So the general way of soft or hard thresholding to choose wavelet coefficients of natural images is weak because it ignores the dependencies between the coefficients.

In order to take dependencies between a coefficient and its parent (adjacent coarser scale at the same position) into consideration, bivariate shrinkage [45, 46] is applied to all framelet coefficients in our comparison test. Let σ denote the standard deviation of the i.i.d. Gaussian noise. For a frame coefficient c, bivariate shrinkage is defined by the shrinkage function η_λ^{bs} as follows:

$$\eta_\lambda^{bs}(c) = \eta_{\lambda_c}^{soft}(c) = \begin{cases} c - \lambda_c \frac{c}{|c|}, & |c| > \lambda_c, \\ 0, & \text{otherwise}, \end{cases} \quad \text{with} \quad \lambda_c := \frac{\sqrt{3}\sigma_n^2}{\sigma_c \sqrt{1 + |c_p/c|^2}}, \tag{6.1.2}$$

where $\sigma_n := \sigma \|b\|_2$ with b being the high-pass filter inducing the frame coefficient c, the frame coefficient c_p is the parent coefficient of c, and

$$\sigma_c := \begin{cases} \sqrt{\breve{\sigma}_c^2 - \sigma_n^2}, & \breve{\sigma}_c > \sigma_n, \\ 0, & \text{otherwise}, \end{cases} \quad \text{with} \quad \breve{\sigma}_c^2 := \frac{1}{N_c} \sum_{j \in N_c} |c_j|^2,$$

where N_c is the number of framelet coefficients in the window centering around the frame coefficient c at the band induced by the filter b.

The bivariate shrinkage is originally derived from real-valued orthogonal wavelet coefficients. Two main adaptations have to be made for over-complete complex framelet coefficients. First, the variance of observed coefficients $\breve{\sigma}_c^2$ is estimated from the magnitude of the complex framelet coefficients. Second, the $\|b\|_2$ is calculated with respect to the complex high-pass filter b instead of real and imaginary part of b separately.

The decomposition level for all TP-$\mathbb{C}$TF$_m$ is set to be $J = 5$ for 512×512 images and $J = 4$ for 256×256 images, so that the denoised subband has at least 16×16 framelet coefficients. The decomposition level for the dual tree complex wavelet transform is set to be $J = 6$ (see [44, 46]). Symmetric boundary extension with 16 pixels is applied to all test images to avoid the boundary effect.

See Figure 6.1 for the grayscale test images: *Barbara*, *Lena*, *Fingerprint*, and *Boat*.

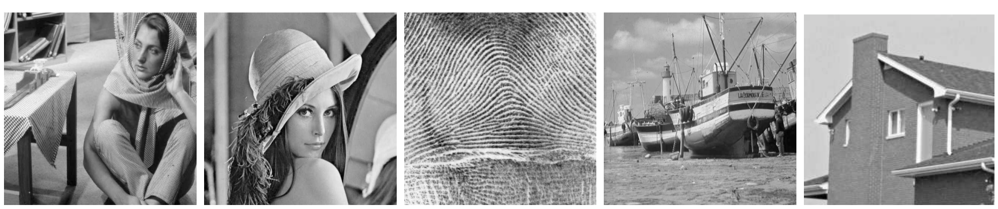

(a) Barbara (b) Lena (c) Fingerprint (d) Boat (e) House

Figure 6.1: (a)-(d) are the four 512×512 grayscale test images: *Barbara*, *Lena*, *Fingerprint*, and *Boat*. (f) is the 256×256 grayscale test image *House*.

The image denoising results for directional tensor product complex framelets by bivariate shrinkage in terms of PSNR are reported in Table 6.1.

Table 6.1 demonstrates that the image denoising results of compactly supported directional tensor product complex tight framelets are comparable to those of their bandlimited counterparts. TP-$\mathbb{C}$TF$_3$ performs less well than others due to insufficient directional selectivity. TP-$\mathbb{C}$TF$_6$ performs significantly better than the

	512 × 512 Lena						
σ	DT-$\mathbb{C}$WT	TP-$\mathbb{C}$TF$_3$	Example 7	TP-$\mathbb{C}$TF$_4$	Example 14	TP-$\mathbb{C}$TF$_6$	Example 14
5	38.26	37.98	38.01	38.12	38.17	38.37	38.38
10	35.20	34.93	34.93	35.16	35.21	35.48	35.49
15	33.46	33.26	33.21	33.51	33.55	33.80	33.80
20	32.23	32.09	32.00	32.33	32.36	32.57	32.56
25	31.27	31.17	31.05	31.39	31.42	31.60	31.57
30	30.48	30.42	30.28	30.62	30.64	30.80	30.76
40	29.20	29.24	29.06	29.40	29.41	29.52	29.47
50	28.20	28.34	28.12	28.46	28.46	28.54	28.47
80	26.14	26.42	26.16	26.48	26.48	26.47	26.40
100	25.19	25.52	25.29	25.55	25.56	25.52	25.45
	512 × 512 Barbara						
5	37.37	37.16	37.02	37.42	37.28	37.84	37.76
10	33.54	33.19	32.98	33.65	33.45	34.18	34.12
15	31.41	30.91	30.71	31.51	31.31	32.07	32.05
20	29.91	29.30	29.10	29.97	29.77	30.54	30.55
25	28.76	28.04	27.84	28.77	28.56	29.35	29.37
30	27.83	27.04	26.83	27.79	27.58	28.38	28.40
40	26.40	25.53	25.33	26.29	26.08	26.86	26.87
50	25.32	24.48	24.29	25.21	25.01	25.71	25.72
80	23.27	22.82	22.67	23.21	23.10	23.53	23.52
100	22.44	22.25	22.11	22.45	22.40	22.64	22.62
	512 × 512 Boat						
5	36.73	36.45	36.52	36.53	36.57	36.92	36.87
10	33.19	32.97	33.03	33.10	33.16	33.41	33.37
15	31.33	31.18	31.22	31.30	31.38	31.56	31.51
20	30.02	29.94	29.94	30.03	30.12	30.26	30.19
25	29.00	28.98	28.94	29.06	29.13	29.26	29.16
30	28.18	28.20	28.12	28.26	28.32	28.44	28.34
40	26.93	26.98	26.87	27.03	27.07	27.19	27.07
50	26.01	26.07	25.95	26.12	26.15	26.25	26.13
80	24.20	24.29	24.15	24.33	24.36	24.41	24.31
100	23.40	23.50	23.36	23.53	23.57	23.58	23.50
	512 × 512 Fingerprint						
5	35.97	35.29	35.51	35.56	35.57	36.27	36.27
10	31.83	30.97	31.18	31.42	31.42	32.10	32.23
15	29.81	28.81	28.98	29.33	29.33	29.77	30.02
20	28.41	27.48	27.64	27.99	27.99	28.17	28.49
25	27.30	26.56	26.69	27.00	26.99	26.98	27.34
30	26.39	25.86	25.92	26.20	26.19	26.06	26.43
40	24.98	24.75	24.63	24.93	24.93	24.68	25.06
50	23.94	23.84	23.57	23.95	23.92	23.67	24.04
80	21.90	21.73	21.27	21.92	21.79	21.66	21.99
100	21.00	20.69	20.21	21.01	20.80	20.75	21.05

Table 6.1: Denoising results, in terms of PSNR values, of directional tensor product complex tight framelets. TP-$\mathbb{C}$TF$_m$ with $m = 3,\ 4,\ 6$ stands for bandlimited directional tensor product complex tight framelets. Example 7 stands for the compactly supported TP-$\mathbb{C}$TF$_3$. Example 14 stands for the compactly supported TP-$\mathbb{C}$TF$_4$ and TP-$\mathbb{C}$TF$_6$ in the corresponding column.

DT-$\mathbb{C}$WT. In particular, the performance of compactly supported TP-$\mathbb{C}$TF$_4$ is comparable to that of the DT-$\mathbb{C}$WT; that is, the compactly supported TP-$\mathbb{C}$TF$_4$ offers an alternative to the famous DT-$\mathbb{C}$WT.

The performance of TP-$\mathbb{C}$TF$_6^{\downarrow}$ for image denoising are compared with two groups of different approaches. The first group tensor product approach includes TP-$\mathbb{C}$TF$_3$ (which has the same redundancy rate $2\frac{2}{3}$ as that of TP-$\mathbb{C}$TF$_6^{\downarrow}$), TP-$\mathbb{C}$TF$_6$ (which has the same directional selectivity as TP-$\mathbb{C}$TF$_6^{\downarrow}$ with a higher redundancy rate $10\frac{2}{3}$), and DT-$\mathbb{C}$WT (which has redundancy rate 4). The second group consists of non-tensor-product approaches including curvelets [2], shearlets [33, 34], and smooth affine shear tight frames [26].

The software for curvelets is CurveLab at http://www.curvelab.org. The frequency wrapping package in CurveLab is applied for comparison. Detailed information on CurveLab package can be found in [2]. The redundancy rate of the CurveLab wrapping is about 2.8. The shearlets software ShearLab is at http://www.shearlab.org. Here two subpackages using compactly supported shearlets are chosen: one is DST (discrete shearlet transform) described in [33] and the other one is DNST (discrete nonseparable shearlet transform) in [34] which has the best performance so far in ShearLab packages. The redundancy rates for DST and DNST are 40 and 49, respectively. For the smooth affine shear tight frames (ASTF) in [26]. The redundancy rate for this system we choose is about 5.8. See [26] for more details. The comparison results of performance are reported in Table 6.2.

For texture-rich images such as *Barbara* and *Fingerprint*, Table 6.2 shows that TP-$\mathbb{C}$TF$_6^{\downarrow}$ outperforms TP-$\mathbb{C}$TF$_3$, DT-$\mathbb{C}$WT, CurveLab, DST, and DNST. It also has a better performance than that of TP-$\mathbb{C}$TF$_6$ for *Fingerprint* but slightly worse performance for *Barbara*. Though CurveLab (wrap) has low redundancy rate, its

σ	TP-$\mathbb{C}$TF$_6^{\downarrow}$	TP-$\mathbb{C}$TF$_6$	TP-$\mathbb{C}$TF$_3$	DT-$\mathbb{C}$WT	CurveLab	DST	DNST	ASTF
	512×512 Barbara							
5	37.63	37.84(-0.21)	37.16(0.47)	37.37(0.26)	33.83(3.80)	37.76(-0.13)	37.17(0.46)	37.40(0.23)
10	33.97	34.18(-0.21)	33.19(0.78)	33.54(0.43)	29.17(4.80)	33.94(0.03)	33.62(0.35)	33.74(0.23)
25	29.28	29.35(-0.07)	28.04(1.24)	28.81(0.47)	24.83(4.45)	28.90(0.38)	28.93(0.35)	29.29(-0.01)
40	26.85	26.86(-0.01)	25.53(1.32)	26.45(0.40)	23.87(2.98)	26.36(0.49)	26.48(0.37)	27.08(-0.23)
50	25.73	25.71(0.02)	24.48(1.25)	25.36(0.37)	23.38(2.35)	25.22(0.51)	25.31(0.42)	26.05(-0.32)
80	23.51	23.53(-0.02)	22.82(0.69)	23.27(0.24)	22.22(1.29)	23.11(0.40)	22.96(0.55)	23.97(-0.46)
100	22.58	22.64(-0.06)	22.25(0.33)	22.42(0.16)	21.61(0.97)	22.23(0.35)	22.06(0.52)	23.02(-0.44)
	512×512 Fingerprint							
5	36.29	36.27(0.02)	35.29(1.00)	35.82(0.47)	33.35(2.94)	36.02(0.27)	35.28(1.01)	35.20(1.09)
10	32.23	32.10(0.13)	30.97(1.26)	31.74(0.49)	30.61(1.62)	31.95(0.28)	31.76(0.47)	30.97(1.26)
25	27.27	26.98(0.29)	26.56(0.71)	27.26(0.01)	26.03(1.24)	27.04(0.23)	27.10(0.17)	26.95(0.32)
40	25.02	24.68(0.34)	24.75(0.27)	24.98(0.04)	23.92(1.10)	24.79(0.23)	24.82(0.20)	25.01(0.01)
50	24.01	23.67(0.34)	23.84(0.17)	23.95(0.06)	23.00(1.01)	23.77(0.24)	23.78(0.23)	24.07(-0.06)
80	21.99	21.66(0.33)	21.73(0.26)	21.91(0.08)	21.18(0.81)	21.65(0.34)	21.63(0.36)	22.11(-0.12)
100	21.09	20.75(0.34)	20.69(0.40)	21.01(0.08)	20.37(0.72)	20.63(0.46)	20.56(0.53)	21.22(-0.13)
	512×512 Lena							
5	38.16	38.37(-0.21)	37.98(0.18)	38.25(-0.09)	35.77(2.39)	38.22(-0.06)	38.01(0.15)	38.19(-0.03)
10	35.22	35.48(-0.26)	34.93(0.29)	35.19(0.03)	33.37(1.85)	35.19(0.03)	35.35(-0.13)	35.18(0.04)
25	31.20	31.60(-0.40)	31.17(0.03)	31.29(-0.09)	30.07(1.13)	31.09(0.11)	31.51(-0.31)	31.40(-0.20)
40	29.10	29.52(-0.42)	29.24(-0.14)	29.22(-0.12)	28.15(0.95)	28.92(0.18)	29.32(-0.22)	29.40(-0.30)
50	28.11	28.54(-0.43)	28.34(-0.23)	28.22(-0.11)	27.19(0.92)	27.89(0.22)	28.21(-0.10)	28.46(-0.35)
80	26.11	26.47(-0.36)	26.42(-0.31)	26.15(-0.04)	25.16(0.95)	25.71(0.40)	25.78(0.33)	26.44(-0.34)
100	25.21	25.52(-0.31)	25.52(-0.31)	25.20(0.01)	24.22(0.99)	24.67(0.54)	24.58(0.63)	25.48(-0.27)
	512×512 Boat							
5	36.74	36.92(-0.18)	36.45(0.29)	36.73(0.01)	33.59(3.15)	36.51(0.23)	36.04(0.70)	36.66(0.08)
10	33.10	33.41(-0.31)	32.97(0.13)	33.19(-0.09)	30.60(2.50)	33.07(0.03)	33.15(-0.05)	33.07(0.03)
25	28.81	29.26(-0.45)	28.98(-0.17)	29.03(-0.22)	27.51(1.30)	28.75(0.06)	29.23(-0.42)	29.10(-0.29)
40	26.72	27.19(-0.47)	26.98(-0.26)	26.99(-0.27)	25.96(0.76)	26.71(0.01)	27.20(-0.48)	27.14(-0.42)
50	25.79	26.25(-0.46)	26.07(-0.28)	26.06(-0.27)	25.18(0.61)	25.78(0.01)	26.23(-0.44)	26.23(-0.44)
80	24.05	24.41(-0.36)	24.29(-0.24)	24.22(-0.17)	23.55(0.50)	23.90(0.15)	24.17(-0.12)	24.41(-0.36)
100	23.27	23.58(-0.31)	23.50(-0.23)	23.39(-0.12)	22.79(0.48)	23.05(0.22)	23.17(0.10)	23.57(-0.30)

Table 6.2: Comparison results, in terms of PSNR values, of several image denoising methods using proposed directional tensor product complex tight framelet TP-$\mathbb{C}$TF$_6^{\downarrow}$, TP-$\mathbb{C}$TF$_3$, TP-$\mathbb{C}$TF$_6$, DT-$\mathbb{C}$WT, CurveLab (wrap) with redundancy rate 2.8 in [2], DST with redundancy rate 40 in [33], DNST with redundancy rate 49 in [34], and ASTF with redundancy 5.8 in [26].

performance is not as good as others for all the test images under bivariate shrinkage. Despite the fact that DST and DNST have much higher redundancy rates than that of $\text{TP-}\mathbb{C}\text{TF}_6^{\downarrow}$, the performance of DST or DNST is not as good as $\text{TP-}\mathbb{C}\text{TF}_6^{\downarrow}$ for *Barbara* and *Fingerprint*. With twice redundancy rate of $\text{TP-}\mathbb{C}\text{TF}_6^{\downarrow}$, ASTF performs better than $\text{TP-}\mathbb{C}\text{TF}_6^{\downarrow}$ only when the noise level is high $\sigma > 40$.

For *Lena* and *Boat*, $\text{TP-}\mathbb{C}\text{TF}_6^{\downarrow}$ does not perform as well as $\text{TP-}\mathbb{C}\text{TF}_3$ and $\text{DT-}\mathbb{C}\text{WT}$ only when σ is high ($\sigma \geqslant 40$) within less than 0.3dB loss in PSNR. For comparison among $\text{TP-}\mathbb{C}\text{TF}_6^{\downarrow}$, $\text{TP-}\mathbb{C}\text{TF}_6$, DNST, and ASTF, we see at most 0.48dB loss of performance of $\text{TP-}\mathbb{C}\text{TF}_6^{\downarrow}$ for both *Lena* and *Boat*. $\text{TP-}\mathbb{C}\text{TF}_6^{\downarrow}$ outperform DST and CurveLab for the test images of *Lena* and *Boat*.

Advanced statistical modeling can improve the estimation of framelet coefficients in transform-based image restoration methods. Gaussian Scale Mixture (GSM) [41, 51] model has been used to describe the behavior of the wavelet/framelet coefficients of natural signals, which is given by

$$x(t) = \sqrt{z(t)}u(t),$$

where t is a positive location vector. GSM model assumes that each coefficient x is specified by a Gaussian probability density function u with zero mean and a hidden multiplier z to adapt spatial fluctuation. In a neighborhood of wavelet/framelet coefficients at nearby location, the GSM model vector x is the product of two independent random variables: a positive hidden multiplier z and Gaussian random vector u with probability density function $N(0, C_u)$.

Note that conditioned on z, the distribution for the coefficient vector x is Gaussian with zero mean and covariance zC_u. Following [41], the probability density function is given by

$$p(x|z) = \frac{1}{(2\pi)^{N/2}|zC_u|^{1/2}} \exp\left(-\frac{x^\mathsf{T} C_u^{-1} x}{2z}\right),$$

and the distribution for x can be calculated from

$$p(x) = \int_0^\infty p(x|z)p(z)dz = \int_0^\infty \frac{1}{(2\pi)^{N/2}|zC_u|^{1/2}} \exp\left(-\frac{x^\mathsf{T} C_u^{-1} x}{2z}\right) p(z)dz.$$

Then the denoising model (6.1.1) combined with GSM becomes

$$y = \sqrt{z}u + n.$$

Specified by the hidden multiplier z in a neighborhood, the observed y is Gaussian distributed with zero mean and covariance $zC_u + C_n$ as given in

$$p_{y|z}(y|z) = \frac{1}{(2\pi)^{N/2}|zC_u + C_n|^{1/2}} \exp\left(-\frac{y^\mathsf{T}(zC_u + C_n)^{-1} y}{2}\right). \tag{6.1.3}$$

From Bayesian perspective, the image denoising is to calculate the Bayesian estimator for the center coefficient in a neighborhood of wavelet/framelet coefficients modeled by GSM. The estimator is given by

$$\begin{aligned} \widehat{x_c} &= \mathrm{E}\{x_c|y\} \\ &= \int x_c p(x_c|y) dx_c = \iint_0^\infty x_c p(x_c, z|y) dz dx_c \\ &= \iint_0^\infty x_c p(x_c|y,z) p(z|y) dz dx_c = \int_0^\infty p(z|y)\, \mathrm{E}\{x_c|y,z\} dz, \end{aligned} \tag{6.1.4}$$

where x_c stands for the center coefficient in the neighborhood [41]. In implementation, (6.1.4) is discretized as

$$\widehat{x_c} = \sum_{k=1}^{K} p(z_k|y)\, \mathrm{E}\{x_c|y, z_k\}, \tag{6.1.5}$$

where K is the number of discretized z.

Conditioned on z, the observed y is Gaussian distributed. Then $\mathrm{E}\{x_c|y,z\}$ in (6.1.5) is the Wiener estimation

$$\mathrm{E}\{x_c|y,z\} = zC_u(zC_u + C_n)^{-1}y,$$

please refer [32, 40, 50] for more information on the Wiener estimation. The posterior density $p(z|y)$ in (6.1.5) can be calculated using Bayes formula by

$$p(z|y) = \frac{p(y|z)p_z(z)}{\int p(y|a)p_z(a)da},$$

where $p(y|z)$ is given by (6.1.3). As for the $p_z(z)$, Portilla *et al.* chose a Jeffrey's prior in [41]

$$p_z(z) \propto \frac{1}{z},$$

due to its superior performance to other options.

In traditional GSM model [51], the signal covariance is assumed to be the same within each subband. Improvement can be made to catch the different local covariance. This is implemented by estimating local covariance in non-overlapping areas as Spatial Variant GSM (SVGSM) [8], by adapting the local directions to the covariance as Orientation Adaptive GSM (OAGSM) [11], or by clustering the coefficients in one subband into many similar components as mixtures of Gaussian Scale Mixture models (MGSM) [9, 39] and mixtures of projected Gaussian Scale Mixture models (MPGSM) [7]. MGSM model can capture the local covariance on each component. The denoising result can be significantly improved. We choose mixtures of Gaussian Scale Mixture models (MGSM) as our advanced statistical model for testing. However, we do not estimate the multiplier z_k for each component k. Instead, we take Jeffrey's prior for all the components to reduce the number of parameters.

To implement either GSM or MGSM model, we have to calculate the covariance matrix C_u in the transform domain. If n_j and y_j are the vectors of wavelet/framelet coefficients of the noise and noisy observation, respectively, then C_n and C_y can be calculated by

$$C_n = \frac{1}{J}\sum_{j=1}^{J} n_j n_j^{\mathsf{T}} \quad \text{and} \quad C_y = \frac{1}{J}\sum_{j=1}^{J} y_j y_j^{\mathsf{T}}, \tag{6.1.6}$$

where J is the total number of coefficients in the neighborhood. With C_n and C_y, the signal covariance C_u can be computed from

$$C_u = C_y - C_n,$$

with a normalization $\mathrm{E}\{z\} = 1$. Hence, the covariance of the noise C_n in the transform domain is essential to the calculation of the signal covariance. The orthonormal wavelet transform preserves the variance of the white Gaussian noise in the transform domain. However, for over-complete transforms, the covariance of the noise in the transform domain is more complicated.

Though the covariance of the noise coefficients in the transform domain can be obtained by (6.1.6), it is an approximation. Based on the notion of discrete affine system, the exact covariance of the noise coefficients can be calculated. It can be generated to other over-complete transforms. Since the noise n is i.i.d. Gaussian with zero mean and covariance σ^2, the covariance of two noise coefficients in the transform domain between positions k_1 and k_2 can be calculated from

$$\begin{aligned}
&\mathrm{E}\{\langle n, b_{j,l;k_1}\rangle\langle n, b_{j,l;k_2}\rangle\}\\
=&\,\mathrm{E}\left\{\left(\sum n(\cdot)b_{j,\ell}(\cdot - 2^j k_1)\right)\left(\sum n(\cdot)b_{j,\ell}(\cdot - 2^j k_2)\right)\right\}\\
=&\,\mathrm{E}\left\{\sum_p n(\cdot)n(p-\cdot)b_{j,\ell}(\cdot - 2^j k_1)b_{j,\ell}(p - \cdot - 2^j k_2)\right\} = \langle b_{j,l;k_1}, b_{j,l;k_2}\rangle\,\mathrm{E}\{n^2\}\\
=&\langle b_{j,l;k_1}, b_{j,l;k_2}\rangle\sigma^2,
\end{aligned}$$

where $b_{j,l;k_1}$ and $b_{j,l;k_2}$ are the filters applied corresponding to position k_1 and k_2 in the discrete affine system and the property of i.i.d. Gaussian with zero mean for the noise n is applied to simplify the expectation.

Above calculation demonstrates that the covariance of the Gaussian noise in the transform domain completely depends on the corresponding filters applied in the discrete affine systems. Thus, the exact covariance of wavelet/framelet coefficients of the noise in the transform domain can be calculated by the inner product of corresponding filters in discrete affine systems.

The denoising results using advanced statistical models are reported in Table 6.3 for bandlimited $\mathrm{TP\text{-}\mathbb{C}TF}_4$ and $\mathrm{TP\text{-}\mathbb{C}TF}_6$. In order to capture the local covariance, the neighborhood size is set to be 5×5.

	$\mathrm{TP\text{-}\mathbb{C}TF}_4$				$\mathrm{TP\text{-}\mathbb{C}TF}_6$			
σ	*Lena*	*Barbara*	*Boat*	*House*	*Lena*	*Barbara*	*Boat*	*House*
10	35.55	34.58	33.50	35.35	35.73	34.81	33.66	35.90
15	33.77	32.53	31.58	33.31	34.03	32.82	31.76	33.99
20	32.51	31.05	30.22	32.06	32.80	31.39	30.43	32.61
25	31.51	29.89	29.22	30.93	31.83	30.26	29.41	31.55
30	30.66	28.93	28.38	29.80	31.01	29.33	28.59	30.65
50	28.34	26.27	26.19	27.27	28.70	26.74	26.39	28.05

Table 6.3: Image denoising results, in terms of PSNR values, of bandlimited $\mathrm{TP\text{-}\mathbb{C}TF}_4$ and $\mathrm{TP\text{-}\mathbb{C}TF}_6$ with advanced statistical model MGSM.

Table 6.3 demonstrates the performance of proposed directional tensor product complex tight framelet with advanced statistical models (MGSM) in image denoising has significant improvement comparing with simple statistical models (bivariate shrinkage). There is an average of $0.2 \sim 0.3$ dB improvement in terms of PSNR for all test images for all standard deviation levels.

It is comparable to the reported best performance in [7] under the transform thresholding philosophy.

6.2 Video denoising

The redundancy rate is crucial for video denoising in three dimensions (3D), since the computational cost is the bottleneck for high-dimensional data processing. Our proposed $\text{TP-}\mathbb{C}\text{TF}_6^{\downarrow}$ only has the redundancy rate $3\frac{5}{7}$ in 3D.

We compare the performance of $\text{TP-}\mathbb{C}\text{TF}_6^{\downarrow}$ with the directional tensor product complex tight framelet $\text{TP-}\mathbb{C}\text{TF}_3$ (which has the same redundancy rate $3\frac{5}{7}$ as $\text{TP-}\mathbb{C}\text{TF}_6^{\downarrow}$), $\text{TP-}\mathbb{C}\text{TF}_6$ (which has the same directionality as $\text{TP-}\mathbb{C}\text{TF}_6^{\downarrow}$ but has the redundancy rate $29\frac{5}{7}$), the 3D $\text{DT-}\mathbb{C}\text{WT}$ (which has the redundancy rate 8), the 3D nonseparable surfacelets in [36] (which has the redundancy rate 6.4), and the 3D nonseparable compactly supported shearlet frames DNST^{3D}–42 and DNST$_2^{3D}$–154 in [34] in ShearLab with DNST^{3D}–42 and DNST$_2^{3D}$–154 having the redundancy rates 42 and 154, respectively. The decomposition level for all tensor product complex tight framelets $\text{TP-}\mathbb{C}\text{TF}_m$ is set to be $J = 4$ and the boundary extension size for all $\text{TP-}\mathbb{C}\text{TF}_m$ is set to be 16 pixels. The strategy for processing frame coefficients for all $\text{TP-}\mathbb{C}\text{TF}_m$ and $\text{DT-}\mathbb{C}\text{WT}$ is the 3D bivariate shrinkage as outlined in (6.1.2) but with window size 3 instead of 7. The constant $\sqrt{3}$ in the bivariate shrinkage function in (6.1.2) for $\text{DT-}\mathbb{C}\text{WT}$ is still set to be $\sqrt{3}$, but this constant is replaced by $\sqrt{4}$ for $\text{TP-}\mathbb{C}\text{TF}_m$ (though there are no significant performance differences if the constant $\sqrt{3}$ is used for $\text{TP-}\mathbb{C}\text{TF}_m$). All parameters for 3D surfacelets and the two 3D shearlets DNST^{3D}–42 and DNST$_2^{3D}$–154 are the same as those described in [34, 36]. The two video sequences *Mobile* and *Coastguard* are used for comparison, which are the same test videos as used in the paper [34] and can be downloaded from the ShearLab 3D package at `http://www.shearlab.org`. See Figure 6.2 for the first frame of these two videos *Mobile* and *Coastguard*.

(a) Mobile (b) Coastguard

Figure 6.2: The first frame of the test videos *Mobile* and *Coastguard*.

The comparison results of performance are reported in Table 6.4 under i.i.d. Gaussian noise with standard deviation $\sigma = 10, 20, 30, 40, 50, 80, 100$.

	$192 \times 192 \times 192$ Mobile						
σ	$\text{TP-}\mathbb{C}\text{TF}_6^{\downarrow}$	$\text{TP-}\mathbb{C}\text{TF}_6$	$\text{TP-}\mathbb{C}\text{TF}_3$	$\text{DT-}\mathbb{C}\text{WT}$	Surfacelets	DNST^{3D}-42	DNST^{3D}-154
10	35.26	35.52(-0.26)	33.40(1.86)	34.11(1.15)	32.79(2.47)	35.27(-0.01)	35.91(-0.65)
20	31.58	31.77(-0.19)	29.90(1.68)	30.53(1.05)	29.95(1.63)	31.32(0.26)	32.18(-0.60)
30	29.52	29.66(-0.14)	28.03(1.51)	28.55(0.97)	28.26(1.26)	29.00(0.52)	29.99(-0.47)
40	28.10	28.20(-0.10)	26.76(1.34)	27.17(0.93)	27.05(1.05)	27.37(0.73)	28.42(-0.32)
50	27.01	27.08(-0.07)	25.79(1.22)	26.15(0.86)	26.11(0.90)	26.13(0.88)	27.22(-0.21)
80	24.82	24.82(0.00)	23.87(0.95)	24.03(0.79)	24.25(0.57)	23.69(1.13)	24.75(0.07)
100	23.87	23.82(0.05)	23.06(0.81)	23.06(0.81)	23.40(0.47)	22.63(1.24)	23.62(0.25)
	$192 \times 192 \times 192$ Coastguard						
10	33.86	34.15(-0.29)	32.59(1.27)	33.16(0.70)	30.86(3.00)	33.13(0.73)	33.81(0.05)
20	30.26	30.62(-0.36)	29.21(1.05)	29.66(0.60)	28.26(2.00)	29.45(0.81)	30.28(-0.02)
30	28.38	28.73(-0.35)	27.46(0.92)	27.82(0.56)	26.87(1.51)	27.50(0.88)	28.40(-0.02)
40	27.13	27.45(-0.32)	26.28(0.85)	26.58(0.53)	25.91(1.21)	26.17(0.96)	27.13(-0.00)
50	26.18	26.48(-0.30)	25.40(0.78)	25.66(0.52)	25.17(1.01)	25.17(1.01)	26.17(0.01)
80	24.30	24.53(-0.23)	23.67(0.63)	23.84(0.46)	23.61(0.69)	23.17(1.13)	24.17(0.13)
100	23.47	23.65(-0.18)	22.91(0.56)	22.98(0.49)	22.87(0.60)	22.24(1.23)	23.22(0.25)

Table 6.4: Video denoising results, in terms of PSNR values, of several methods using proposed 3D $\text{TP-}\mathbb{C}\text{TF}_6^{\downarrow}$ with the redundancy rate $3\frac{5}{7}$, 3D $\text{TP-}\mathbb{C}\text{TF}_6$ with the redundancy rate $29\frac{5}{7}$ (having the same directionality as $\text{TP-}\mathbb{C}\text{TF}_6^{\downarrow}$), 3D $\text{TP-}\mathbb{C}\text{TF}_3$ with the redundancy rate $3\frac{5}{7}$ (having the same redundancy rate as $\text{TP-}\mathbb{C}\text{TF}_6^{\downarrow}$), the 3D $\text{DT-}\mathbb{C}\text{WT}$ with the redundancy rate 8, the 3D nonseparable surfacelets in [36] with the redundancy rate 6.4, and the 3D nonseparable compactly supported shearlet frames DNST^{3D}-42 and DNST_2^{3D}-154 with the redundancy rates 42 and 154, respectively.

From Table 6.4, we see that the loss of performance of $\text{TP-}\mathbb{C}\text{TF}_6^{\downarrow}$ is not significant in comparison with $\text{TP-}\mathbb{C}\text{TF}_6$ for both *Mobile* and *Coastguard*. $\text{TP-}\mathbb{C}\text{TF}_6^{\downarrow}$

can outperform DNST_2^{3D}-154 when the noise level σ is high ($\sigma > 50$) despite the fact that DNST_2^{3D}-154 has the highest redundancy rate 154 which is 41.5 times the redundancy of $\text{TP-}\mathbb{C}\text{TF}_6^{\downarrow}$. Generally, $\text{TP-}\mathbb{C}\text{TF}_6^{\downarrow}$ outperforms all other methods for any noise level σ (except a slightly worse performance at $\sigma = 10$ comparing with DNST^{3D}-42 for *Mobile*). Significant improvement can be seen in comparison with the nonseparable 3D surfacelets in [36] (up to 2.47dB for *Mobile* and 3dB for *Coastguard*) and DNST^{3D}-42 in [34] (up to 1.24dB for *Mobile* and 1.23dB for *Coastguard*).

Bibliography

[1] *Wavelet*, 2015 (accessed February 3, 2015). http://en.wikipedia.org/wiki/Wavelet.

[2] E. Candès, L. Demanet, D. Donoho, and L. Ying. Fast discrete curvelet transforms. *Multiscale Modeling & Simulation*, 5(3):861–899, 2006.

[3] E. Candès and D. Donoho. Curvelets and curvilinear integrals. *Journal of Approximation Theory*, 113(1):59–90, 2001.

[4] I. Daubechies. *Ten lectures on wavelets*, volume 61. SIAM, 1992.

[5] M. N. Do and M. Vetterli. The contourlet transform: an efficient directional multiresolution image representation. *IEEE Transactions on Image Processing*, 14(12):2091–2106, 2005.

[6] R. J. Duffin and A. C. Schaeffer. A class of nonharmonic Fourier series. *Transactions of the American Mathematical Society*, pages 341–366, 1952.

[7] B. Goossens, A. Pizurica, and W. Philips. Image denoising using mixtures of projected Gaussian scale mixtures. *IEEE Transactions on Image Processing*, 18(8):1689–1702, 2009.

[8] J. A. Guerrero-Colón, L. Mancera, and J. Portilla. Image restoration using space-variant Gaussian scale mixtures in overcomplete pyramids. *IEEE Transactions on Image Processing*, 17(1):27–41, 2008.

[9] J. A. Guerrero-Colón, E. P. Simoncelli, and J. Portilla. Image denoising using mixtures of Gaussian scale mixtures. In *Image Processing, 2008. ICIP 2008. 15th IEEE International Conference on*, pages 565–568. IEEE, 2008.

[10] K. Guo, G. Kutyniok, and D. Labate. Sparse multidimensional representations using anisotropic dilation and shear operators. *Wavelets and Splines (Athens, GA, 2005), G. Chen und MJ Lai, eds., Nashboro Press, Nashville, TN*, pages 189–201, 2006.

[11] D. K. Hammond and E. P. Simoncelli. Image modeling and denoising with orientation-adapted Gaussian scale mixtures. *IEEE Transactions on Image Processing*, 17(11):2089–2101, 2008.

[12] B. Han. On dual wavelet tight frames. *Applied and Computational Harmonic Analysis*, 4(4):380–413, 1997.

[13] B. Han. Matrix extension with symmetry and applications to symmetric orthonormal complex m-wavelets. *Journal of Fourier Analysis and Applications*, 15(5):684–705, 2009.

[14] B. Han. Pairs of frequency-based nonhomogeneous dual wavelet frames in the distribution space. *Applied and Computational Harmonic Analysis*, 29(3):330–353, 2010.

[15] B. Han. Symmetric orthonormal complex wavelets with masks of arbitrarily high linear-phase moments and sum rules. *Advances in Computational Mathematics*, 32(2):209–237, 2010.

[16] B. Han. Symmetric orthogonal filters and wavelets with linear-phase moments. *Journal of Computational and Applied Mathematics*, 236(4):482–503, 2011.

[17] B. Han. Symmetric orthogonal filters and wavelets with linear-phase moments. *Journal of Computational and Applied Mathematics*, 236(4):482–503, 2011.

[18] B. Han. Nonhomogeneous wavelet systems in high dimensions. *Applied and Computational Harmonic Analysis*, 32(2):169–196, 2012.

[19] B. Han. Properties of discrete framelet transforms. *Mathematical Modelling of Natural Phenomena*, 8(01):18–47, 2013.

[20] B. Han. Algorithm for constructing symmetric dual framelet filter banks. *Mathematics of Computation*, 84(292):767–801, 2015.

[21] B. Han, G. Kutyniok, and Z. Shen. Adaptive multiresolution analysis structures and shearlet systems. *SIAM Journal on Numerical Analysis*, 49(5):1921–1946, 2011.

[22] B. Han, Q. Mo, and Z. Zhao. Construction and application of compactly supported directional tensor product complex tight framelets. preprint.

[23] B. Han, Q. Mo, and Z. Zhao. Compactly supported tensor product complex tight framelets with directionality. *SIAM Journal on Mathematical Analysis*, 47(3):2464 – 2494, 2015.

[24] B. Han and Z. Zhao. Tensor product complex tight framelets with increasing directionality. *SIAM Journal on Imaging Sciences*, 7(2):997–1034, 2014.

[25] B. Han, Z. Zhao, and X. Zhuang. Directional tensor product complex tight framelets with low redundancy. *Applied and Computational Harmonic Analysis*, 2015.

[26] B. Han and X. Zhuang. Smooth affine shear tight frames with MRA structure. *Applied and Computational Harmonic Analysis*, 2015.

[27] N. Kingsbury. Image processing with complex wavelets. *Philosophical Transactions of the Royal Society of London A: Mathematical, Physical and Engineering Sciences*, 357(1760):2543–2560, 1999.

[28] N. Kingsbury. Complex wavelets for shift invariant analysis and filtering of signals. *Applied and Computational Harmonic Analysis*, 10(3):234–253, 2001.

[29] G. Kutyniok et al. *Shearlets: Multiscale analysis for multivariate data*. Springer Science & Business Media, 2012.

[30] G. Kutyniok, M. Shahram, and X. Zhuang. Shearlab: A rational design of a digital parabolic scaling algorithm. *SIAM Journal on Imaging Sciences*, 5(4):1291–1332, 2012.

[31] M. Lebrun, M. Colom, A. Buades, and J. Morel. Secrets of image denoising cuisine. *Acta Numerica*, 21:475–576, 2012.

[32] J.-S. Lee. Digital image enhancement and noise filtering by use of local statistics. *IEEE Transactions on Pattern Analysis and Machine Intelligence*, (2):165–168, 1980.

[33] W.-Q. Lim. The discrete shearlet transform: A new directional transform and compactly supported shearlet frames. *IEEE Transactions on Image Processing*, 19(5):1166–1180, 2010.

[34] W.-Q. Lim. Nonseparable shearlet transform. *IEEE Transactions on Image Processing*, 22(5):2056–2065, 2013.

[35] J.-M. Lina and M. Mayrand. Complex Daubechies wavelets. *Applied and Computational Harmonic Analysis*, 2(3):219–229, 1995.

[36] Y. M. Lu and M. N. Do. Multidimensional directional filter banks and surfacelets. *IEEE Transactions on Image Processing*, 16(4):918–931, 2007.

[37] S. G. Mallat. A theory for multiresolution signal decomposition: the wavelet representation. *IEEE Transactions on Pattern Analysis and Machine Intelligence*, 11(7):674–693, 1989.

[38] Q. Mo. *Compactly supported symmetric MRA wavelet frames*. PhD thesis, University of Alberta, 2003.

[39] J. Portilla and J. A. Guerrero-Colon. Image restoration using adaptive Gaussian scale mixtures in overcomplete pyramids. In *Optical Engineering +Applications*, pages 67011F–67011F. International Society for Optics and Photonics, 2007.

[40] J. Portilla, V. Strela, M. J. Wainwright, and E. P. Simoncelli. Adaptive Wiener denoising using a Gaussian scale mixture model in the wavelet domain. In *Image Processing, 2001. Proceedings. 2001 International Conference on*, volume 2, pages 37–40. IEEE, 2001.

[41] J. Portilla, V. Strela, M. J. Wainwright, and E. P. Simoncelli. Image denoising using scale mixtures of Gaussians in the wavelet domain. *IEEE Transactions on Image Processing*, 12(11):1338–1351, 2003.

[42] I. W. Selesnick. Hilbert transform pairs of wavelet bases. *Signal Processing Letters, IEEE*, 8(6):170–173, 2001.

[43] I. W. Selesnick. The design of approximate Hilbert transform pairs of wavelet bases. *IEEE Transactions on Signal Processing*, 50(5):1144–1152, 2002.

[44] I. W. Selesnick, R. G. Baraniuk, and N. C. Kingsbury. The dual-tree complex wavelet transform. *IEEE Signal Processing Magazine*, 22(6):123–151, 2005.

[45] L. Sendur and I. W. Selesnick. Bivariate shrinkage functions for wavelet-based denoising exploiting interscale dependency. *IEEE Transactions on Signal Processing*, 50(11):2744–2756, 2002.

[46] L. Sendur and I. W. Selesnick. Bivariate shrinkage with local variance estimation. *IEEE Signal Processing Letters*, 9(12):438–441, 2002.

[47] Y. Shen, B. Han, and E. Braverman. Image inpainting using directional tensor product complex tight framelets. *arXiv preprint arXiv:1407.3234*, 2014.

[48] E. P. Simoncelli, W. T. Freeman, E. H. Adelson, and D. J. Heeger. Shiftable multiscale transforms. *IEEE Transactions on Information Theory*, 38(2):587–607, 1992.

[49] H. J. S. Smith. On systems of linear indeterminate equations and congruences. *Philosophical Transactions of the Royal Society of London*, 151:293–326, 1861.

[50] V. Strela. Denoising via block Wiener filtering in wavelet domain. In *European Congress of Mathematics*, pages 619–625. Springer, 2001.

[51] V. Strela, J. Portilla, and E. P. Simoncelli. Image denoising using a local Gaussian scale mixture model in the wavelet domain. In *International Symposium on Optical Science and Technology*, pages 363–371. International Society for Optics and Photonics, 2000.